Åbo Akademi University

Hanna Kinnunen

The Role and Corrosivity of Lead in Recycled Wood Combustion

The Role and Corrosivity of Lead in Recycled Wood Combustion

Hanna Kinnunen

Laboratory of Inorganic Chemistry
Åbo Akademi University
Åbo, Finland, 2019

Supervisors

D.Sc. Docent Patrik Yrjas
Åbo Akademi University

D.Sc. Sonja Enestam
Valmet Technologies Oy

Opponent and reviewer

Professor Franz Winter
Vienna University of Technology

Reviewer

Professor Rainer Backman
Umeå University

ISBN 978-952-12-3847-5 (print)
ISBN 978-952-12-3848-2 (digital)
Painosalama Oy – Turku, Finland 2019

In any field, find the strangest thing and then explore it.

- J. Archibald Wheeler

Preface

The research in this thesis was carried out as part of my work at Valmet Technologies Oy between 2014 and 2019. Firstly, I would like to warmly thank my supervisor D.Sc. Sonja Enestam. This thesis would not have been possible without her valuable help. She always had confidence in me and made this thesis happen, technically and financially. Her encouragement and our common interest in corrosion and lead brought this thesis to at least its halfway point. My other supervisor, D.Sc. Docent Patrik Yrjas is also gratefully acknowledged. His valuable comments gave me new perspectives and broadened my ways of thinking.

This thesis would not have been completed without the help of my co-authors and colleagues. I would like to warmly thank Prof. Daniel Lindberg for sharing his endless knowledge of thermodynamics. Discussions with Daniel always provided new and mind-broadening aspects to my work. I'm also grateful to my other co-authors: D.Sc. Mikko Uusitalo, D.Sc. Dorota Bankiewicz, D.Sc. Markus Engblom, Mr. Tor Laurén, Ms. Annika Talus, D.Sc. Rikard Norling and Mr. Jonne Niemi for their time and valuable input. I deeply appreciate our fruitful co-operation with Annika and Rikard and I hope we will continue our interesting research expedition. In addition, I would like to express special thanks to personnel in Top Analytica for helping me with the analysis. It's always exciting and inspiring to visit their lab.

I want to express my deepest gratitude to my former colleagues, Ms. Johanna Tuiremo and Ms. Merja Hedman. Johanna's guidance and knowledge in steels and Merja's combustion experience provided the basis for this work. It has been a pleasure to follow in their footsteps. I'm also extremely grateful to our "BFB guys," Mr. Risto Eteläaho and Mr. Jukka-Pekka Leppälä, who have always shown interest in my work. I would like to warmly thank Jukka-Pekka for helping me with the site measurements and Risto for always having time and patience for my questions and explaining to me the principles of boilers. Help from both of them has been invaluable. I would also like to thank Ms. Silja Inkinen for her valuable advice; she always had time for me despite her numerous other commitments. I am also grateful to Mr. Kari Mäkelä for his time and guidance. No matter what I asked, he had the answers.

Huge thanks belong as well to each and every member of our combustibility and corrosion team. I wouldn't have had time to finish this thesis without their efforts and help. It's a pleasure to work in a group like

that! I would also like to sincerely thank our Valmet ladies' group. Our discussions and laughs during coffee breaks have cheered me up on hard days and have given me something other than work to think about.

I'm also grateful for all the friends who have lived this together with me. Our jogs, journeys, dinners, escape rooms and never-ending laugh have given me a good balance for the work. I feel privileged to have so many friends around me willing to help.

Finally, I wish to express my greatest thanks to my parents for being good role models for me and giving me the freedom to make my own decisions whether they were wise or not. My mother has shown me that there is no such thing that we should give up and I've learned from my father that studying always pays. And Ilari, love of my life - Thanks for being there, sharing this road with me, sensing the tone when I needed cheering up and showing me that everything is not always that serious.

Tampere, August 2019

Hanna Kinnunen

Abstract

Combustion of various waste-derived fuels has been increasing during the recent decades due to their low price, good availability, CO_2 neutrality and legislation. Fossil fuels are being replaced by renewable and waste-derived fuels as the European strategy requires increased use of renewable sources for heat and power production. In addition, landfilling of combustible waste is restricted by legislation. Recycled wood is one of the example fuels used to replace fossil fuels. It has a heterogeneous nature, as it might derive from several different sources, such as construction, demolition and refurbishment work, and may also include furniture and packaging materials. This type of wood waste is typically surface-treated with different chemical agents such as paints and lacquers and mechanical contaminants, such as plastics and metallic components might be present. Due to these impurities, elevated concentrations of Pb, Zn, Cl, Na and K may exist within recycled wood. These elements contribute to corrosion, fouling and slagging during combustion, each of which reduces the boiler efficiency.

Corrosion is usually the main limiting factor to achieve higher steam parameters. During untreated virgin wood combustion, alkali chlorides might form and cause corrosion at the superheater area where the material temperature exceeds 450 °C. In recycled wood firing, alkali chlorides are present in combination with heavy metals, and the corrosion starting temperature may be considerably lower than with virgin wood combustion. In practice, this means that corrosion issues might be present in furnace walls, low-temperature superheaters and economisers. Pb and Zn are known to decrease the first melting temperature of ash deposits, and together with alkali chlorides, the first melting temperature can be close to 200 °C. These low-melting mixtures promote molten phase corrosion, which may lead to catastrophic corrosion rates.

Intelligent and optimised boiler design requires an understanding of how and why corrosion occurs. The role and corrosivity of Pb compounds during recycled wood combustion were studied in this thesis. Full-scale measurements were carried out in fluidised bed boilers combusting recycled wood. The results gained from the measurements were utilised in laboratory-scale corrosion experiments. Thermodynamic modelling was used to predict the formation and condensation of Pb including compounds.

Fine particle measurements in a full-scale fluidised bed boiler revealed over 70 % of Pb to be present as chlorides in the furnace. The highest share was observed between the secondary and tertiary air levels. Short- and long-

term deposits revealed Pb to be bound with K and Cl, as KPb_2Cl_5 and K_2PbCl_4. Zn was not found at all in long-term deposits. The share of Pb in the deposits was lower on warmer surfaces, and no Pb was found in the uncooled sample probe, indicating that Pb-including compounds will deposit through condensation. Clear differences in the corrosion rates (0.8 mm/year vs. 0.4 mm/year) were observed between the samples exposed to hot (800 °C) and cooler (490 °C) flue gas temperature using the same material temperature (360 °C).

The formation mechanisms of solid KPb_2Cl_5 and K_2PbCl_4 are assumed to proceed via $PbCl_2$ (g, l, s) and KCl (g, s) or via a gaseous intermediate product, $KPbCl_3$. This $KPbCl_3$ (g) was added to the thermodynamic database to study whether its presence changes the stability of $PbCl_2$. The calculations suggested that $KPbCl_3$ (g) is stable between 400 and 900 °C. Most of the Pb is still suggested to be present as $PbCl_2$ within this temperature range. At conditions corresponding to the ones between the secondary and tertiary air levels, the thermodynamic calculations propose gaseous PbO be present as the major component. Thermodynamic calculations suggested solid KPb_2Cl_5 to be stable below 285 °C. Solid K_2PbCl_4 was predicted to be stable on surfaces with temperatures between 285 °C and 365 °C which are typical furnace wall temperatures. The highest condensation temperature of $PbCl_2$ was predicted to be ~440 °C.

In laboratory-scale corrosion experiments, $PbCl_2$ was observed to interact with KCl, forming KPb_2Cl_5 and K_2PbCl_4. In addition, interactions with Na_2SO_4 and K_2SO_4 forming $Na_3Pb_2(SO_4)_3Cl$ and $K_3Pb_2(SO_4)_3Cl$, respectively, were observed. No solid-solid interaction with $PbCl_2$ and NaCl was observed.

Most of the corrosion findings reported in this thesis occurred below the first melting temperature of the deposit. The results quite clearly show that corrosion proceeds via $FeCl_2$ formation with Fe-based steels. $FeCl_2$ was observed to form in the full- and laboratory-scale studies as a corrosion product beneath the K-Pb-Cl-including mixtures. A solidus projection for the $PbCl_2$-KCl-$FeCl_2$ system was calculated to determine whether corrosion occurring at low temperatures could be explained by the formation of the eutectic melt between the deposit and $FeCl_2$. The melting temperatures vary between 312 °C and 334 °C depending on the composition. Corrosion study with $FeCl_2$-$PbCl_2$-KCl mixture showed that these compounds may interact, and form melt or sintered particles together already at 300 °C. $PbCl_2$-including deposits getting into contact with the steel initiate the corrosion reaction. To initiate the corrosion, no molten phase is needed in the

beginning. In the second stage, as the corrosion proceeds, $FeCl_2$ may form a local melt together with Pb-including particles.

Laboratory exposures showed no corrosion with carbon steel at 200 °C when exposed to $PbCl_2$-containing deposits. Corrosion was noticed to occur at 300 °C and above. Threshold temperatures for severe corrosion with a synthetic deposit including 5 wt-% $PbCl_2$ and 95 wt-% K_2SO_4 for the low-alloy 16Mo3 and 10CrMo9-10 were 325 °C and 350 °C, respectively. Ni-based alloy 625 was not corroding at the highest test temperature of 375 °C.

Keywords: High temperature corrosion, furnace wall, superheater, lead potassium chloride, recycled wood combustion

Sammanfattning

Förbränning av avfall och återvinningsbränslen har ökat under de senaste decennierna tack vare deras låga priser, goda tillgänglighet, CO_2-neutralitet och lagstiftningen. Fossila bränslen ersätts av förnybara bränslen, eftersom den europeiska strategin förpliktar att öka användningen av förnybara energikällor. Därtill är deponi av brännbart avfall begränsat av lagstiftningen. Returträ är ett av de bränslen som används för att ersätta fossila bränslen. Returträ är heterogent till sin natur, eftersom det kan innehålla material från byggnads-, rivnings- och renoveringsarbeten, och kan omfatta möbler och förpackningsmaterial. Denna typ av träavfall är typiskt ytbehandlad med färger och lacker för att förbättra och förlänga livslängden. Det kan också innehålla mekaniska föroreningar, till exempel plast och metalliska komponenter. På grund av dessa föroreningarna kan förhöjda koncentrationer av Pb, Zn, Cl, Na och K existera i returträ. Alla dessa element har stor inverkan på korrosion och beläggningsbildning som minskar pannans tillgänglighet och effektivitet.

Korrosion är vanligtvis den huvudsakliga begränsande faktorn för högre ångparametrar. Vid förbränning av obehandlat trä, kan alkaliklorider bildas och förorsaka korrosion på överhettare där materialtemperaturen överstiger 450 °C. Vid returträförbränning förekommer alkaliklorider i kombination med tungmetaller och korrosion kan börja vid lägre temperaturer än vid förbränning av obehandlad trä. I praktiken betyder detta att korrosionsproblem kan förekomma i eldstadsväggar, primär överhettare och ekonomisers. Pb och Zn minskar påslagets första smälttemperatur och tillsammans med alkaliklorider kan den första smältemperaturen vara ~200 °C. Dessa lågsmältande blandningar främjar smältfaskorrosion, vilket kan leda till katastrofala korrosionshastigheter.

För att kunna uppnå en intelligent och optimerad pannkonstruktion är det viktigt att förstå hur och varför korrosion händer. Korrosivitet av Pb samt roll under returträförbränning studerades i denna avhandling. Fullskaliga mätningar utfördes i fluidiserade bäddpannor som använder returträ. Resultaten från de fullskaliga mätningarna användes i pannsimulerade korrosionsförsök i laboratorie-skala. Termodynamisk modellering användes för att prediktera bildning och kondensation av Pb-föreningar.

Finpartikelmätningar visade att över 70 % av Pb förekommer främst som klorid i eldstaden. Koncentrationen var högst mellan de sekundära och tertiära luftnivåerna. Pb kunde identifieras både i korttidpåslag (två timmars sondprov) och i påslag som bildats i pannan under en längre tid. Pb

konstaterades reagera med K och Cl under bildning av KPb_2Cl_5 och K_2PbCl_4. Zn hittades inte alls i de långvariga beläggningarna. Andelen Pb minskade när man gick från de kallare materialtemperaturerna till de varmare ytorna. Inget Pb hittades i okylda prov vilket indikerar att Pb-föreningar fastnar genom kondensation. Samma K-Pb-Cl förening identifierades emellertid i påslagen tagna vid olika rökgas temperaturer. Tydliga skillnader i korrosionshastigheter (0.8 mm/år vs. 0.4 mm/år) noterades mellan proverna som var utsatta för heta (800 °C) och svalare (490 °C) rökgastemperatur men densamma materialtemperaturen (360 °C).

Fast KPb_2Cl_5 och K_2PbCl_4 bildas från $PbCl_2$ (g, l, s) och KCl (g, s) eller från en gasformig mellanprodukt, $KPbCl_3$. Termodynamiska data för $KPbCl_3$ (g) har tidigare saknats i de databaser som använts för att beräkna de stabila Pb-föreningarna i förbränningsförhållanden. I detta arbete inkluderades data för $KPbCl_3$ (g) i de termodynamiska jämviktsberäkningarna för att undersöka om detta påverkar $PbCl_2$-stabiliteten. Beräkningarna antyder att $KPbCl_3$ (g) är stabilt mellan 400 och 900 °C. Det mesta av Pb är enligt de termodynamiska jämviktsberäkningarna fortfarande i form av $PbCl_2$ inom detta temperaturområdet. Mellan de sekundära och tertiära luftnivåerna beräknas Pb förekomma huvudsakligen som PbO (g). Beräkningarna antyder att KPb_2Cl_5 (s) är stabilt nedan 285 °C och K_2PbCl_4 mellan 285 °C and 365 °C vilka är typiska eldstadstemperaturer. Den beräknade högsta kondensationstemperaturen för $PbCl_2$ är ca 440 °C.

I laboratorie-experimenten, observerades $PbCl_2$ reagera med KCl under bildning av KPb_2Cl_5 och K_2PbCl_4. Dessutom noterades reaktioner med Na_2SO_4 och K_2SO_4 under bildning av $Na_3Pb_2(SO_4)_3Cl$ respektive $K_3Pb_2(SO_4)_3Cl$. Ingen fast fas reaktion mellan $PbCl_2$ och NaCl observerades.

Det mesta av rapporterade korrosionsfall i denna avhandling uppstod under den första smält-temperaturen för saltblandningen. Resultaten från detta arbete understöder att korrosionen fortskrider via $FeCl_2$-bildning med Fe-baserade stål. $FeCl_2$ bildades i försök i både full- och laboratorieskala under K-Pb-Cl blandningar. En solidusprojektion för $PbCl_2$-KCl-$FeCl_2$ -systemet beräknades för att undersöka om korrosionen som uppstår vid låga temperaturer kan förklaras av bildandet av en eutektisk smälta mellan saltblandningen och $FeCl_2$. De beräknade smältemperaturerna varierade mellan 312 °C och 334 °C beroende på sammansättningen. Korrosionstest med en blandning av $FeCl_2$-$PbCl_2$-KCl visade att dessa föreningarna kan bilda en smälta eller sintrade partiklar tillsammans redan vid 300 °C. Pb-haltiga beläggningar som kommer i kontakt med stålet initierar korrosionsreaktionen. För att initiera korrosionen, behövs ingen smältfas. I

det andra steget när korrosionen fortskrider kan $FeCl_2$ bilda en lokal smälta tillsammans med Pb-haltiga partiklar.

I laboratorie-experimenten ingen korrosion noterades med kolstål under $PbCl_2$-innehållande saltblandningar vid 200 °C. Tröskeltemperaturen för signifikant korrosion med en syntetisk saltblandning som bestod av 5 vikt-% $PbCl_2$ och 95 vikt-% K_2SO_4 var 325 °C för de låglegerade stålen 16Mo3 och 350 °C 10CrMo9-10. Den Ni-baserade legeringen (Alloy 625) korroderade inte i dessa experiment. Den högsta test-temperaturen var 375 °C.

Tiivistelmä

Jäteperäisten polttoaineiden käyttö on lisääntynyt viime vuosikymmenten aikana, mikä johtuu niiden matalasta hinnasta, hyvästä saatavuudesta, CO_2-neutraaliudesta sekä lainsäädännöstä. Eurooppa 2020-strategia velvoittaa korvaamaan fossiilia polttoaineita uusiutuvilla polttoaineilla ja lisäämään uusiutuvien energianlähteiden käyttöä lämmön- ja sähköntuotannossa. Lisäksi poltettavan jätteen kaatopaikkasijoitusta on rajoitettu lainsäädännössä. Yksi fossiilisten polttoaineiden korvaavista vaihtoehdoista on kierrätyspuu. Kierrätyspuu on tyypillisesti peräisin useista eri lähteistä, mikä tekee kierrätyspuun koostumuksesta hyvin heterogeenisen. Se voi sisältää esimerkiksi rakennus-, purku- ja remontointijätteitä sekä huonekaluja ja pakkausmateriaaleja. Tämän tyyppinen jätepuu on usein käsitelty erilaisilla kemiallisilla pintakäsittelyaineilla, kuten maaleilla ja lakoilla, ja niissä voi olla mekaanisia epäpuhtauksia, kuten muovia ja metallisia komponentteja. Näiden epäpuhtauksien vuoksi kierrätyspuussa voi olla kohonneita lyijy- ja sinkkipitoisuuksia, klooria, natriumia ja kaliumia. Kaikki nämä alkuaineet vaikuttavat korroosioon ja likaantumiseen polton aikana, jotka puolestaan laskevat kattilan tehokkuutta.

Korroosio on yleensä höyryn arvoja rajoittava päätekijä. Käsittelemättömän luonnonpuun poltossa voi muodostua alkalikloridеja, jotka voivat aiheuttaa korroosiota tulistinalueella, jossa materiaalilämpötila ylittää 450 °C. Kierrätyspuuta poltettaessa alkalikloridit yhdessä raskasmetallien kanssa aiheuttavat korroosiota jo paljon alhaisemmissa lämpötiloissa kuin luonnonpuuta poltettaessa. Käytännössä tämä tarkoittaa, että korroosiota voi esiintyä tulipesän seinissä, matalamman lämpötilan tulistimissa sekä syöttöveden esilämmittimissä. Lyijy ja sinkki tunnetusti laskevat kerrostuman sulamispistettä ja yhdessä alkalikloridien kanssa voivat muodostaa kerrostuman, jonka sulamispiste voi olla lähes 200 °C. Matalalla sulavat yhdisteet edistävät sulafaasikorroosiota, jonka tiedetään aiheuttavan suuria korroosionopeuksia.

Korroosioilmiöiden ymmärtäminen on avain optimaaliseen kattilasuunnitteluun. Tässä työssä tutkittiin lyijyn roolia ja korrosiivisuutta kierrätyspuupolton aikana. Täyden mittakaavan mittauksia tehtiin leijukattiloissa, joiden polttoaineena käytetään kierrätyspuuta. Näistä saatuja tuloksia hyödynnettiin laboratoriomittakaavan korroosiouunikokeissa. Termodynaamista tasapainolaskentaa käytettiin apuna ennustamaan lyijyä sisältävien yhdisteiden stabiilisuutta.

Pienhiukkasmittaukset leijukattilan tulipesässä osoittivat, että yli 70 % lyijystä on sitoutuneena klooriin. Pitoisuus oli suurimmillaan sekundääri- ja tertiääri-ilmatasojen välissä. Lyijyä löydettiin sekä pitkän että lyhyen ajan kerrostumista yhdisteinä, joissa on mukana kaliumia ja klooria; KPb_2Cl_5 ja K_2PbCl_4. Sinkkiä ei havaittu pitkän ajan kerrostumista. Lyijyä ei löydetty jäähdyttämättömästä kerrostumanäytteestä, mikä indikoi, että lyijyä sisältävät yhdisteet kerrostuvat kondensoitumalla. Korroosionopeuksissa havaittiin suuria eroja (0.8 mm/vuosi vs. 0.4 mm/vuosi) kuuman (800 °C) ja kylmemmän (490 °C) savukaasulämpötilan välillä huolimatta siitä, että materiaalilämpötila oli molemmissa alueissa sama (360 °C).

Kiinteät yhdisteet KPb_2Cl_5 ja K_2PbCl_4 voivat muodostua lyijykloridin ja kaliumkloridin (s, l, g) reagoidessa keskenään tai kaasumaisen välituotteen $KPbCl_3$ kautta. $KPbCl_3$ (g) -yhdiste lisättiin termodynaamiseen tietokantaan, jotta nähtäisiin, vaikuttaako sen muodostuminen lyijykloridin stabiilisuuteen. Laskennat osoittivat, että $KPbCl_3$ (g) on stabiili lämpötila-alueella 400-900 °C. Suurin osa lyijystä on kuitenkin edelleen lyijykloridina tällä lämpötila-alueella. Termodynaamiset laskennat ennustavat suurimman osan lyijystä muodostavan kaasumaista lyijyoksidia sekundääri- ja tertiääri-ilmatasojen välissä. Kiinteä KPb_2Cl_5 on termodynaamisten laskentojen mukaan stabiili 285 °C:seen asti. Kiinteä K_2PbCl_4 on puolestaan stabiili lämpötila-alueella 285-365 °C, jotka ovat tyypillisiä tulipesän seinien lämpötiloja. Laskennat ennustavat lyijykloridin korkeimman kondensoitumislämpötilan olevan noin 440 °C.

Laboratoriomittakaavan korroosiouunikokeissa lyijykloridin havaittiin reagoivan kaliumkloridia sisältävien kerrostumien kanssa ja muodostavan KPb_2Cl_5- ja K_2PbCl_4-yhdisteitä. Tämän lisäksi lyijykloridin havaittiin reagoivan alkalisulfaattien Na_2SO_4 ja K_2SO_4 kanssa ja muodostavan vastaavasti $Na_3Pb_2(SO_4)_3Cl$- ja $K_3Pb_2(SO_4)_3Cl$-yhdisteitä. Kiinteä-kiinteä-reaktiota ei kuitenkaan havaittu lyijykloridin ja natriumkloridin välillä.

Suurin osa tässä työssä tehdyistä korroosiohavainnoista tapahtuivat alle kerrostuman ensisulamispisteen. Rautakloridia havaittiin muodostuvan korroosiotuotteena sekä täyden mittakaavan että laboratoriomittakaavan testeissä K-Pb-Cl yhdisteitä sisältävien kerrostumien alla rautapohjaisilla teräksillä. $PbCl_2$-KCl-$FeCl_2$-yhdistelmälle määritettiin faasidiagrammi, jotta voitaisiin selvittää, johtuuko suuret korroosionopeudet matalissa lämpötiloissa eutektisen sulan muodostumisesta rautakloridin ja kerrostuman välillä. Sulamislämpötilat yhdistelmälle vaihtelivat välillä 312-334 °C seoksen koostumuksesta riippuen. Korroosiotestit $FeCl_2$-$PbCl_2$-KCl-suolaseoksella osoittivat, että kyseiset komponentit voivat reagoida

keskenään ja muodostaa sulaa tai sintraantuneita partikkeleita jo 300 °C:n lämpötilassa. Lyijykloridia sisältävät kerrostumat, jotka pääsevät kosketuksiin teräksen pinnan kanssa, aikaansaavat korroosioreaktion. Korroosioreaktion alkamiseksi ei tarvita välttämättä sulafaasin läsnäoloa. Korroosioreaktion jatkuessa muodostunut rautakloridi voi muodostaa paikallisia sula-alueita lyijyä sisältävien partikkeleiden kanssa.

Laboratoriomittakaavan testeissä hiiliteräksellä havaittiin korroosiota 300 °C:ssa ja sen yläpuolella erilaisilla lyijykloridia sisältävillä suolaseoksilla. Korroosiota ei havaittu alle 200 °C:n testilämpötilassa. Korroosion alkamislämpötiloja eri teräksillä testattiin synteettisellä suolaseoksella, joka sisälsi 5 paino-% lyijykloridia ja 95 paino-% kaliumsulfaattia. Matalaseosteisen teräksen 16Mo3 korroosion alkamislämpötila oli 325 °C ja 10CrMo9-10-teräksen 350 °C. Nikkelipohjainen teräs Alloy 625 ei korrodoitunut korkeimmassakaan testilämpötilassa, joka oli 375 °C.

List of publications and contributions of the author

This thesis is based on the work contained in the following papers:

Paper I

The influence of flue gas temperature on lead chloride induced high temperature corrosion. Fuel (2017), 1-11, doi: 10.1016/j.fuel.2017.01.082.

Hanna Kinnunen, Merja Hedman, Markus Engblom, Daniel Lindberg, Mikko Uusitalo, Sonja Enestam, Patrik Yrjas

Kinnunen planned and prepared the probe measurements and performed the wall thickness measurements of the corrosion probe rings. SEM/EDX analyses were performed by Kinnunen together with laboratory personnel. Engblom calculated the intra-deposit temperature gradients and Lindberg calculated the solidus projection of the system $PbCl_2$-KCl-NaCl. The results were evaluated by Kinnunen in co-operation with the other authors. Kinnunen was the corresponding author of the paper.

Paper II

High-temperature corrosion due to lead chloride mixtures simulating fireside deposits in boilers firing recycled wood. Fuel Processing Technology (2017), 306-313, doi: 10.1016/j.fuproc.2017.07.017.

Hanna Kinnunen, Daniel Lindberg, Tor Laurén, Mikko Uusitalo, Dorota Bankiewicz, Sonja Enestam, Patrik Yrjas

Kinnunen planned the corrosion measurement tests. SEM/EDX analyses were performed by Kinnunen together with laboratory personnel. Lindberg calculated the solidus projection for the $FeCl_2$-KCl-$PbCl_2$ system. Interpretation of the results was done by Kinnunen together with the other authors. Kinnunen was the main author of the paper.

Paper III

Interactions of $PbCl_2$ with alkali salts in ash deposits and effects on boiler corrosion. Energy & Fuels (2018), 8519-8529,
doi: 10.1021/acs.energyfuels.8b01722.

Jonne Niemi, Hanna Kinnunen, Daniel Lindberg, Sonja Enestam

The corrosion measurements were planned by Kinnunen and Niemi. Niemi performed the experimental part of the laboratory measurement and Kinnunen made the analyses of the boiler deposit. Evaluation of the results was performed by Niemi and Kinnunen together with the other authors.

Kinnunen and Niemi focused on the corrosion and deposit chemistry, respectively. Niemi was the corresponding author of the paper.

Paper IV

Corrosion in recycled wood combustion – reasons, consequences and solutions. Energy & Fuels (2019), doi: 10.1021/acs.energyfuels.8b04168.

Hanna Kinnunen, Merja Hedman, Daniel Lindberg, Sonja Enestam, Patrik Yrjas

Kinnunen planned the corrosion oven measurements and thermodynamic calculations. SEM/EDX analyses were performed by Kinnunen together with laboratory personnel. Interpretation of the corrosion measurement was performed by Kinnunen. Lindberg performed the thermodynamic calculations. Fine particle measurements were carried out by Technical Research Centre of Finland (VTT). Interpretation of the fine particle results was done by Kinnunen and Hedman. Kinnunen was the main author of the paper.

Paper V

Corrosion of carbon steel underneath a lead/potassium chloride salt mixture. Materials & Corrosion (2019), doi: 10.1002/maco.201810650.

Annika Talus, Hanna Kinnunen, Rikard Norling, Sonja Enestam

Kinnunen planned the corrosion measurement matrix in co-operation with Talus. The experimental part and analyses were carried out by Talus and Kinnunen. Talus was the main author of the paper.

Related publications not included in the thesis:

VI Influence of the deposit CO_3/SO_4 ratio on superheater corrosion. International chemical recovery conference (2014) Tampere, Finland. Conference proceedings.
Hanna Kinnunen, Dorota Bankiewicz, Daniel Lindberg, Sonja Enestam, Kari Haaga, Mikko Hupa

VII Erosive wear of boiler steels by sand and ash. Wear (2014), 213-224, doi: 10.1016/j.wear.2014.06.007.
Elina Huttunen-Saarivirta, Hanna Kinnunen, Johanna Tuiremo, Mikko Uusitalo, Maksim Antonov

VIII Corrosivity of lead chloride containing salt mixtures. 22nd International Conference on Fluidized Bed Combustion (2015) Turku, Finland. Conference proceedings.
Hanna Kinnunen, Dorota Bankiewicz, Merja Hedman, Mikko Uusitalo, Sonja Enestam

IX Boiler atmosphere profile with focus on heavy metal behaviour in a full-scale recovered fuel-fired CFB boiler. The 22nd International Conference on Fluidized Bed Combustion (2015) Turku, Finland. Conference proceedings.
Merja Hedman, Sonja Enestam, Hanna Kinnunen, Niklas Engblom, Juha Roppo

X Corrosivity of lead chloride containing salt mixtures – characterization of corrosion products. Nordic Flame Days (2015), Copenhagen, Denmark. Conference proceedings.
Hanna Kinnunen, Dorota Bankiewicz, Kristina Hellström, Mikko Uusitalo, Sonja Enestam

XI High temperature corrosion due to lead chloride mixed with potassium sulphate. The 26th International Conference on Impacts of Fuel Quality on Power Production (2016), Prague, Czech Republic. Conference proceedings.
Hanna Kinnunen, Dorota Bankiewicz, Sonja Enestam, Patrik Yrjas

XII Presence and behaviour of lead in a full-scale waste wood fired BFB-boiler. Nordic Flame Days (2017), Stockholm, Sweden. Conference proceedings.
Merja Hedman, Hanna Kinnunen, Niklas Engblom, Sonja Enestam

List of abbreviations

ACZA	ammoniacal copper zinc arsenate
BFB	bubbling fluidised bed
BHF	bag-house filter
BSE	backscatter electron
CCA	chromated copper arsenate
CFB	circulated fluidised bed
dp	fine-mode cut size
DLPI	Dekati Ltd. -type low-pressure mass impactor
DSC/TGA	Differential scanning calorimetry/thermogravimetric analyses
ELPI	electrical low-pressure impactor
ESP	electrostatic precipitator
FB	fluidised bed
IC	ion chromatography
ICP-MS	inductively coupled plasma mass spectrometer
MSW	municipal solid waste
OW	overlay welding
PCP	pentachlorophenol
PVC	polyvinyl chloride
SCR	selective catalytic reduction
SEM/EDX	Scanning Electron Microscope/Energy Dispersive X-ray
SH	superheater
SNCR	selective non-catalytic reduction
SRF	solid recovered fuel
T_0	first melting temperature
T_{100}	complete melting point
XRD	X-ray diffraction

Table of contents

1. Introduction

In the evolution of cleaner energy production, fossil fuels are being replaced by various renewable energy sources. Biomass has been used for decades to produce heat and electricity and also in the production of transport fuels. Use of bioenergy helps to reduce greenhouse gas emissions by providing an option for carbon dioxide (CO_2)-neutral power production. As the regulations for landfilling are getting stricter and the concept of a circular economy has become more familiar, the use of different waste fuel fractions has increased in the power production field. The share of renewable energy has been increasing in the European Union (EU) over the last 15 years, as shown in Figure 1 [1, 2]; its utilisation is expected to grow even further due to the Europe 2020 strategy. The strategy states that 20 % of total energy consumption must be produced by renewable sources by 2020 and increase to 27 % by 2030; the 2030 figure was recently proposed to be increased to 32 % [3, 4]. Individual renewable energy targets have been set for each European country. For example, in Finland the target level of 38 % was already achieved by 2014 (38.7 %) [2]. Since then, the level has remained approximately the same. Based on the estimation, the level in Finland in 2018 was 37 % [5]. Sweden has also already achieved its target value; more than half of its energy (53.8 %) was coming from renewable sources in 2016 [2, 4, 6].

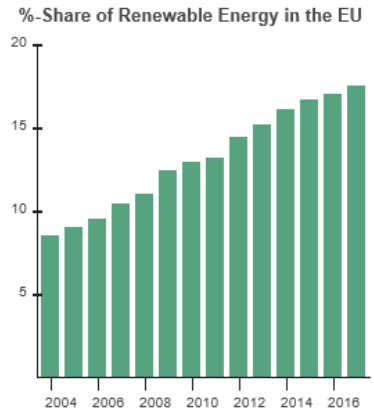

Figure 1. Percental share of renewable energy in the EU from 2004 to 2016. The figure is adapted from [1].

In the past, incineration was seen as a disposal method for different waste fractions. Currently, wastes are seen as potential fuels to replace fossil fuels. This has decreased the treatment costs of the wastes and increased the external transportation of waste-derived fuels. Recycled wood is one

example of the waste fractions utilised in power production. For example, Sweden imported 2.1 million tons of waste in 2013 to be utilised as an energy source; 85 % of the provided waste was recycled wood and municipal waste [7]. Another country utilising and producing a great deal of recycled wood is the UK. In 2017, 1.7 million tons of recycled wood were utilised in biomass power plants and about 300 000 tons were exported [8]. Besides offering green energy benefits, recycled wood is also a cheaper fuel compared to other biomass fuels. According to the Swedish Energy Agency, the price of recycled wood is about half the price of wood chips, Figure 2 [9].

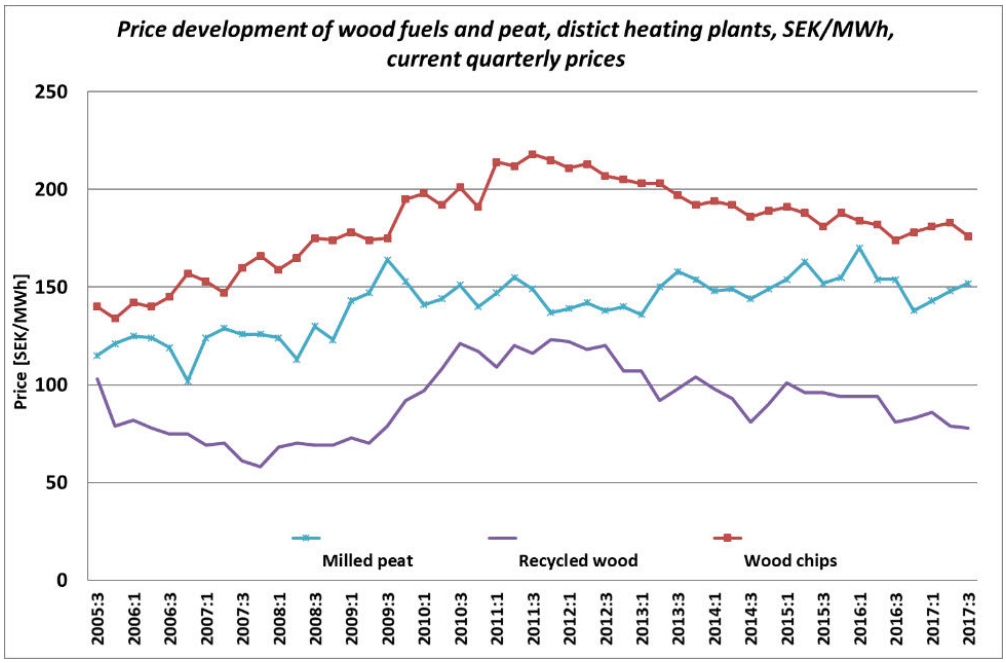

Figure 2. Price development of peat, recycled wood and wood chips in Sweden. 100 SEK equals roughly 10 euro. The figure is adapted from [9].

Recycled wood typically comprises different wood fractions from sources such as construction, demolition and refurbishment works, and may include furniture and packaging materials such as wood pallets [10-12]. This kind of wood waste may contain different chemical contaminants, such as paints, lacquer and siccatives. It can also be contaminated with mechanical contaminants such as plastics and metallic components. Thus, recycled wood typically includes elevated concentrations of heavy metals, such as lead (Pb), zinc (Zn) and chlorine (Cl), as well as alkali metals, such as sodium (Na) and potassium (K).

During combustion of alkali- and Cl-containing fuels, alkali chlorides may form; these are known to increase the corrosion risk on low-alloy steel superheaters where surface temperatures exceed 450 °C [13, 14]. Corrosion is usually the main limiting factor for higher steam parameters. Alkali chloride-induced corrosion has been widely studied; there are now effective solutions against this type of corrosion. The use of highly alloyed steels, sulphur (S)-based additives, co-combustion with high S-containing fuels, and superheater placement are the most commonly-known solutions. Superheaters can be located after the empty pass where the flue gas temperature is already reduced. In the case of a circulated fluidised bed (CFB) boiler, the hottest superheater can be placed in the loop seal, where the amount of corrosive chlorides is lower compared to the furnace or convective pass after the cyclone.

In waste fuel firing, alkali chlorides are present in combination with elevated heavy metal concentrations, and the corrosion starting temperature can be as low as 250-300 °C [15]. In practice, this means that corrosion issues may be present in furnace walls, low-temperature superheaters and economisers in the power boilers. Lack of a detailed understanding of corrosion phenomena and corrosion-preventing actions, may lead to unexpected and costly shutdowns. In waste-to-energy plants, over 70 % of the shutdowns are related to high-temperature corrosion issues [16]. It has been estimated that corrosion-related maintenance costs can constitute one-third of the annual maintenance budget and can be as high as 10 % of the annual turnover [16].

In the last decade, as the use of waste-based fuels has been increasing, there has been a focus on heavy metal-induced corrosion in order to understand the corrosion phenomena during waste fuel combustion [17-21]. Corrosivity and corrosion mechanisms of heavy metals including deposits have been studied by means of thermodynamic calculations and field studies with different material candidates to protect the most vulnerable areas of the boiler. However, many of the corrosion tests have been carried out in rather high material temperatures (≥ 400 °C), although corrosion problems are seen on the heat transfer surfaces at considerably lower temperatures. Zn has been studied to a higher extent than Pb; the role of Pb is not yet fully understood. Pb combined with K and Cl has been found in boiler deposits, and the formation of KPb_2Cl_5 and K_2PbCl_4 compounds have been predicted with thermodynamic calculations [19]. However, the formation mechanisms of such compounds and their impacts on corrosion are not known.

1.1. Objectives and approach

The focus of this work was determined to be the presence, behaviour and corrosivity of Pb in fluidised bed (FB) boilers during recycled wood combustion as there were open questions related to the corrosion mechanism, critical temperature areas and form and presence of heavy metals in different parts of the boiler. The experimental work was performed with the use of full- and laboratory-scale measurements in different environments and temperatures. The effect of flue gas temperature on corrosion and deposit composition was studied in a CFB boiler firing recycled wood (**Paper I**). Long-term corrosion probe measurements and short-term deposit probe measurements were carried out. As Pb was present in larger shares than Zn in the deposits, the overall focus was set more to the role of Pb. The formation and corrosivity of KPb_2Cl_5 and K_2PbCl_4 compounds were studied in the laboratory (**Papers II, III, IV, V**). An isothermal corrosion test method was used to examine the corrosivity and corrosion threshold temperature of K-Pb-Cl including compounds. The novel gradient test method was used to study the interactions of $PbCl_2$ within the deposit containing other possible compounds present in full-scale boiler deposits (**Paper III**). Corrosion was shown to occur at temperatures below the deposit's first melting point. The role of iron (Fe) in corrosion reactions was studied in more detail as it could explain the increased corrosion (**Papers IV and V**). The presence and form of heavy metals in fine particles was studied in a recycled wood firing bubbling fluidised bed (BFB) boiler (**Paper IV**). The results gained from the full- and laboratory-scale tests were further used in thermodynamic calculations. The calculations were done in order to study stability of Pb-including compounds in gas phase and within deposits (**Paper IV**). The results and understanding gained from this work are to be used in boiler design when challenging Pb-containing fuels are under consideration.

2. Background

The most commonly-used combustion technologies for recycled wood are FB- and grate-firing, which are presented in this chapter. Recycled wood, as a fuel for power production, is discussed further in Chapter 2.2. Typical composition and sources of harmful elements, such as Pb, Zn and Cl are presented. Ash formation and deposition are described in Chapter 2.3. Due to the elevated concentrations of heavy metals and Cl in recycled wood, corrosion is one of the major operational challenges, which limits the final steam parameters. The current understanding of corrosion caused by heavy metal chlorides is summarised in Chapter 2.4. Finally, an overview of the most commonly-used materials in boilers is given in Chapter 2.5.

2.1. Combustion technologies

The two main technologies in current power production using challenging fuels are FB- and grate-firing boilers. Grate-firing is the oldest combustion technology and is still widely used, for example in waste combustion. One advantage of grate-firing is the ability to handle different fuel particle sizes without costly fuel pre-treatment. FB technology has become a competitive option alongside grate-firing technology due to FB's ability to handle high moisture-containing fuels; in addition, they have better response to load changes in combined heat and power plants. FB boilers enable efficient and environmentally-friendly use of a large variety of challenging fuels, such as biomass, sludges and different waste-derived fuels. The main emphasis of this thesis is on FB technology, since all the full-scale studies were carried out in either a BFB or a CFB boiler. In addition, FB technology has a high development potential due to a combined load and fuel flexibility. However, the results generated from the field tests and laboratory corrosion tests may also be adapted to grate-firing. All FB boiler data presented in this chapter originate from the company that the author represents.

2.1.1. Bubbling fluidised bed boiler

One of the first industrial BFB boilers for biomass combustion was delivered to the Finnish pulp and paper industry in 1982 to combust sludge and bark residues not suitable for grate-firing. The development of the BFB boilers grew rapidly in terms of size; within 15 years the boiler capacity reached today's level, 200-300 MW_{th}. The dimensions of the boiler and the steam parameters are defined based on the fuel or fuel mixture composition,

moisture content and heating value. In the 1990s, different recycled fuel fractions were introduced as a part of the fuel palette; since then, the share of these types of fuels has increased. Nowadays, combustion of 100 % recycled wood is no longer an exception.

BFB boiler uses the principle of natural water circulation based on different densities of water and steam. Boiler feed water is heated in the economisers from which it goes to the steam drum. The drum separates the water, which continues as boiler water to the bottom part of the boiler through downcomers. Water is heated along the furnace walls and turns into steam as the temperature increases in the upper part of the furnace. The produced steam-water mixture is led to the steam drum, where the steam is separated from the water and the steam continues to the superheaters. Steam could also be led to convective pass walls or to the roof if they are part of the superheating surfaces. The water-steam circulation is presented in Figure 3. The pressure parts of a BFB boiler consist of the furnace, steam drum, superheaters, economisers and in some boilers, boiler bank. The boiler bank absorbs heat from the flue gas between economisers and superheaters and reduces steaming in the economiser sections. It is typically used with high heating value fuels to increase the boiler efficiency. Air preheaters are used in some boilers to preheat the combustion air.

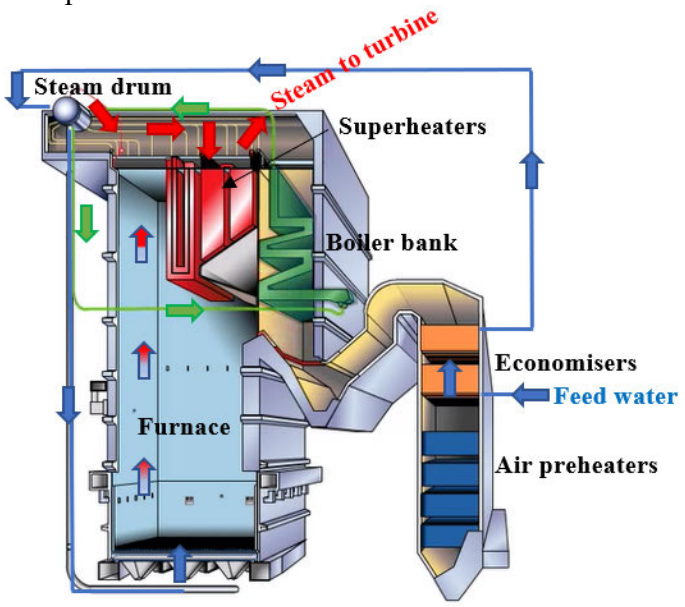

Figure 3. Water-steam circulation and main components in a BFB boiler. Blue arrows indicate water circulation, red arrows steam circulation and green arrows indicate boiler bank water-steam circulation.

Bottom part of the furnace, reducing zone $\lambda < 1$

Solid fuel or a fuel mixture is fed into the furnace through fuel feeding conveyors and fuel chutes either by the side walls or by the front wall. Primary air can be used to improve fuel feeding and to reduce the conveyor temperature. The primary air is blown through the bottom of the furnace, which makes the bed fluidised and the material starts to bubble. The stage of the fluidisation can be stationary, bubbling, turbulent or circulating depending on the fluidising gas velocity and particle size. In the case of a BFB boiler, the bed material average particle size is 1 mm and velocity around 1 m/s. The bottom part of the boiler is called the dense bed area, above which there is a splash zone that reaches to about 2 m above the bed. Combustion occurs in the lower part of the furnace. The bed temperature is typically 800-900 °C, but lower bed temperatures (650-750 °C) can be used when combusting fuels with a high bed agglomeration tendency. The bed temperature can be controlled by a recirculation gas system, which has a significant cooling effect as it decreases the stoichiometric ratio of the combustion reactions in the bed area. The bed temperature also depends on the fuel properties, such as moisture content. Atmosphere at the bottom of the furnace is reducing (air-to-fuel ratio, λ=0.4), meaning that there is a lack of oxygen to achieve complete combustion.

Sand particles that are too big to fluidise accumulate at the bottom of the furnace, and too-small particles escape to the upper furnace as a part of the fly ash. Efficient bed material removal is needed as bed material becomes coarser during combustion. Bigger particles, such as stones, over-sized sand and impurities of the fuel will be removed through the furnace bottom as bottom ash. The lower part of the furnace is covered with a refractory lining to protect the tube materials from erosion, to reduce heat transfer to the walls and to minimise heat losses from the bed. Silica sand is commonly used as the bed material, but in the case of high alkali-containing fuels inert, quartz-free bed material, diabase, or kaolin-additive ($Al_2Si_2O_5(OH)_4$) can be used to prevent the formation of low melting alkali silicates. The lower part of the furnace is typically refractory covered during biomass combustion.

Upper part of the furnace, oxidising zone $\lambda \geq 1$

Secondary and tertiary airs are used to complete the combustion. The area above the secondary air level is called the freeboard area. The atmosphere is changing towards the oxidising side and the air-to-fuel ratio is around 1 at the secondary air level. Combustion is completed after the final air inlet and the air-to-fuel ratio increases to around 1.2, meaning that there is already

excess amount of oxygen in the flue gas. After the secondary air level, the flue gas temperature is about 1000-1200 °C. Tertiary air is used to complete combustion when low nitrogen oxide (NO_x) emissions are required.

Superheaters

The saturated steam from the steam drum is heated up in several stages in the superheaters: primary, secondary, tertiary and sometimes quaternary superheaters. Steam is said to be superheated when its temperature is higher than the vaporisation temperature. In the superheater area, steam absorbs heat from the flue gases. Superheaters can be located in the upper part of the furnace (radiative, vertical superheaters) or in the second pass (convective, horizontal superheaters). In some boiler designs, a nose arch protects vertical superheaters from the furnace radiation. Superheater steam flow direction in comparison with flue gas direction can be either co-current or counter-current. Counter-current is usually more beneficial from the heat transfer perspective as hot flue gas faces the coldest steam temperature. Sootblowers are used to clean the superheater and economiser areas to maintain good heat transfer. Empty pass can be designed for boilers firing fuels with elevated risk of fouling and corrosion. The idea behind the empty pass is to cool down the flue gases in order to reduce the amount of corrosive chlorides in the gas phase before they reach the superheaters. The flue gas temperature before the empty pass is typically 850 °C and after the empty pass about 650 °C. A sideview of a BFB boiler designed for recycled wood fuel is presented in Figure 4.

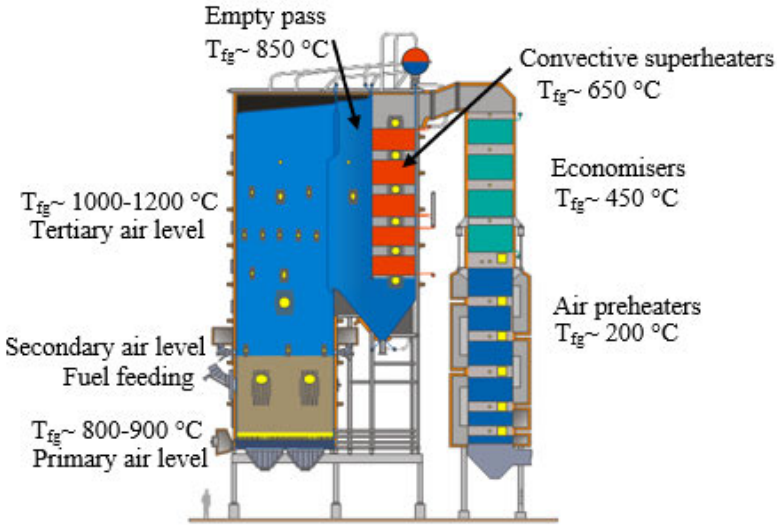

Figure 4. Sideview of a BFB boiler designed for recycled wood fuel with main features and temperatures described. Superheaters are located after the empty pass to reduce the amount of gaseous corrosive chlorides in the vicinity of the tube surfaces.

Emission control

Produced flue gases are cleaned with flue gas cleaning systems and the fly ash formed is usually collected and removed with a bag-house filter (BHF) or an electrostatic precipitator (ESP). Primary harmful emissions, NO_x, sulphur dioxide (SO_2) and carbon monoxide (CO), can be controlled through the air staging system, air ratio and furnace temperatures. Naturally, the fuel mixture can also be optimised, according to availability, to minimise the emissions. NO_x emissions can be efficiently reduced by tertiary air feeding or as a secondary option by ammonia/urea injection (selective non-catalytic reduction, SNCR) or by the use of catalysts (selective catalytic reduction, SCR). SNCR is located in the upper part of the furnace and catalysts at the end of the flue gas channel. If both of the systems are used, it is called a slip catalyst. The SO_2 level is reduced when fuel S-content is reduced or by self-reduction by elements in the ash-forming matter, such as K, Na, and calcium (Ca). Limestone ($CaCO_3$) injection to the freeboard can be used to reduce SO_2 emissions, or optionally feeding hydrated lime ($Ca(OH)_2$) to BHF. $CaCO_3$ decomposes in the furnace to calcium oxide (CaO) and CO_2. Formed CaO further reacts with SO_2 and forms calcium sulphate ($CaSO_4$). Ca also occurs naturally in the biomass, as organically-bonded and as crystalline salt particles. The organic part of the Ca produces CaO during combustion [22].

2.1.2. Circulating fluidised bed boiler

CFB technology has become one of the main combustion technologies for coal, biomass and waste fractions, especially in industrial and municipal power plants. Just like BFB boilers, CFB boilers are easily able to combust a wide fuel palette. The size of the boilers has increased incrementally, starting from heating plants of few MW_{th} up to utilities in the 600 MW_e class.

Steam-water cycles of CFB boilers are most often based on a natural circulation, even though once-through designs are available for the utility boiler market. In a typical boiler with natural circulation, feedwater passes through the economisers to the steam drum. The steam leaving the boiler is replaced with the corresponding amount of feedwater. Boiler water from the steam drum flows through downcomers to the furnace bottom, loop seal and in some boiler designs, to the boiler bank. A boiler bank is used for cases in which the economisers and superheaters are not cooling down enough flue gases to avoid major heat losses, for example in cases with high moisture fuels. As the water heats up with increasing temperature, it flows upwards through the furnace and cyclone walls back to the steam drum. As in the case of BFB boilers, the steam is led from the steam drum to the superheaters. The pressure parts of a CFB boiler consist of a furnace, cyclone, loop seal, second pass, steam drum, superheaters and economisers. The furnace, cyclone and loop seal are often referred to as a hot loop. In CFB boilers as compared to BFB boilers, used fluidisation velocity is higher (3-5 m/s) and bed material size smaller (0.1-0.6 mm) to enable sand circulation. Circulating solid material in the hot loop ensures even temperature profiles, good mixing and effective heat transfer. A solid bed material consists of sand, fuel ash and in some cases S-capturing additives and related reaction products (e.g., limestone and $CaSO_4$).

Furnace

As in BFB boilers, CFB combustion is ensured through primary and secondary air feedings. Primary air is fed through the nozzles from the bottom of the furnace. Primary air keeps the bed in the fluidising stage and ensures stable combustion, whereas secondary air finalises the combustion. Lower secondary air is fed from the fuel feeding level and upper secondary air is fed from approximately two meters above the lower air feeding. The air-to-fuel ratio in the bottom of the furnace is commonly 0.6 and 1.2 in the upper part of the furnace after the lower and upper secondary air inlets. The furnace temperature is about 850-900 °C during high load combustion. The temperature of the bed can be controlled with recirculation gas. In contrast

to the BFB boiler, the heat is evenly distributed through the whole furnace, so no large temperature variations occur at different heights of the furnace. In the case of high agglomeration tendency fuels, additives such as kaolin or quartz-free bed material are used rather than lowering the furnace temperature. The furnace walls are made of membrane tubes that are typically at least partly covered with refractory lining to reduce erosion and corrosion problems.

Cyclone and loop seal

The purpose of the cyclone is to separate solid particles from the flue gas flow based on centrifugal forces. Bigger particles are circulated back to the furnace through the loop seal. Flue gases and smaller particles are led to a vortex finder due to increased gas velocity, and further to a manifold duct and to a superheater pass. The vortex finder is an uncooled component. Cyclone efficiency determines the particle size of the circulating material; typically, particles over 100 μm are recycled back to the furnace. High particle velocities induce high erosion risk, and thus the cyclone membrane structure is covered with refractory lining. The cyclone can be either cooled or non-cooled. However, non-cooled cyclones are prone to suffer from significant mechanical problems; as a result most cyclones are currently water- or steam-cooled. The temperature of the flue gas entering and exiting the cyclone is typically a little lower than in the lower part of the furnace (< 900 °C).

Circulated solid particles from the cyclone are lead to the loop seal, which returns the particles back to the lower furnace. The loop seal is part of the same cooling circulation system as the cyclone and has a membrane wall construction. It has its own fluidising air system to ensure continuous operation and to prevent sand accumulation and further sintering. Schematic pictures of both a cyclone and a loop seal are presented in Figure 5.

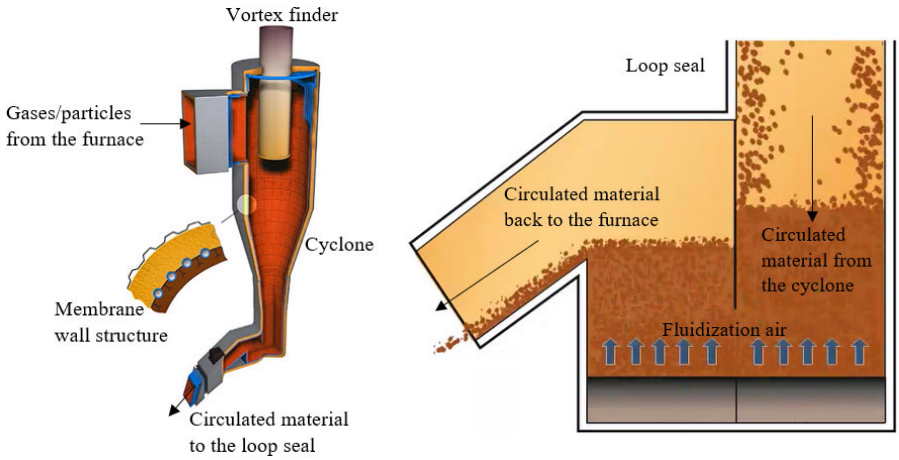

Figure 5. Schematic pictures of a cyclone (on the left) and a loop seal (on the right).

Superheaters

The steam coming from the drum is led to the primary, secondary and tertiary superheaters. Superheaters can be located in the furnace as a wing wall superheater, in the convective pass after the cyclone or in the loop seal. Wing wall superheaters are used with fuels with good heating value, typically in coal firing boilers. The hottest superheater can be located in the loop seal in the case of high Cl-containing fuels. A picture of a CFB boiler designed for waste fuel firing is presented in Figure 6.

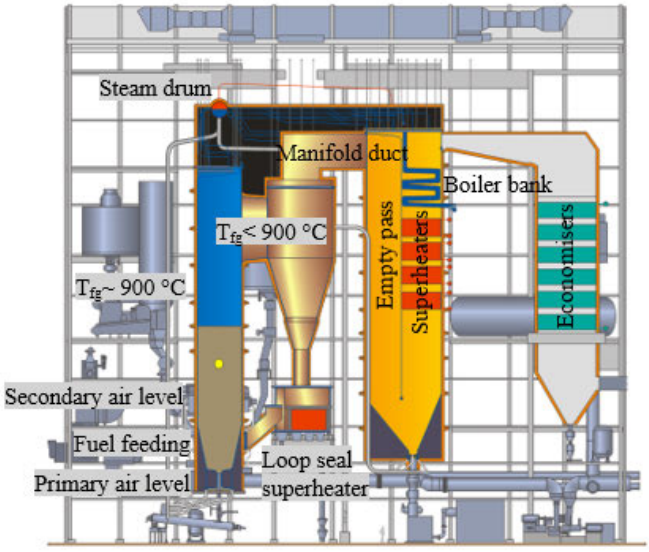

Figure 6. Sideview of a CFB boiler designed for waste fuels. The hottest superheater is located in the loop seal and other superheaters after the empty pass to avoid chloride-induced corrosion.

Emission control

The same principles for reducing primary emissions and flue gas cleaning apply to CFB boilers as those described in the BFB boiler chapter. Good mixing and effective heat transfer in a CFB boiler offer favourable emission performance and low unburnt losses. NO_x emissions are extremely low compared to the BFB boilers due to a low primary NO_x level which may be further reduced with the use of SNCR and/or SCR. SO_2 reduction by in-furnace self-reduction is more efficient in CFB boilers compared to BFB boilers.

2.1.3. Grate-firing boiler

Grate-firing technology is one of the oldest combustion technologies for waste incineration. It can be used for a wide range of solid fuels, mainly for biomass and waste but also for low quality coals. The boiler sizes currently range between 4 and 300 MW_e although many are on the smaller side [23, 24]. Fuel is fed onto the grate with mechanical stokers. The grate has two main functions: to transport the fuel and to distribute the primary air flow through the grate. Combustion occurs at a temperature of about 1000 °C. Grates can be either air- or water-cooled; the mode depends on the fuel type. For challenging fuels with high moisture content, air-cooled grates are typically used [23]. The amount of bottom ash produced in grate-firing is typically larger compared to fluidised bed combustion.

Grate-types can be divided into four categories depending on their main characteristics: stationary sloping grate, travelling grate, reciprocating grate and vibrating grate [23, 24]. The latter one usually has the highest availability and the lowest maintenance costs; thus, the vibrating water-cooled grate type is the most commonly-used solution. The shaking movement spreads the fuel evenly and improves carbon burnout [24]. The travelling grate literally moves the fuel from one side to the other and combustion occurs during this transportation. The reciprocating grate moves back and forth, which transports the fuel. Both mixing of the fuel and carbon burnout are enhanced. The stationary sloping grate is the only type in which the grate does not move. Fuel is fed to the slope where it burns while sliding downwards. The biggest disadvantages of this type of grate are uncontrolled combustion and fuel avalanche risk [24].

The main benefits with grate-firing boilers are relatively low capital and operational costs. In addition, no fuel pre-treatment is needed. In contrast, emission control is difficult in grate-firing. Incomplete combustion and improper air mixing create challenges for primary emissions control. ESP

and scrubbers can be used to decrease emissions. Agglomeration is not a typical problem in grate-firing boilers. However, they are prone to fouling, slagging and corrosion as are FB boilers. Additives such as aluminium oxide (Al_2O_3), CaO, magnesium oxide (MgO), $CaCO_3 \cdot MgCO_3$ and kaolin can be used to prevent the formation of low-melting ash. S-based additives can also be used to prevent corrosion in the superheater area [23, 24].

2.2. Recycled wood as a fuel

Recycled wood has become an attractive replacement for fossil fuels, due to its low price and ready availability. Many countries are trying to decrease landfilling by increasing recycling; at the same time, energy recovery from wastes is increasing. According to European legislation, waste must primarily be utilised; if not possible, the secondary option is landfilling [25]. In some countries, however, for example in Sweden, landfilling of combustible waste is not allowed at all [12, 26].

Recycled wood goes by several names. Terms such as used wood, waste wood and recovered wood are used in addition to recycled wood [27]. Demolition wood is a term used for one subtype of recycled wood. Recycled wood may derive from several different waste-based sources, such as manufacturing industries, construction and demolition contractors and municipal recycling centers. The amount of possible contaminants in the recycled wood determines whether it will be treated as a biofuel or as waste [27]. It may contain leftover pieces from furniture manufacturing, packaging material and wood pallets [12]. This kind of wood waste contains a variety of chemical contaminants based on the source entity's efforts to extend product service life, prevent physical damages and mitigate pest infestation. In addition, plastics, metals, glass, stones, concrete and soil may be present, which increase the ash content of the fuel, Figure 7 [10, 11, 26]. Impurities not removed in the pre-treatment stage accumulate on the bottom part of the furnace during combustion. The contaminants can be divided into two categories: chemical and mechanical contaminants. Chemical contaminants are permanently adhered and cannot be economically removed from the wood material whereas the amount of mechanical contaminants can be reduced through actions such as sorting [27, 28]. Mechanical treatments such as crushing and sieving followed by fine fraction removal can reduce the concentrations of contaminants in the recycled wood [28].

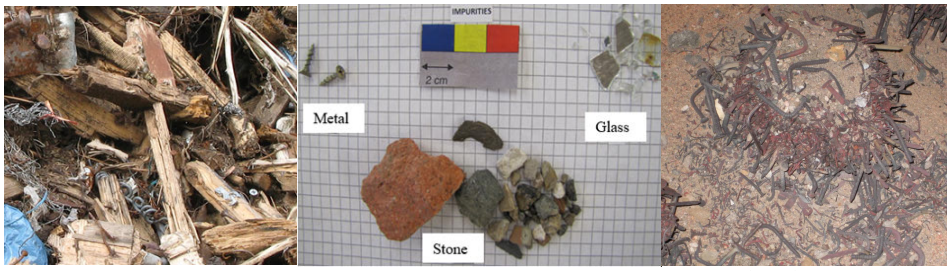

Recycled wood fuel *Impurities of the fuel* *Accumulated impurities at the furnace bottom*

Figure 7. Photo of the recycled wood (on the left) and found impurities such as metal, stones and glass (in the middle). Impurities found on the furnace bottom after a recycled wood firing (on the right).

Recycled wood can be divided into different categories based on levels of contamination. The following categorisation is based on Technical Research Centre of Finland's (VTT) guidelines for the Finnish wood industry in accordance with the European Waste List reported by Alakangas et al. [27]:

Category A • EN ISO 17225-1 Solid biofuels • clean, chemically untreated, non-hazardous wood • residues from forests, parks and gardens and from the wood processing industry • combustion in biomass plants	Category B • EN ISO 17225-1 Solid biofuels • chemically treated, non-hazardous wood • shall not contain halogenated organic compounds (PVC) and preservatives • elemental limits: Cl ≤0.1 wt-%, S ≤0.2 wt-%, N ≤0.9 wt-%, Pb ≤50 mg/kg, Zn ≤200 mg/kg, Hg ≤0.1 mg/kg, Ar + Cr + Cu Σ ≤74 mg/kg • combustion in biomass plants
Category C • EN ISO 15359 Solid recovered fuels • chemically treated wood, such as demolition wood • can be contaminated e.g. with halogenated organic compounds • incineration according to Finnish waste incineration directive	Category D • hazardous waste • includes preservative-treated wood • railway sleepers • can be used as energy only in waste incineration

Categories C and D may include elevated concentrations of corrosion-enhancing elements, such as Pb, Zn and Cl. Elemental composition may vary significantly due to the heterogeneous nature of the recycled wood [11].

The ash-forming matter, the inorganic non-combustible part of the fuel, is composed of organically bound material, dissolved salts, included minerals and contaminants derived from the fuel itself or the impurities from soil [22]. The major ash-forming elements present in biomass combustion are silicon (Si), K, Na, Ca, magnesium (Mg), aluminium (Al), titanium (Ti), and Fe which are typically connected with S, phosphorus (P) and Cl. These elements affect ash behaviour, such as bed agglomeration, slagging, fouling and corrosion. The term slagging is used for furnace wall deposition and fouling refers to superheater area deposition. All of these can result in unscheduled shutdowns due to failures or bed sintering, leading to decreased availability and higher maintenance costs. The minor ash-forming elements of the ash include trace metals and heavy metals, which mainly affect emissions. However, in the case of recycled wood, Pb and Zn concentrations are also important from the perspective of ash behaviour as they lower the melting point of the ash [15].

Table 1 presents the composition of over 100 recycled wood fuels compared to barkless stem wood data of 10 analyses. The data are gained from a database [29]. The fuel data are gathered from several fuel analyses collected from existing boiler plants in Europe. Due to the heterogeneous nature of recycled wood, minimum and maximum values of the elements are presented.

Table 1. Comparison of the elemental composition of stem wood and recycled wood, d.s. = dry solids [29].

[wt-% d.s.] *if no other unit*	**Stem wood** *Average values*	**Recycled wood** *Min. – Max.*
Moisture	34	6 – 51
Ash	1.2	1.4 – 8.4
C	51	28 – 52
H	5.9	3.7 – 6.5
N	0.48	0.22 – 2.5
O (calculated)	40.9	31.6 – 43.6
S	0.03	0.01 – 0.4
Cl	0.02	0.02 – 0.7
LHV dry [MJ/kg]	19.4	11.7 – 19.9
LHV wet [MJ/kg]	11.6	8.2 – 18.9
Major ash-forming elements [mg/kg d.s.]		
Al	430	100 – 2760
Si	2040	880 – 23300
Ti	115	29 – 4500
Na	166	200 – 2500
Mg	342	250 – 1300
K	787	350 – 1500
Ca	2227	1200 – 12000
Fe	614	190 – 4800
P	132	36 – 340
Mn	117	55 – 300
Minor ash-forming elements [mg/kg d.s.]		
Sb	< 5	0.25 – 15
As	< 10	0.8 – 118
Cd	< 1	0.2 – 486
Cr	5.2	6.2 – 130
Co	< 2	0.6 – 17
Cu	3.8	0.2 – 580
Pb	< 6	11.4 – 790
Hg	not analysed	0.01 – 132
Ni	< 2	1.2 – 31
Sn	< 0.5	0.3 – 47
V	< 0.5	0.3 – 113
Ba	not analysed	0.03 – 920
Mo	not analysed	0.2 – 1.72
Zn	32	9 - 2000

Recycled wood is usually a drier fuel and its ash content is elevated due to the impurities in the fuel compared to stem wood. Barkless stem wood has typically low ash contents, ~1 wt-% [26]. Alkali metals (Na and K) as well as Zn are naturally occurring in wood plants at some level [30]. However,

increased levels of Na in recycled wood usually originate from plywood residues, paints and wood preservatives [26]. The sources for elevated concentrations of Pb, Zn and Cl are presented in Chapter 2.2.1.

2.2.1. Sources of lead, zinc and chlorine

Lead (Pb) Typical sources of Pb in waste wood originate from various wood treatment agents and stabilisers [31-33]. Lead sulphates and -phosphates have been used as polyvinyl chloride (PVC) stabiliser agents in plastics. For example, lead stearate, tribasic lead sulfate and dibasic lead phosphite are typical PVC stabilizers. Lead chromate ($PbCrO_4$) was commonly used in paints for colouring pigments in the past, but it has been banned since 1990. Pb can also be found in lacquers, preservatives and siccatives; thus, buildings and furniture waste may include elevated concentrations of Pb. Pb concentrations are elevated in recycled wood by a factor of about 480 compared to stem wood, mainly due to surface-treated wood [11].

Zinc (Zn) Zn is naturally present in wood, at roughly 10 mg/kg [30]. Elevated concentrations of Zn in recycled wood originate mainly from metals, paints, lacquers, binders and siccatives [10, 31, 34, 35]. Approximately 70 % of Zn in Swedish recycled wood comes from surface-treated wood [31]. Zinc oxide (ZnO) is used as a white pigment in paints and as a preservative agent. The yellow colour in paints originates from zinc chromate ($ZnCrO_4$). Zn, like Pb, can also be used as a PVC stabiliser. Siccatives typically include zinc carboxylate as a drying agent. In addition to ZnO, other preservatives used for woody construction materials include zinc sulphate ($ZnSO_4$) and ammoniacal copper zinc arsenate (ACZA). It has also been reported that wood-plastic composites might be treated with zinc borate [32]. Zn has been widely used in galvanised systems, which is one of the biggest applications of Zn [34]. Metallic parts, especially the ones made of brass (Cu-Zn alloy), can be one of the major Zn sources in waste wood. Krook et al. [11] estimated that the median Zn concentration of recycled wood is 50 times higher than in stem wood.

Chlorine (Cl) The major proportion of Cl found in recycled wood derives from chlorinated plastics, such as PVC. Chlorinated compounds are also found in plywood, coated particleboard and wood painted before the 1990s. In addition, Cl compounds can be used as a flame retardant [32]. One other Cl source is pentachlorophenol (PCP) which has been used as a wood preservative. This highly toxic compound is nowadays forbidden, but it may still exist in smaller amounts in recycled wood. Cl-containing agents have

also been used against fungi in products such as wood pallets. In addition, sea water and road salting are other possible chlorine sources [32].

2.3. Ash formation, deposition and adhesion

During combustion, fuel particles go through different physicochemical transformations and ash is formed from the inorganic part of the fuel constituents [22, 36, 37]. Formed ash is either bottom ash or fly ash. In FB technology, during biomass and waste combustion, the majority (over 90 %) of the formed ash is fly ash. The fly ash follows the flue gas flow and is the major concern in terms of corrosion, erosion, slagging and fouling.
The fly ash is composed of fine and coarse particles [37]. Fine particles or sub-micron particles (< 1 μm) are formed from volatilised ash-forming species by homogeneous condensation as the flue gases cool down [22, 36, 37]. These particles typically include sulphates, chlorides and carbonates as well as Pb- and Zn-salts in the case of recycled wood [36]. Coarse particles, or supermicron particles (> 1 μm), are composed of non-volatilised ash residuals including volatilised species that have come to the particle surface by heterogeneous condensation [22, 36, 37].

Ash deposition starts with formation of ash particles, followed by transport and adhesion to the heat transfer surfaces, and finally interaction with the deposit [22, 38]. Transportation of fine and coarse particles is mainly driven by diffusion, inertial impaction and thermophoresis mechanisms [22, 37, 38]. In the case of gaseous compounds, condensation is the main mechanism. Fine particles are transported by thermophoresis driven by a temperature gradient [22, 36, 37]. Gas molecules located on the hot side of the fine particles has more kinetic energy compared to cold-side particles, and they can push the fine particles towards the colder region [37]. Diffusion is based on local concentration differences, moving from high gas concentrations to lower concentrations, typically for particles below 10 μm [22, 37]. Particles over 10 μm are transported by inertial impaction driven by a gas flow [36]. These coarse particles have a higher probability of impacting the heat exchanger surfaces, but they do not easily adhere to the surface [37]. Deposition to the heat transfer surfaces happens by van der Waals forces or by adhering to partly molten particles [22]. Gaseous ash-forming compounds can condense directly on the tube surfaces or by nucleating on to the other particles first [22, 37]. Smaller fly ash particles (< 10 μm) have higher sticking efficiency compared to the larger particles [37].

The most essential elements in the development of corrosion are K, Na, Ca, Cl, Pb, Zn and S [22]. Their release, reactivity and stability depend on the mode of occurrence in the fuel matrix. The behaviour of K and Na during biomass combustion is a well-known phenomenon. They will be released during combustion as hydroxides KOH/NaOH (g), elemental alkalis K/Na (g), chlorides KCl/NaCl (g) and/or sulphates K_2SO_4/Na_2SO_4 (g, s) depending on the availability of Cl, S, Ca and the air-to-fuel ratio [22]. In the absence of S, gaseous elemental alkali and -hydroxide might condense as carbonate aerosols, K_2CO_3/Na_2CO_3 [22]. Part of the alkalis may be captured by silicates in the bed. Cl is known to be released completely during combustion as sodium chloride (NaCl), potassium chloride (KCl) and hydrochloric acid (HCl) and in the case of recycled wood combustion, also as lead chloride ($PbCl_2$) and zinc chloride ($ZnCl_2$) [22].

2.3.1. Release and speciation of lead- and zinc-including compounds

The formation and behaviour of heavy metal compounds are not yet as widely understood as those of the above-mentioned alkali metals. Chemical fractionation is a method of studying how ash-forming elements are bound in the fuel and how reactive they are during combustion. The method was first developed for coal and was later modified for biomass fuels [39-41]. It is based on selective leaching by different solvents: water, ammonium acetate (NH4Ac) and HCl. Water leaches alkali sulphates, -carbonates and -chlorides. NH4Ac leaches organically associated matter, such as Mg, Ca, K, Na and barium (Ba). The materials that are soluble in water and NH4Ac are likely to vaporise during combustion [40]. Finally, HCl leaches carbonates and sulphates of metals and alkaline earth metals. The non-soluble remainder typically contains oxides, silicates and sulphides. The fractionation method can be applied for materials such as fuels and ashes.

Vainikka et al. studied the presence of corrosive ash-forming elements in a solid recovered fuel (SRF)-firing BFB boiler by fine particle measurements [33]. The water-soluble fraction of Pb and Zn were assumed to be present as chlorides or sulphates. The remaining fraction was thought to be elemental Zn and Pb or oxides or sulphides. According to the leaching results, 40 % Pb and 50 % Zn were present in water-soluble compounds. Based on the calculated atomic ratios of water-soluble Na, K, Cl, Pb, Zn and S, Vainikka indicated that the formation of alkali and heavy metal sulphates was negligible, and the major part of the fraction was in the form of chlorides.

The release of Pb and Zn during combustion and gasification of different wood-based fuels has been reported by several authors [42-46]. Based on the combustion tests reported, the release started around 400-500 °C and was observed to be strongly related to the temperature and Cl content. Heavy metal release was reported to be 85-100 % at 1000 °C during combustion of chromated copper arsenate (CCA)-impregnated recovered waste wood [42]. According to another study [43] about 85 % of Zn was released at 850 °C during demolition wood combustion. The release correlated with Cl content, indicating that Zn was released as $ZnCl_2$. Jones [47] observed that Zn content in deposits decreased by approximately 25 % when operating the BFB boiler with reduced bed temperature (~724 °C).

The form and compounds of released heavy metals can be further predicted by thermodynamic modelling. It can be used to predict the chemical behaviour of multicomponent multiphase mixtures of ash-forming elements [48]. One of the best-known modelling programs is SOLGASMIX which is an integral part of the thermochemical software, FactSage [49]. The calculations provide information about stable phases, condensing compounds and melting properties of inorganic condensed phases. The calculations are based on Gibbs energy minimisation and require representative comprehensive databases. A significant amount of work has been done in this field. For example, the thermodynamic database of Åbo Akademi University currently contains 14 elements: Al, C, Ca, Cl, H, K, Mg, Mn, N, Na, O, P, S, and Si with 120 gaseous compounds, 2 liquid solutions phases, 12 solid solution phases and 73 pure condensed phases [49]. In addition, Pb and Zn have been implemented. The major restrictions for thermodynamic equilibrium modelling are the lack of physical properties, such as chemical kinetics and mass transport phenomena [50]. In addition, local conditions such as mixing and residence times are not taken into account.

Thermodynamic modelling has been used by several authors to predict the stability of Zn and Pb compounds during different types of wood and waste fuel combustion [19, 43-45, 47, 51-53]. Ménard et al. [53] made a thermodynamic study of heavy metal behaviour during municipal waste incineration. The software used was GEMINI (Gibb Energy MINImiser) with 29 elements in the database (C, H, O, N, S, Cl, F, Si, Ca, Mg, Na, K, Al, Fe, P, Mb, Ti, Cr, Zn, Pb, Cd, Hg, B, Cu, Ni, Co, As, Ba, Sn), including 1772 chemical species in total. As a result of the calculations, the stable form of Pb at the entrance of the grate was solid lead sulphide (PbS). In the combustion front, the stable gaseous phases were elemental Pb, lead sulphide (PbS), and lead

chlorides (PbCl and $PbCl_2$). Some gaseous lead oxide (PbO) was also predicted. However, they observed that the thermodynamic approach was inadequate in the case of Pb whose volatilisation seems overestimated. Zinc was predicted to form gaseous elemental Zn and $ZnCl_2$ and the calculation results seemed to correlate well with the reported combustion observations.

Bankiewicz et al. [52] made thermodynamic equilibrium modelling for ash and gaseous species at 1100 °C using FactSage 6.1 when simulating combustion of SRF, bark and sludge-containing fuel mixture. Pb was predicted to be present as gaseous Pb or PbS under reducing (λ = 0.8) conditions and as gaseous PbO under oxidising (λ = 1.2) conditions. A minor amount of gaseous PbCl was predicted to be stable at reducing conditions and PbCl and $PbCl_2$ at oxidising conditions. Zn was predicted to be volatilised as gaseous Zn at reducing conditions and to form a solid silicate ($Ca_2ZnSi_2O_7$) at oxidising conditions. A small fraction was predicted to volatilise as gaseous $ZnCl_2$. Comparison with the fine particle samples collected from the full-scale BFB boiler supported the speciation and formation of $ZnCl_2$, but not with Pb-including compounds, as a major portion of Pb was present as $PbCl_2$ in the fine particle fraction. As a second stage, the stable phases at 400 °C were predicted by using the gaseous equilibrium phase composition obtained from calculations at 1100 °C as an input. Pb was estimated to be present as stable solid PbS and gaseous $PbCl_2$ in reducing conditions and as solid lead sulphate ($PbSO_4$) in oxidising conditions. Zn formed solid ZnS and $ZnSO_4$. Some collected boiler deposits, however, revealed the presence of $PbCl_2$ and KCl in the most corroded parts of the front wall.

The behaviour of Pb and Zn during FB combustion of recycled wood was studied further by Enestam [19] in both reducing (λ = 0.5) and oxidising conditions (λ = 1) by FactSage. In the reducing conditions at flue gas temperatures of 700-900 °C, Pb and Zn were estimated to exist as gaseous elemental metals, Pb and Zn. Some gaseous PbS, PbCl, $PbCl_2$ and $ZnCl_2$ may be stable as well. Pb and Zn were predicted to deposit through condensation of gaseous compounds. In oxidising conditions, $PbCl_2$ (g) was predicted to be stable until ~700 °C and oxidise to PbO (g) at higher temperatures. The major portion of Zn was estimated to be present as ZnO (g, s). Small proportions of $ZnCl_2$ (g) can be present. Due to its lower condensation temperature (179-283 °C), it is expected to condense in the colder surfaces of the flue gas channel.

Under the oxidising conditions, Enestam [19] predicted ZnO (s) and double salts KPb_2Cl_5 (s), K_2PbCl_4 (s) and K_2ZnCl_4 (s) to be stable for the

condensed species. This indicates that deposited Pb and Zn might react with K in the deposit. Similar double salts have been reported to exist in actual boiler deposits and in laboratory tests with synthetic deposits [46, 54-56]. These condensed double salts can either be formed within the deposit or already be in the gas phase, according to the reactions 1-4 [57]. An intermediate gaseous compound, $KPbCl_3$, may form at the first stage and further re-react with KCl as presented in reactions 3 and 4.

$$PbCl_2\ (g, l, s) + 2\ KCl\ (g, s) \rightarrow K_2PbCl_4\ (s) \quad (1)$$
$$2\ PbCl_2\ (g, l, s) + KCl\ (g, s) \rightarrow KPb_2Cl_5\ (s) \quad (2)$$
$$PbCl_2\ (g, l, s) + KCl\ (g, s) \rightarrow KPbCl_3\ (g) \rightarrow \quad (3)$$
$$KPbCl_3\ (g) + KCl\ (g, s) \rightarrow K_2PbCl_4\ (s) \quad (4)$$

Jones et al. [58] performed thermodynamic calculations using FactSage 6.3 to predict the speciation of ash-forming elements during municipal solid waste (MSW) and industrial waste firing. For oxidising conditions ($\lambda = 1.4$), gaseous $ZnCl_2$ was predicted to be stable above 400 °C, with a maximum at 800 °C. Above 1000 °C, gaseous Zn was the main volatile Zn species. Above around 800 °C, $PbCl_2$ was predicted to oxidise to PbO. Under reducing conditions ($\lambda = 0.7$), the stability of $ZnCl_2$ was similar to oxidising conditions. A significant amount of gaseous Zn was observed to be stable at 700-800 °C; the level stabilised at higher temperatures. PbCl and $PbCl_2$ were present at lower temperatures, and PbS was the prevailing Pb component above ~600 °C. Jones et al. [58] stated that the reducing conditions give rise to the corrosive elements in higher concentrations compared to the oxidising conditions. During studies of the thermal stability of zinc, Jones et al. [59] concluded that $ZnCl_2$ should not easily form deposits in a boiler due to its low melting point and instability when molten under oxidising conditions. Experiments with differential scanning calorimetry / thermogravimetric analysis (DSC/TGA) showed that $ZnCl_2$ melts at 320 °C and vaporises and partly oxidises to ZnO above 400 °C. In addition, they found out that chlorination of ZnO to $ZnCl_2$ is possible at temperatures of 240-330 °C with high HCl (500 ppm)-containing environments.

In addition to the existing combustion environment estimating techniques, promising new methods have been developed. A novel, laser-based measurement technique, CPFAAS (collinear photofragmentation and atomic absorption spectroscopy), has been demonstrated to monitor gaseous KCl content effectively during biomass combustion [60, 61]. Measured KCl gas concentrations were reported to vary between 25 and 249 ppm during

combustion of straw and wood in a CFB boiler [62]. A method based on the same measurement technique has been developed to measure gaseous $PbCl_2$ in boiler environments [63]. However, the measurements carried out in a full-scale boiler environment firing recycled wood showed surprisingly low concentrations (0.4-0.8 ppm) of gaseous $PbCl_2$ [63].

2.4. Corrosion

Corrosion of the heat transfer surfaces has been and still is the limiting factor for higher steam parameters. The role and importance of Cl and formation of metal chlorides in high-temperature corrosion was already understood decades ago [64-69]. However, the penetration of Cl-including species through the oxide scale is not fully understood [14]. Chlorine is suggested to penetrate through the scale as a Cl_2 molecule or as a Cl^- anion [68, 70]. Cl can be present as alkali chlorides, heavy metal chlorides or in the form of HCl gas during biomass and waste combustion, which can all destroy the protective metal oxide and initiate corrosion. Depending on the prevailing conditions, temperatures and chlorides present, gaseous phase corrosion, solid phase corrosion or molten phase corrosion may occur. Besides the effect of fuel mixture composition on corrosion, two other crucial elements have been observed to affect corrosion rates as well: material and flue gas temperatures. The higher the flue gas or the material temperature, the higher the measured corrosion rate [67, 71-74]. The impacts of heat flux and temperature gradient on corrosion and on the composition of the ash and fused salt layers are highlighted in the literature [75-78]. Temperature gradient was observed to have an effect on deposit morphology and to induce alkali chloride transport within the deposit according to the laboratory measurements [76]. A partially or completely molten layer was observed in the outer layer of the deposit. Alkali chlorides were observed to be transported towards the air-cooled steel surface by evaporating from the hotter particles and condensing on colder particles on the deposit.

2.4.1. Gaseous phase corrosion

For gaseous phase corrosion to occur, gas molecules react directly with the tube material without condensation. Corrosion is caused by gaseous corrodents, such as HCl or Cl_2. As a rule of thumb, 0.1 wt-% of Cl in the waste fuel generates about 80-100 ppm HCl to the flue gas [14, 67, 79]. Corrosion caused by gaseous Cl_2 in oxidising conditions was studied by Grabke et al. [68], and the commonly-known name of the reaction mechanism, active

oxidation, was proposed by McNallan et al. [69]. Corrosion is suggested to start as gaseous Cl_2 is formed and reacts with a metal surface [68]. Gaseous Cl_2 can be formed from HCl and oxygen by the Deacon process as described in reaction 5.

$$2\ HCl\ (g) + ½\ O_2\ (g) = Cl_2\ (g) + H_2O\ (g) \quad (5)$$

The Deacon process is typically slow but it could be catalyzed by an oxidised metal surface. Gaseous Cl_2 is claimed to be able to penetrate through cracks and pores to the metal-oxide interface by creating diffusion paths at the grain boundaries. In the metal-oxide interface, where partial pressure of oxygen is small, solid metal chlorides are formed according to reaction 6.

$$Me^*(s) + Cl_2\ (g) \rightarrow MeCl_2\ (s) \quad (6)$$

*Me = Fe, chromium (Cr) or nickel (Ni)

Metal chlorides have high vapour pressure, especially iron chloride ($FeCl_2$), and are highly volatile at the prevailing conditions, causing solid metal chlorides to evaporate according to reaction 7. For example, at 500 °C $FeCl_2$ has the vapour pressure of $4 \cdot 10^{-5}$ bar [68]. It has been suggested that volatilisation can promote corrosion when the vapour pressure is > 10^{-6} bar [14].

$$MeCl_2\ (s) \rightarrow MeCl_2\ (g) \quad (7)$$

Metal chlorides are proposed to penetrate upwards to the oxide-gas interface and form metal oxides as oxygen partial pressure increases, as presented in reactions 8 and 9. In the case of high-alloy steel, formation of chromates instead of oxides are reported to occur.

$$3\ MeCl_2\ (g) + 2\ O_2\ (g) = Me_3O_4\ (s) + 3\ Cl_2\ (g) \text{ or} \quad (8)$$

$$2\ MeCl_2\ (g) + 3/2\ O_2\ (g) = Me_3O_4\ (s) + 2\ Cl_2\ (g) \quad (9)$$

When the metal chlorides are oxidised, a porous non-protective metal oxide layer forms. Cl is released in this reaction as Cl_2, which is supposed to penetrate back to the steel surface and react again with the steel [68]. This causes a corrosion cycle known as active oxidation. The rate-determining factor of gaseous phase corrosion was suggested to be controlled by the

outward diffusion of metal chlorides. In the case of reducing conditions, metal chlorides can form directly on the metal surface [68]. Formed metal chlorides are not oxidised but vaporised instead.

2.4.2. Solid phase corrosion

Solid phase corrosion is probably the most typical corrosion mechanism in the boiler fireside heat transfer surfaces as the partial pressure of HCl is not high enough in biomass-derived flue gases to cause severe gas phase corrosion [14]. In biomass combustion, KCl is the dominant chloride [14] whereas corrosion in recycled wood combustion has been shown to be caused by heavy metals or by a combination of heavy metals and alkali chlorides [15, 17, 18, 21, 64, 65, 67, 72, 80, 81]. Solid phase corrosion has been reported to initiate corrosion with low-alloy steel already at 450 °C [13]. Chlorides may initially be present as gaseous chlorides, which then condense to a cooler heat transfer surfaces, forming solid particles. These solid particles initiate corrosion reactions in direct contact with the steel surface [14]. The same active oxidation mechanism as described above has been proposed for solid phase corrosion according to reaction 10 forming alkali ferrates ($K_2Fe_2O_4$ or $Na_2Fe_2O_4$) and Cl_2 [68]. In the case of higher alloyed steel, alkali chromates (K_2CrO_4 or Na_2CrO_4) are suggested to form as described in reaction 11 [68]. The presence of water vapour has been suggested to promote HCl formation according to reaction 12 [82]. Formed Cl_2 gas is proposed to be able to penetrate to the steel surface and corrosion proceeds as described in equations (6-9).

$$2\ NaCl\ (s) + Fe_2O_3\ (s) + \tfrac{1}{2}\ O_2\ (g) \rightarrow Na_2Fe_2O_4\ (s) + Cl_2\ (g) \quad (10)$$

$$4\ NaCl\ (s) + Cr_2O_3\ (s) + 5/2\ O_2\ (g) \rightarrow 2\ Na_2CrO_4\ (s) + 2\ Cl_2\ (g) \text{ or} \quad (11)$$

$$4\ NaCl\ (s) + Cr_2O_3\ (s) + 2\ H_2O\ (g) + 3/2\ O_2\ (g) \rightarrow 2\ Na_2CrO_4\ (s) + 4\ HCl\ (g) \quad (12)$$

In cases of higher alloyed steels, the rate determining step in the corrosion is more connected to the destruction of a protective layer rather than to the formation of Cl_2 or HCl [83, 84]. Pettersson et al. [82] suggested that alkali cations, such as K^+, destroys the protective oxide layer at the intial stage of corrosion followed by Cl_2 or HCl.

In the active oxidation mechanism, the question of Cl_2 ability to penetrate the oxide scale has been raised. Cl_2 is a larger molecule than O_2, which does not support the theory of why Cl_2 is able to diffuse through the scale but O_2 is not. If this was the case, the prevailing conditions close to steel surface would no longer have low partial oxygen pressure to support the

thermodynamic favour for metal chloride formation. Folkeson et al. [70] proposed Cl^- formation with solid KCl on the low-alloy steel surface. An electrochemical corrosion mechanism is initiated by the dissociation of KCl on the steel surface and forming Cl^- and KOH in the presence of H_2O and O_2. Fe is suggested to oxidize to Fe^{2+} at the metal/oxide interface. Cl^- anions migrates down through the oxide grain boundaries and forms $FeCl_2$ with Fe^{2+} ions. Cl^- theory has also been proposed by others [85-87].

Sulphation of alkali chlorides on tube surfaces has been shown to form Cl_2 gas. Sulphation of alkali chlorides on tube surfaces has been claimed to enhance corrosion by the mechanisms presented in reactions 13 and 14 [68, 88].

$$2\ KCl\ (s) + SO_2\ (g) + O_2\ (g) \rightarrow K_2SO_4\ (s) + Cl_2\ (g) \text{ or} \quad (13)$$

$$2\ KCl\ (s) + SO_2\ (g) + ½\ O_2\ (g) + H_2O\ (g) \rightarrow K_2SO_4\ (s) + 2\ HCl\ (g) \quad (14)$$

Released HCl may diffuse towards the steel surface and form metal chlorides, which later become oxidized, or HCl oxidises and produces Cl_2 gas according to reaction 5 [14].

2.4.3. Molten phase corrosion

Daniel et al. [65] understood nearly 40 years ago that corrosion in waste-derived boilers cannot be explained only by alkali chlorides or by gaseous HCl. They proposed that corrosion is caused by molten heavy metal salts or molten heavy metal salts mixed with alkali chlorides. In the presence of heavy metals, the corrosion mechanism is often referred to as a molten phase corrosion because heavy metals decrease the first melting temperature of deposits as shown in Table 2. Deposits rarely have one specific melting temperature, but rather a temperature range where the melting occurs. The first melting temperature of the deposit, T_0, describes the temperature at which the first liquid phase appears [89]. In the complete melting point, T_{100}, the last solid particles are dissolved, and the deposit becomes completely molten. Laboratory tests have shown that the existence of a molten phase of in a deposit drastically increases the corrosion rate [13]. However, increased corrosion has also been observed below the first melting temperature of the deposits [13, 14].

Table 2. Melting points and lowest melting temperatures of some compounds.

Composition [wt-%]	Melting point and lowest melting temperatures [°C]	Reference
Pure compounds		
Pb	327	[19]
Zn	420	[19]
$ZnCl_2$	318	[54]
$PbCl_2$	501	[90]
$FeCl_2$	677	[19]
KCl	771	[90]
NaCl	801	[90]
PbO	886	[19]
ZnO	1975	[19]
Mixed compounds		
$ZnCl_2$–NaCl–KCl	203	[91]
68 $ZnCl_2$ - 32 KCl	230	[67]
51 $ZnCl_2$ - 43 KCl - 6 $PbCl_2$	238	[67]
KCl - $ZnCl_2$ - K_2SO_4 - $ZnSO_4$	292	[54]
73 $ZnCl_2$ - 27 $PbCl_2$	300	[54]
K_2SO_4 - Na_2SO_4 - $ZnSO_4$	384	[54]
16 $NaCl_2$ - 40 KCl - 44 $PbCl_2$	400	[54]
KCl - $PbCl_2$	409	[92]
NaCl - $PbCl_2$	409	[92]
KCl - NaCl	657	[93]
Compounds including elements from the steel		
$FeCl_2$ - $ZnCl_2$	300	[19]
KCl - $FeCl_2$	350	[93]
NaCl - $FeCl_2$	378	[93]
$FeCl_2$ - $PbCl_2$	420	[94]

The corrosion of furnace walls cannot be explained solely by the active oxidation mechanism due to the relatively low vapour pressures of different metal chlorides, such as $FeCl_2$, chromium chloride ($CrCl_2$) and nickel chloride ($NiCl_2$), at 250-350 °C [64]. Instead, corrosion has been explained by molten phase formation and fluxing of the protective oxide in the fused salt, sometimes termed a hot corrosion mechanism, which can be divided into two types [95]. Hot corrosion type I occurs above the melting point of the deposit and type II occurs at temperatures below the melting point of the deposit [15]. The increased corrosion rate and in type II is reported to be caused by the electrolytic phase that forms between the steel surface and the deposit. The molten phase is known to produce catastrophic corrosion rates

due to faster reactions in the liquid phase compared to solid-solid reactions; the liquid phase provides electrolyte for the electrochemical attack [14].

The main corrosion mechanism has been proposed to be dissolution of metal/metal oxide in the molten salt as soluble metal chlorides [15, 54, 65, 88, 96]. Corrosion starts with the dissolution of metal or metal oxide at the metal/salt melt interface, according to reaction 15 [15, 64]. The Cl_2 gas produced is dissolved in the melt and transported to the metal surface, as described in reaction 16. Metal is dissolved as metal chloride, which forms a eutectic mixture together with the deposit. Eutectic melt forms at a certain temperature from phases that have limited solubility with each other in the solid state [97]. Eutectic temperature refers to the lowest melting temperature of the system at which all components form a homogeneous melt. Depending on the number of components - binary, ternary and quaternary, etc.-eutectics may exist.

$$ZnCl_2\ (l) + 2\ Fe_2O_3\ (s) \rightarrow (Zn,Fe)O\ (s) + Fe_3O_4\ (s) + Cl_2\ (g) + \tfrac{1}{2}\ O_2\ (g) \quad (15)$$

$$Fe + Cl_2\ (diss.) \rightarrow FeCl_2\ (diss.) \quad (16)$$

The concentrations of dissolved metal chloride are high at the inner interface and lower at the salt/gas interface. This results in metal chloride diffusion outwards through the salt melt. At the salt/gas interface, metal chlorides will be oxidised as the oxygen partial pressure increases and Cl_2 gas is released, as presented in reaction 17. Cl_2 partial pressure is high enough to penetrate to the metal-oxide interface to react with the metal and enhance further material degradation.

$$2\ FeCl_2\ (diss.) + 3/2\ O_2\ (g) \rightarrow Fe_2O_3 + 2\ Cl_2\ (diss.) \quad (17)$$

Higher-alloyed steels have been proposed to corrode in a similar way (reaction 18) by dissolution of the protective oxide in molten salt, destroying the protective oxide and forming chromates and Cl_2 gas [54, 98-100].

$$2\ PbCl_2\ (l) + Cr_2O_3\ (s) + 5/2\ O_2\ (g) \rightarrow 2\ PbCrO_4\ (s) + 2\ Cl_2\ (g) \quad (18)$$

The solubility of metal chlorides in molten salts has been reported to be the corrosion rate determining factor [64]. Solubility of $FeCl_2$ in the molten $ZnCl_2$-KCl mixture was shown to be higher compared to the solubilities of $CrCl_2$ and $NiCl_2$. In fact, $CrCl_2$ and $NiCl_2$ have almost no solubility [96]. Thus, Fe-based low-alloy steels are much more prone to molten phase corrosion

compared to Ni-based alloys. Kawahara [74] reported that in molten phases, volatile chlorides with high vapour pressures ($ZnCl_2$, $PbCl_2$, NaCl, KCl) and gas components (HCl, Cl_2, SO_2, O_2) penetrate through the scale defects into the scale. The extent of penetration was proposed to depend on the stability of oxides against the chlorination reaction, and the penetration extent is the highest with Fe-oxides. Viklund et al. [56] proposed that alloying with sufficient Cr content could increase the resistance against chlorination.

In addition, Spiegel also suggested that direct oxidation of molten $ZnCl_2$ in the top of the steel at 500 °C and 600 °C forms Cl_2 (reaction 19), followed by further reaction with the Cr_2O_3 layer, forming Zn-rich spinel (reaction 20) [54].

$$ZnCl_2\ (l) + ½\ O_2\ (g) \rightarrow ZnO\ (s) + Cl_2\ (g) \quad (19)$$

$$ZnO + Cr_2O_3 \rightarrow ZnCr_2O_4 \quad (20)$$

Alkali chlorides have also been shown to induce corrosion by forming a liquid phase with the salt and corrosion product (metal chloride) [85]. Jonson et al. [85] reported that when low-alloy steel was exposed to KCl salt at 400 °C, a KCl-$FeCl_2$ liquid phase was formed on the Fe oxide surface. KCl dissociation was suggested to produce Cl^- anions which reacted with Fe^{2+} ions as described by Folkeson et al. [70]. $FeCl_2$ has been suggested to form according to reaction 21 (in the scale-gas interface) and reaction 22 (in the scale-metal interface).

$$2\ KCl\ (s) + ½\ O_2\ (g) + H_2O\ (g) + 2\ e^- \rightarrow 2\ KOH + 2\ Cl^- \quad (21)$$

$$Fe \rightarrow Fe^{2+} + 2\ e^- \quad (22)$$

The overall result would be according to reaction 23.

$$2\ KCl\ (s) + ½\ O_2\ (g) + H_2O\ (g) + Fe \rightarrow 2\ KOH\ (s) + FeCl_2 \quad (23)$$

Okoro et al. [101, 102] reported similar melt formation between the reaction product and the deposit at 560 °C and Fantozzi et al. [103] observed melt formation between KCl and Cr_2O_3 at 550 °C.

2.4.4. Corrosion tests with heavy metal chlorides

A short summary of the heavy metal-including corrosion tests found from the literature is presented in Table 3. The summary of the literature data shows that corrosion caused by heavy metal-including salts has been observed at low material temperatures (at 316 °C) [65]. $PbCl_2$ was found to be more corrosive than $ZnCl_2$ [98]. However, a rapid volatilization of $ZnCl_2$

during the tests was observed. Based on one study, KCl was found to be more corrosive than $PbCl_2$ at 400 °C [104]. However, $PbCl_2$ was oxidised to PbO. Pb- and Zn oxides and -sulphates are reported to be less corrosive than their corresponding chlorides [98, 105]. Although melt formation is often detected, the presence of a melt is not necessarily needed for severe corrosion to occur [18].

In addition to the previously-presented corrosion mechanisms, other theories have been proposed in the literature for corrosion during combustion of different waste fuels. Talus et al. [46] proposed a solid PbO to react with $FeCl_2$ (reaction 24) and form Fe oxide and $PbCl_2$. Formed $PbCl_2$ could further react with alkali chlorides present in the deposit, and thus form low melting mixtures that could enhance corrosion.

$$PbO\ (s) + FeCl_2\ (s) + \tfrac{1}{6}\ O_2\ (g) \rightarrow \tfrac{1}{3}\ Fe_3O_4\ (s) + PbCl_2\ (s) \qquad (24)$$

Not only carbon steels and low-alloy steels suffer from corrosion; high-alloy stainless steels and Ni-based alloys also suffer from it as well. However, corrosion initiated at temperatures higher than those for the low-alloyed steels. Alipour et al. [106] proposed different corrosion mechanisms depending on the steel grade. Low-alloy steel was suggested to corrode by HCl, leading to the formation of $FeCl_2$. Ni-based alloy 625 was found to be attacked by a K-Pb compound. FeCrAl alloys were corroded by K together with Cl. K destroyed the protective alumina layer and Cl attacked the base material. Stainless steel was corroded by both chloride-containing species and a compound containing Pb and K.

Table 3. Summary of corrosion tests with heavy metal salts based on the literature.

Laboratory-scale testing *(atmosphere assumed as oxidising if not otherwise specified)*				
Test materials	**Tempera-tures [°C]**	**Salts (wt-%)**	**Results**	**Ref.**
10CrMo9-10, AISI347	350, 400, 450, 500, 550, 600	100% $PbCl_2$ 100% $ZnCl_2$	$PbCl_2$ corrosive at 400 °C against 10CrMo9-10. $ZnCl_2$ corrosive at 350 °C against 10CrMo9-10.	[98, 107]
	350, 450, 550	100% PbO 100% ZnO	$PbCl_2$ corrosive at 450 °C against AISI 347. No corrosion with $ZnCl_2$ at 450 °C against AISI 347. PbO corrosive against 10CrMo9-10 at 550 °C. No corrosion with AISI 347	
10CrMo9-10, AISI347	400, 500, 600	5% $PbCl_2$- 5% $ZnCl_2$-90% KCl 5% $PbCl_2$- 95% KCl 5% $PbCl_2$- 95% K_2SO_4	All mixtures corrosive at 400 °C against 10CrMo9-10 and at 500 °C against AISI 347. No clear trend between corrosivity of different salts.	[107]
carbon steel	316	84% $ZnCl_2$-16% NaCl	Corrosion observed in the carbon steel sample.	[65]
10CrMo9-10, AC66 (X5NiCr CeNb32 27)	400, 500, 600	$PbCl_2$	Accelerated corrosion at 500 °C with 10CrMo9-10. Corrosion also with AC66 but clearly less.	[54]
	400, 500, 600	$ZnCl_2$	Accelerated corrosion at 600 °C with 10CrMo9-10. Corrosion also with AC66 but clearly less.	
	300, 400	50% $ZnCl_2$-50% KCl	Severe corrosion at 300 °C with 10CrMo9-10. No corrosion with AC66.	
carbon steel, 2.25CrMo, SS304	400, 500 reducing condit.	55% $ZnCl_2$-45% KCl (mol-%)	All materials corroded already at 400 °C.	[99]
carbon steel, P91, SS310	450	55% $ZnCl_2$-45% KCl (mol-%)	All materials corroded.	[100]

Fe-based alloys: 825 & 803, Ni-Cr-Fe alloys: 600 & 690	550, 650	20% $ZnCl_2$-40.9% $PbCl_2$-21.9% KCl-17.2% NaCl 4.7% $ZnCl_2$-9.7% $PbCl_2$-2% KCl-2.6% NaCl-6.1% K_2SO_4-4.9% Na_2SO_4-70% Al_2O_3	Increasing test temperature resulted increased corrosion attack with Fe-based alloys. Ni-Cr-Fe alloys exhibited similar levels of corrosion at both temperatures.	[108]
2.23Cr-1Mo,	400	KCl-$ZnCl_2$	Corrosion observed and formation of KCl-$FeCl_2$ eutectic melt was suggested.	[64]
T22	400 5% N_2 + 40% H_20	$ZnCl_2$ KCl-$ZnCl_2$ NaCl-$ZnCl_2$	KCl-$ZnCl_2$ salt resulted in the thickest oxide scale, also signs of molten phase were observed with this salt	[109]
2.25Cr-1Mo	400 5% N_2 + 40% H_20	KCl $PbCl_2$	KCl more severe than $PbCl_2$. $PbCl_2$ oxidised to PbO.	[104]
Laboratory-scale combustion testing				
Test materials	**Tempera-tures [°C]**	**Environment**	**Results**	**Ref.**
16Mo3, 304L, Alloy 625	material: 350, 400 flue gas: 930	wood pellets doped with different Pb-levels: 10, 100, 1000 mg/kg (+ Cl, K, Zn) λ = 0.7	300 °C: no lead in the deposit except at Pb-level 1000 mg/kg. 400 °C: Pb in deposit increased with increasing Pb-level in the fuel. KPb_2Cl_5 identified from the deposits. No corrosion with 304L nor with Alloy 625.	[46]
15Mo3, 304, Alloy 625	material: 350, 400, 550, 600	wood pellets doped with different Pb-levels: 10, 100, 1000 mg/kg (+ Cl, K, Zn) λ = 0.7 & 1.3	Pb and Zn found from the furnace walls temperatures (350 °C, 400 °C) with air ratio of 0.7 but not much from the superheater temperatures (550 °C, 600 °C) with air ratio of 1.2. Pb-K-Cl-O deposit formed.	[81]

Full-scale probe samples / Full-scale tube samples				
Test materials	**Tempera-tures [°C]**	**Environment**	**Results**	**Ref.**
13CrMo4-4, super304, 317L, Sanicro28, Alloy 625	material: 440 flue gas: 635	70% / 30% household / industrial waste superheater area	Pb-K-Cl compound observed from the corroded samples 13CrMo corroded the most, followed by super304, then equally 317L and San28. Inc625 yielded the least corrosion of the tested materials.	[56]
16Mo3, 310S, FeCrAl, Alloy 625	material: 390	waste wood furnace wall area	Cl-K-Pb/K-Zn-Cl compounds observed. Order of the test materials starting from the worst corroded: 16Mo3 < 310S < FeCrAl < Alloy 625	[106]
carbon steel, Alloy 625	material: 260-316	refuse-derived fuel (RDF) firing furnace wall area	High concentrations of Cl, Na, K, Zn found in the samples.	[65]
Ni-based overlay weld	material: 300-600	waste incineration	Molten phase in deposits, containing mainly $ZnCl_2$, KCl, some Na and Pb.	[54]
T12, Alloy 625	material: 550, flue gas: 635 material: 465, flue gas: 650	waste incineration	Both samples suffered from corrosion.	[74]

2.4.5. Corrosion control

S-based additives, such as elemental S or liquid sulphate injection, and co-combustion of high S-containing fuels are known to be effective ways to reduce alkali chloride-induced superheater corrosion in boilers [82-88]. S is effectively binding alkalis, thus reducing the amount of gaseous alkali chlorides in the gas phase according to reaction 25.

$$2\ K/NaCl\ (g) + SO_2\ (g) + H_2O\ (g) + \tfrac{1}{2}\ O_2\ (g) \rightarrow K/Na_2SO_4\ (g,l) + 2\ HCl\ (g) \quad (25)$$

It is known that the low S/Cl molar ratio of the fuel poses a high-temperature corrosion risk by forming alkali chlorides instead of non-corrosive alkali sulphates. It has been proposed that the corrosion risk is high with a S/Cl molar ratio below 2, moderate if the ratio is between 2 and 4, and low if the S/Cl molar ratio is above 4 [79]. High Ca-levels may consume S further by forming $CaSO_4$ which could hence limit the sulphation of alkali chlorides [22, 26]. Kaolinite is typically used to prevent bed agglomeration but may also decrease gaseous alkali content by binding alkalis to form alkali-aluminosilicates instead of alkali chlorides [110, 111].

The effectiveness of different additives against heavy metal-induced corrosion is not yet understood. Sewage sludge was reported to decrease the amount of K, Cl and Na in furnace wall deposits, leading to reduced corrosion of Ni-based 625 alloy and FeCrAl-alloys [112]. However, low-alloy steels were not included in the test matrix. Other studies carried out in the waste-fired boilers have focused on the superheater area. Sulphate injection reduced the corrosion in the superheater area [113], sewage sludge effectively decreased alkali chloride concentration in the superheater area [114] and the addition of S into the fuel inhibited superheater corrosion in waste firing [115]. S-based additives might be effective against superheater corrosion by reducing alkali chloride concentrations, but at the same time, they might increase the amount of heavy metal chlorides. The addition of peat ash to demolition wood seemed to decrease chloride concentration in aerosols, but increased the level of Zn and Pb instead [80]. The addition of Zn- and Pb chloride to synthetic sulphate deposits increased the corrosion rate of low-alloy steel [65]. Additives injected into the bottom part of the furnace or mixed with the fuel might not have enough time to react before they reach the furnace walls, and thus are ineffective against furnace wall corrosion.

2.5. Material selection in boilers

Material selection plays an important role in boilers in terms of corrosion and financial considerations. The cost of tube materials and manufacturing increases significantly if high-alloyed materials must be used instead of carbon or low-alloy steels. Disregarding corrosion during material selection, might lead to unexpected shutdowns due to corrosion-related failures of heat transfer surfaces. Pressure vessel legislation and standards also control material selection, design and manufacturing by setting certain limitations and requirements for the materials. Materials must fulfill certain strength

properties and have good ductility and toughness. In addition, pressure bearing materials must have good weldability properties. Fe and carbon (C) are the base elements of the steel; the C content is less than 2 %. In boiler pressure bearing materials, however, the C content is limited to 0.3% to achieve the necessary weldability, ductility and toughness properties.

When steels are exposed to high temperatures, they will become oxidised. The steel surface begins to absorb oxygen from the surrounding air and forms a metal oxide layer [116]. The formed oxide layer can be either protective or non-protective depending on its stability at prevailing conditions. Protective oxide is tightly adhered to the surface. It has a high melting point and low vapour pressure. In addition, the thermal expansion coefficient must be small. If the oxide layer is not protective, corrosion can initiate and proceed by either outward (diffusion of metal ions) or inward (diffusion of oxide ions) growing oxide [116].

2.5.1. Non-alloy steels

Non-alloy steels (or carbon steels) consist primarily of Fe and C. They are widely used in boiler components due to their low price. Non-alloy steels include manganese (Mn) and small amounts of Si or Al. Si and Al are used to de-oxidise the steel to produce a more homogeneous structure and to avoid gas porosities. De-oxidised steels are known as killed or semi-killed steels. Mn is used to improve strength properties. It also binds S to form manganese sulphides (MnS) instead of harmful iron sulphides (FeS), which decrease the mechanical properties. They have fairly favourable strength properties, low price and wide availability. However, due to their lack of alloying elements, they do not provide the best corrosion and oxidation resistance. The formed oxide is Fe oxide, either wüstite (FeO), magnetite (Fe_3O_4) or hematite (Fe_2O_3) depending on the prevailing conditions. All of them are known for their poor oxidation resistance. Fe_3O_4 and Fe_2O_3 are the stable oxides below 570 °C [21]. Non-alloy steels can be used in boiler water-side components, e.g., in feedwater pipes, economisers and furnace walls up to the lower-temperature superheaters and boiler bank. They can be used cost-effectively in pressure bearing components up to about 450 °C; in non-pressure parts, the scaling temperature limits their use to ~540 °C.

2.5.2. Low-alloy steels

Low-alloy ferritic steels used in boiler pressure bearing components include Fe, C and smaller amounts of Cr and molybdenum (Mo). Vanadium (V) and

boron (B) can be used to increase high-temperature strength. The addition of Cr favours the formation of a mixed spinel $Fe(Fe,Cr)_2O_4$ layer, which further enhances oxidation resistance; thus these alloys can be used up to 575 °C in pressure bearing components [21]. The higher level of alloying means that the price is also higher and that manufacturing is more demanding compared to non-alloy steels. In boilers, low-alloy steels are typically used in furnace walls, superheaters, superheater connection pipes and in pipings.

2.5.3. High-alloy ferritic steels

When compared to low-alloy steels, higher amounts of Cr and Mo are added to improve high-temperature oxidation and strength properties. In addition, high-alloy steels are often alloyed with niobium (Nb) and V to further improve high-temperature creep strength properties. Alloying with larger amounts of Cr increases high-temperature oxidation resistance; thus these alloys can be used up to ~600°C in pressure bearing components. While they have better creep properties compared to the low-alloy steels, manufacturing is clearly more demanding. For example, in welding, pre-heating and post-weld heat treatments are typically required as well as use of root gas to protect welds from oxidation. These types of steels are typically used in superheaters, superheater headers and in main steam piping.

2.5.4. Austenitic stainless steels

Stainless steels can be divided into ferritic, martensitic and austenitic stainless steels based on their crystalline structures. Stainless steels include at least 13 % Cr. Ferritic and martensitic stainless steels are not typically used in pressure bearing components due to their low ductility. In contrast, austenitic stainless steels have good ductility properties and are widely used in pressure bearing components. They must include at least 18 % Cr and 7 % Ni to ensure fully austenitic structure. If the Ni content is lower than 7 %, the crystal structure will include both ferritic and austenitic structures. This steel type is called Duplex steel; use of these steels is limited to max. ~300 °C. The unique austenitic-ferritic structure starts to decompose above this temperature. Austenitic stainless steels have strong high-temperature corrosion resistance due to the protective Cr_2O_3 layer. However, they suffer from sensitisation in the temperature range of 550-850 °C. Cr carbides precipitating to the grain boundaries are causing this sensitisation phenomena. In pressure bearing components, stabilised steel grades such as TP310HCbN and TP347HFG are used in that 550-850 °C temperature range

to prevent sensitisation. Typical stabilising agents are Ti or Nb. Due to the higher amounts of alloying elements, austenitic stainless steels are expensive materials; their use must be considered case by case. Typical components made of austenitic stainless steels in pressure bearing parts are the hottest superheaters. Austenitic stainless steel types 304L, 309, 310 and 253Ma are widely used in high-temperature non-pressure parts in boilers as superheater ties and vortex finders. They are also widely used as tube shield materials.

2.5.5. Ni-based alloys

Ni-based alloys have Ni as a main alloying element instead of Fe. These types of steels are much more expensive than austenitic stainless steels due to the high levels of Ni-alloying; thus, these steels are seldom used as solid tubes and are used more frequently as coating materials, such as composite tubes and overlay welded (OW) tube cladding materials. The use of OW coatings has increased during the recent years in boiler applications. They are widely used in furnace walls when more demanding fuels such as recycled wood are combusted. Ni-based alloys offer strong corrosion resistance in places where lower-alloyed materials have suffered from corrosion. In addition to furnace walls, Ni-based overlay weld materials can be used in the hottest superheaters, locating them in the areas with high corrosion risk. Good high-temperature corrosion resistance is based on the increased Cr activity and diffusion rates, as well as low Fe content due to alloying with high amounts of Ni rather than Fe [21]. Table 4 presents a summary of the materials used in boiler pressure bearing components.

Table 4. Summary of the materials used in boiler pressure bearing components.

Main alloying elements [wt-%]					**Steel grade examples:**		**Max temp. [°C]**	**Rel. price**
C	**Cr**	**Ni**	**Mo**	**Other**	**EN**	**ASME**	**Press. vessels / Scaling temp.**[*)]	
Non-alloy steels / carbon steels								
≤ 0.2	≤ 0.3	≤ 0.3	≤ 0.08	Mn, Si, Fe	P265GH	SA-210 Gr.A1 and C	450 / 540	x1
Typically used in economisers, furnace walls, low temp. superheaters, boiler banks								
Low-alloy steels								
0.12 - 0.2	≤ 0.3	≤ 0.3	0.25 - 0.35	Mn, Si, Fe	16Mo3	SA-209 Gr. T1	480 / ~540	x1.3
0.1 - 0.17	0.7 - 1.15	≤ 0.3	0.4 - 0.6	Mn, Si, Fe	13CrMo4-5	SA-213 Gr. T12	550 / ~580	x2
0.08 -0.14	2 - 2.5	≤ 0.3	0.9 - 1.1	Mn, Si, Fe	10CrMo9-10	SA-213 Gr. T22	580 / ~620	x2.5
0.05 - 0.1	2.2 - 2.6		0.9 - 1.1	Mn, Si, V, Ti, B, Fe	7CrMoVTiB10-10	SA-213 Gr. T24	575 / ~620	x3.5
Typically used in furnace walls, superheaters and superheater connection pipes								
High-alloy ferritic steels								
0.08 -0.12	8 - 9.5	≤ 0.4	0.85 - 1.05	Mn, Si, V, Nb, Fe	X10CrMoVNb9-1	SA-213 Gr. T91	600 / ~650	x6
Typically used in superheaters and superheater headers								
Austenitic stainless steels								
≤ 0.035	16 - 18	10 - 15	2-3	Mn, Si, Fe	X2CrNiMo17-12-2	SA-213 TP316L	/ ~800	x4
0.04 - 0.1	17 - 19	9 - 13		Mn, Si, Nb, Fe	X8CrNi19-11	SA-213 TP347HFG	620 / ~800	x9
0.04 - 0.1	24 - 26	19 - 22		Mn, Si, N, Nb, Fe	X6CrNiNb25-20	SA-213 TP310HCbN	650 / ~1000	x12
Typically used in superheaters								

≤ 0.035	18 - 20	8 - 13		Mn, Si, N, Fe	X2CrNi19-11	SA-213 TP304L	/ ~800	x3
0.09	21	11		Si, N, Ce, Fe	1.4835	UNS S30815, 253Ma	/ ~1000	x6
Typically used in superheater ties, vortex finders and tube shields								
Ni-based alloys								
≤ 0.026	20	~60	9	Fe	Alloy 625		/ ~1000	**)
Typically used as cladding material								

*) Maximum scaling temperature is limited in some boiler applications considering the cost-effective use.

**) Alloy 625 is widely used in boiler applications as cladding material in OW tubes. Tube price with OW cladding is typically 100-200 €/m depending on the tube outside diameter and cladding thickness.

2.6. Concluding remarks from the literature

Combustion of different waste fuel fractions, such as recycled wood, is known to cause severe corrosion problems mainly in furnace walls but also in other lower-temperature heat transfer surfaces. Because recycled wood contains elevated concentrations of heavy metals, Cl and alkali metals, the formed ash will have low melting temperatures. For example, a mixture consisting of $ZnCl_2$, KCl and NaCl can have a first melting temperature of 203 °C. Thus, the corrosion mechanism caused by heavy metal-including salts is often referred to as molten phase corrosion. The salt melt reacts with the steel oxide dissolving it into the molten salt as soluble metal chlorides and causing a so-called fluxing mechanism. The mechanism releases Cl, which can chlorinate the metal further. It is proposed that eutectic melt forms between the salt/deposit and the metal chloride. The rate determining factor was reported to be the solubility of metal chloride in molten salts. Many of the reported tests in which the molten phase corrosion mechanism has been studied are performed at rather high temperatures, above 400 °C, whereas furnace wall temperatures are usually lower.

While $ZnCl_2$ and $PbCl_2$ have both proven to be corrosive in laboratory-scale tests, $PbCl_2$ was found to be more corrosive. Their corresponding oxides are not corrosive in the temperatures of the furnace walls or lower-temperature superheaters. Boiler deposits in the areas where furnace wall corrosion has been observed, are often found to consist of mixtures of alkali chlorides and heavy metal chlorides, rather than solely of heavy metal chlorides. According to thermodynamic modelling, ZnO and the double salts, K_2PbCl_4, KPb_2Cl_5 and K_2ZnCl_4 are predicted as condensed phases

during recycled wood combustion under oxidising conditions. However, their formation mechanism, corrosivity, and behaviour have not been studied in the literature. In identifying the most suitable materials, it is crucial to understand the initial reasons for the corrosion. Ni-based alloys have proven to be a good option against corrosive environments; however, their higher costs dictate that their use must be considered carefully.

Zn and Pb are reported to be easily vaporised during combustion and their tendency to form chlorides is known. According to thermodynamic calculations, $PbCl_2$ and $ZnCl_2$ are both predicted to be stable in certain concentrations under oxidising and reducing conditions. The major part of the Zn in the oxidizing part of the furnace is predicted to be in the form of solid ZnO. Only low amounts of gaseous $ZnCl_2$ is expected to be present in the upper part of the furnace; due to a low condensation temperature, it is predicted to condense at the cold end of the flue gas channel. In the case of Pb, which is expected to be present mainly as gaseous PbO and $PbCl_2$, condensation of its quite stable chloride is possible at somewhat higher temperatures compared to Zn.

Some inaccuracies have been observed in the prediction of Pb compounds with thermodynamic modelling. According to the modelling, the major part of the Pb during SRF combustion was predicted to be in the form of gaseous PbO and solid $PbSO_4$ under oxidising conditions. However, Pb was found as $PbCl_2$ based on the fine particle measurements and collected boiler deposits. In addition, a newly-developed laser measurement technique detected rather low levels of gaseous $PbCl_2$ during combustion of recycled wood. One formation route for the double salts K_2PbCl_4 and KPb_2Cl_5 is through $PbCl_2$ (g, l, s) and KCl (g, s) to form gaseous $KPbCl_3$. Formation of $KPbCl_3$ may affect $PbCl_2$ stability during combustion. So far, the thermodynamic data for gaseous $KPbCl_3$ has not been included in the thermodynamic database.

3. Experimental methods

A specific set of measurement methods was used to study the behaviour and form of Pb in different parts of a boiler firing recycled wood. Fine particle measurements were used to study the condensable salts and other fine ash particles in a BFB boiler furnace. The effect of flue gas temperature on the existence and corrosivity of Pb containing compounds was studied with corrosion probes in different parts of a CFB boiler. Both, short-term deposit probes and long-term corrosion probes were used. The information obtained from full-scale measurements and deposit samples was further utilised in simplified laboratory-scale tests. Laboratory corrosion oven tests were used for more detailed corrosion mechanism studies with different materials and temperatures under different Pb-including deposit mixtures. Finally, knowledge gained from full- and laboratory-scale measurements was utilized in thermodynamic modelling. The FactSage-program was used for calculating phase diagrams and evaluating the presence of gas-, solid- and liquid- phases.

3.1. Laboratory-scale experiments

3.1.1. Isothermal corrosion experiments

Some of the corrosion tests were carried out in a tube furnace under isothermal conditions. The method was used in three papers (**Papers II, IV and V**) to study the corrosivity and behaviour of Pb-compounds mixed with other deposit constituents. The steel materials studied were carbon steel (P265GH), two low-alloy steels (16Mo3 and 10CrMo9-10) and Ni-based alloy (Alloy 625). Their standard compositions are presented in Table 4. Test pieces of 20 × 20 mm with a thickness of 5 mm were first ground with ethanol using a 600 and then a 1000- or 1200-grit silicon carbide (SiC) paper. After the final grit, the pieces were cleaned in an ultrasonic bath. In most of the tests, the test pieces were pre-oxidised at 200 °C for 24 hours. One test was performed without pre-oxidation in order to study how pre-oxidation affects possible corrosion and corrosion mechanisms (**Paper V**). Portions of the deposits were pre-melted for 30 minutes before testing as a standard procedure. Pre-melting was performed at different temperatures depending on the melting points of the different mixtures, e.g., the $PbCl_2$-K_2SO_4 pre-melting temperature was 500 °C. This procedure ensured proper mixing of the different deposit components. However, when studying the interaction of $PbCl_2$ with other deposit constituents, pre-melting of the deposit was not

performed (**Papers IV and V**). All the deposit mixtures were ground before the tests.

The edges of the sample piece were covered with a protective paste to prevent the molten salt from falling off the sample surface as presented in Figure 8. After the sample preparation, each test piece was covered with a deposit mixture (0.25 g/specimen). The deposit mixtures used were composed of $PbCl_2$ and different mixtures that included $PbCl_2$, presented in Table 5. In addition, pure K_2SO_4 was used in one test. Exposure times varied from 24 hours to 168 hours (7 days) and temperatures varied between 300 °C and 375 °C. The experiments were carried out in either ambient air or in synthetic air mixture containing 100 ppm HCl and/or 20 vol-% H_2O.

Table 5. Tests carried out in isothermal corrosion oven.

Deposit	Atmosphere	Temperature [°C]	Time [h]	Material	Notes	Paper
100 K_2SO_4 (wt-%)	ambient air	350	24	16Mo3	Samples pre-oxidised and deposits pre-melted	II
50 $PbCl_2$ – 50 K_2SO_4 (wt-%)	ambient air					
50 $PbCl_2$ – 50 SiO_2 (wt-%)	ambient air					
33.3 $PbCl_2$ – 33.3 KCl –33.3 $FeCl_2$ (wt-%)	ambient air	300, 340	8	P265GH	Samples pre-oxidized, no pre-melting of the deposit	IV
5 $PbCl_2$ – 95 $PbCl_2$ (wt-%)	ambient air	310, 325, 350, 375	168	16Mo3, 10CrMo9-10, Alloy 625	Samples pre-oxidised and deposit pre-melted	IV
50 $PbCl_2$ – 50 KCl (mol-%)	100 ppm HCl, 20 vol-% H_2O	300, 340	24	P265GH	Pre-oxidised and not pre-oxidised samples, deposits not pre-melted	V
50 $PbCl_2$ – 50 KCl (mol-%)	20 vol-% H_2O	300, 340	24	P265GH		V

After the corrosion experiments, the steel pieces were cooled to room temperature outside of the furnace. After the cooling, the samples were placed in a mould, cast in epoxy and cut through the middle to reveal the cross-section. The cross-sections were prepared for Scanning Electron Microscope/Energy Dispersive X-ray (SEM/EDX) studies by polishing the

cross-section surfaces in kerosene using 1000, 1200, 2500 (and 4000) grit SiC paper, and then cleaning them in petroleum ether in an ultrasonic bath. The thickness and distribution of the oxide layer were determined using SEM backscatter electron (BSE) mode, Figure 8. Several SEM-BSE images were combined to form a panoramic image, which was digitally treated by using contrast differences.

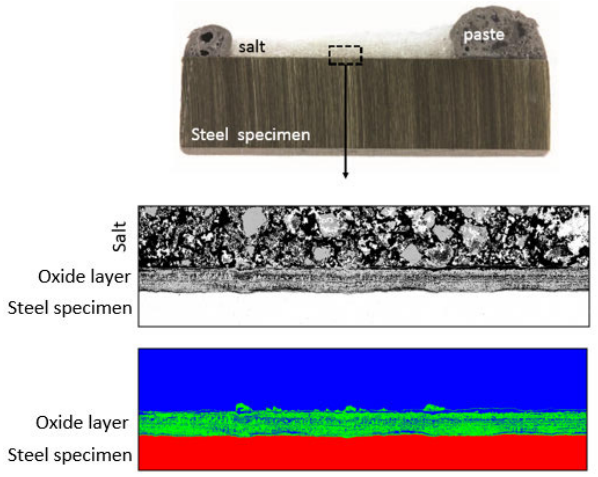

Figure 8. A steel sample covered with synthetic salt (upper), cross-section of the exposed sample (middle) and SEM-panorama image (lower) for determination of oxide layer thickness.

After the panoramic images were coloured, the thickness of the oxide layer was determined for each vertical line of pixels and was recalculated to µm, Figure 9. Mean, median, most occurring and maximum values were determined. The severity of the corrosion was determined by the oxide layer thickness using the mean value. An oxide layer greater than 20 µm is considered to indicate significant corrosion [18]. The corrosion products were identified with SEM/EDX and also with X-ray diffraction (XRD) (**Paper V**).

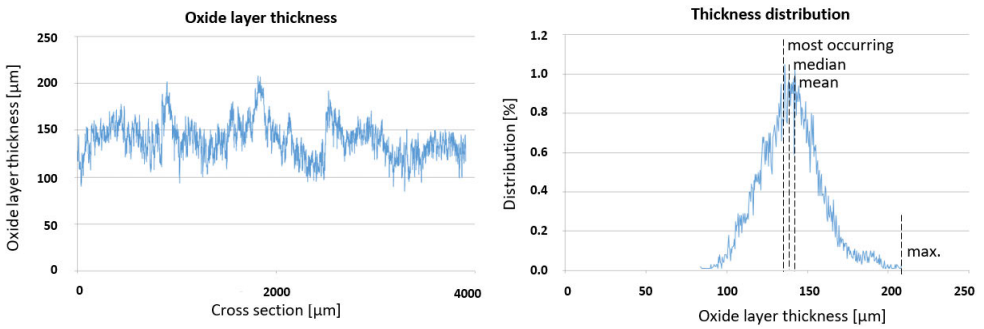

Figure 9. Examples of oxide layer thickness distribution curves.

3.1.2. Corrosion experiments with a temperature gradient over the deposit

Another useful method to simulate boiler conditions in a laboratory-scale studies is to apply a temperature gradient over the deposit [76]. This method enables temperature difference between the exposed steel sample and the gas atmosphere, Figure 10. The difference between the temperatures of a steel sample and a furnace gas results to a relatively steep temperature gradient as in a real boiler environment. It was used to study the reactivity and migration of $PbCl_2$ within the different deposits, Table 6 (**Papers II and III**). The first test was carried out to determine whether $PbCl_2$ reacts with K_2SO_4 when mixed together (**Paper II**). The other test set-up was done to investigate the interaction of gaseous $PbCl_2$ with K and Na salts that are typically found in boiler deposits, with special focus on the formation of corrosive alkali-lead compounds (**Paper III**). The laboratory tests were performed using two synthetic deposit materials that were applied on an air-cooled probe on adjacent alloy samples separated by a heat-resistant barrier. The first deposit component was always $PbCl_2$ and the other was either NaCl, Na_2SO_4, KCl, K_2SO_4, a KCl-NaCl mixture, or inert SiO_2.

Table 6. Test matrix for gradient corrosion tests.

Deposit [wt-%]	Atmosphere	Furnace temp. [°C]	Steel temp. [°C]	Time [h]	Material	Paper
Ring 1: 10 $PbCl_2$ -90 K_2SO_4	ambient air	980	310	24	P235GH	II
Ring 1: $PbCl_2$ Ring 2: SiO_2			200 400	24 4, 24		III
Ring 1: $PbCl_2$ Ring 2: NaCl			400	4, 24		
Ring 1: $PbCl_2$ Ring 2: Na_2SO_4			200, 400	24		
Ring 1: $PbCl_2$ Ring 2: KCl			200, 400	24		
Ring 1: $PbCl_2$ Ring 2: K_2SO_4			200, 400	24		
Ring 1: $PbCl_2$ Ring 2: 50 KCl-50 NaCl			200, 400	24		

Instead of square-shaped steel pieces, ring-shaped samples were used. The material used was a carbon steel (P235GH). An air-cooled probe with sample rings (max. two sample rings at a time) was inserted into a tube

furnace. The corrosion probe consists of a probe and a protective tube, Figure 10. The protective tube surrounds the whole probe except for a window exposing part at the location of the steel rings. The outer protective tube was mounted on the air-cooled probe in order to reduce the probe cooling effect on the furnace, resulting in more stable temperatures. The inner probe has two removable sample rings, which are equipped with thermocouples. Cooling started as the probe material reached the target temperature (200-400 °C). Roughly 0.5 g of the deposit mixture was applied on top of each ring on an area of about 10 mm × 20 mm. It corresponded to a thickness of about 5 mm of deposit prior to the experiment. The edges of the application area on the rings were surrounded by a protective paste to hold the deposit in place in case of melting of the deposits.

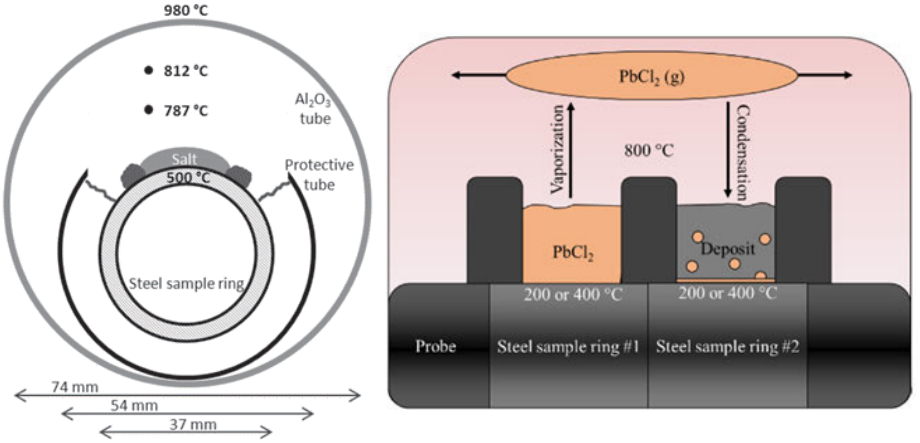

Figure 10. A schematic presentation of the temperature gradient experimental procedure (Paper III).

The temperature of one of the test rings on the probe was regulated with a proportional-integral-derivative controller (PID controller) to adjust the flow of the cooling air. The temperature of the other test ring was monitored and logged during the experiment. Typically, a difference of 5-10 °C is formed between the rings. The furnace set temperature was 980 °C, which gave a gas temperature of around 700-800 °C about 1 cm above the deposit. This resulted in a temperature gradient across the deposits around 50 °C/mm in the radial direction. Two deposits were pre-melted (50 KCl-50 NaCl: 800 °C for 30 min and 10 $PbCl_2$-90 K_2SO_4: 500 °C for 30 minutes) and all the deposits were ground and sieved before the experiments. After each exposure, the probe was cooled rapidly to room temperature and the deposit was glued to the sample ring with a small amount of epoxy. Once the epoxy

was set, the sample piece was cast wholly in epoxy, and cut through for SEM/EDX studies as was done with the isothermal test samples, Figure 8.

3.2. Full-scale measurements

Full-scale measurements were carried out in a 120 MW_{th} CFB boiler and in a 63 MW_{th} BFB boiler, both firing recycled wood (**Papers I and IV**), Figure 11. The purpose was to study the behaviour and form of Pb in different parts of the boiler by means of probe- and fine particle measurements. Short-term deposit probe and long-term corrosion probe measurements were carried out in different parts of the boilers. Fuel samples were collected from both boilers during the measurement campaign.

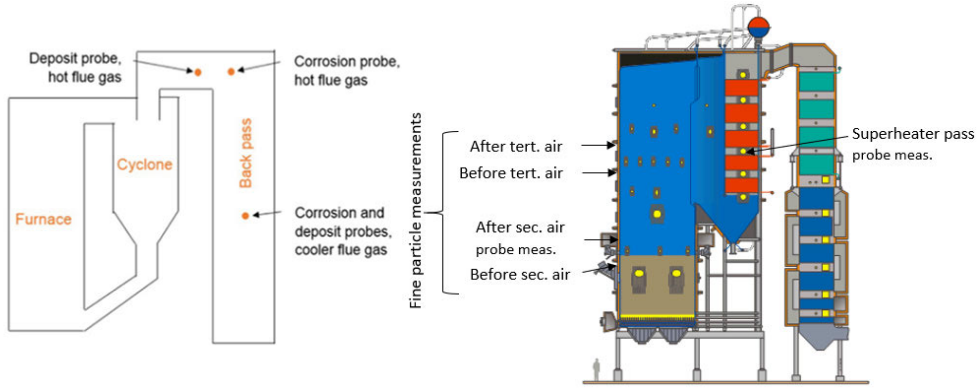

Figure 11. Cross-sections of CFB and BFB boilers firing recycled wood. Probe and fine particle measurement locations are described in the pictures (Papers I and IV).

In the CFB boiler, the effect of flue gas temperature on corrosion was studied (**Paper I**); thus, the deposit and corrosion probe measurements were carried out in the hotter flue gas area (T_{fg} ~800 °C) located in the upper part of the back pass and in the cooler flue gas area (T_{fg} ~490 °C) in the lower part of the back pass, after the boiler bank. The material temperature in each case was adjusted to 360 °C. A tube deposit sample was collected from the superheater area with a sharp knife into a plastic bag (**Paper III**). The bag was closed tightly to prevent humidification of the sample. The superheater material temperature at the sampling location was around 400-420 °C and the flue gas temperature was around 850 °C. A cross-section of the deposit sample was prepared for SEM/EDX analyses.

In the BFB boiler (**Paper IV**), the short-term deposit probe measurements were done after the secondary air feed (T_{fg} ~950 °C) and from the superheater

pass (T_{fg} ~690 °C). Material temperatures were adjusted to 262 °C and 350 °C, respectively. In addition, an uncooled deposit sample was collected after the secondary air. Fine particle samples were collected from four different locations of the furnace: before and after the secondary air inlets and before and after the tertiary air inlets. The flue gas temperatures were measured with a K-type thermocouple corrected with a factor of 1.05 for radiation. The temperature measurements with the thermocouple, especially in the furnace area, may result in considerable inaccuracies. Thus, the temperatures presented are only indicative and the values in the secondary and tertiary air areas may be assumed to be higher. The fuel was fed into the boiler from the front wall. Secondary air was fed from the front and rear walls and tertiary air from the right and left walls. Ammonia feeding was used for SNCR of NO_x emission. Most of the measurement connections in the furnace were located in the right/front corner of the furnace.

3.2.1. Short-term deposit probe measurements

An air-cooled deposit probe was used to collect the initial deposit coming into contact with the steel material (**Papers I and IV**), Figure 12. The ring temperature was adjusted to the desired value with cooling air and monitored with a thermocouple drilled into the material ring and connected to a regulator unit. The thermocouple measuring the flue gas temperature was placed outside of the ring. Elemental composition of the deposits was measured, analysed and evaluated. One ring was exposed at a time and the testing time was two hours. The ring material was made of austenitic stainless steel (SA-213 TP310HCbN) to minimise eventual reactions between the collected deposit and the probe material.

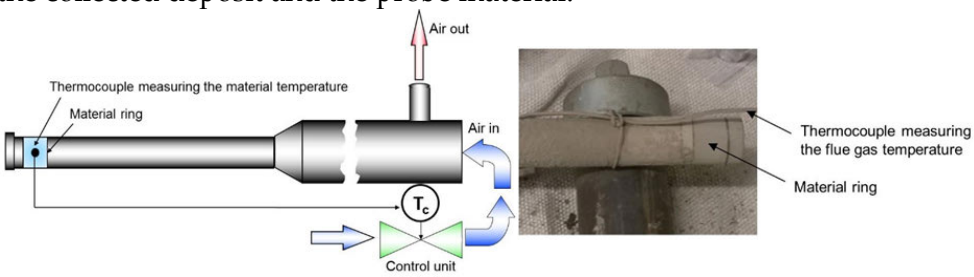

Figure 12. A schematic sketch of the deposit probe (on the left) and a close-up photo of the short-term deposit ring after the exposure (on the right) (Paper I).

The deposit was scratched off from three different locations for chemical analysis after the exposure. The deposits from the wind, side and lee

positions were placed onto a carbon tape and studied with SEM/EDX, Figure 13.

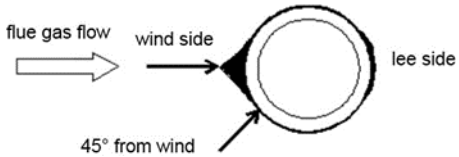

Figure 13. The locations of the collected deposit samples taken for chemical analysis (Paper I).

In addition, the compositions of the wind-side locations were analysed by means of XRD to identify the compounds in the deposits. The XRD analyses were carried out with a Bruker-AXS D8ADVANCE X-ray diffractometer. The compounds were identified using DIFFRAC. EVA [117] with the PDF-2 database [118].

3.2.2. Long-term deposit probe measurements

The purpose of the long-term corrosion probe measurements was to evaluate the effect of flue gas temperature on corrosivity. The corrosion probe's working principle is similar to that of the deposit probe described above, Figure 12. The test material used in the corrosion probes was low-alloy steel (16Mo3). The measurement time was five months.

After the exposures, the corrosion probe rings were cut in half along its radial direction. The one half was mechanically cleaned while the other half was polished and prepared for SEM/EDX analyses. The ring wall thicknesses were measured before and after the exposure from the mechanically cleaned sample half around the ring. The measurements were carried out with a device designed for this purpose, Figure 14. Cross-sections of the uncleaned sample were cast in epoxy and polished with SiC paper to a grit of 4000. Polishing occurred without the water-containing lubricants to avoid dissolving the chlorides. After grinding, the samples were sputtered with carbon, then placed in the SEM/EDX and analysed with the secondary electron detector using a voltage of 20 keV.

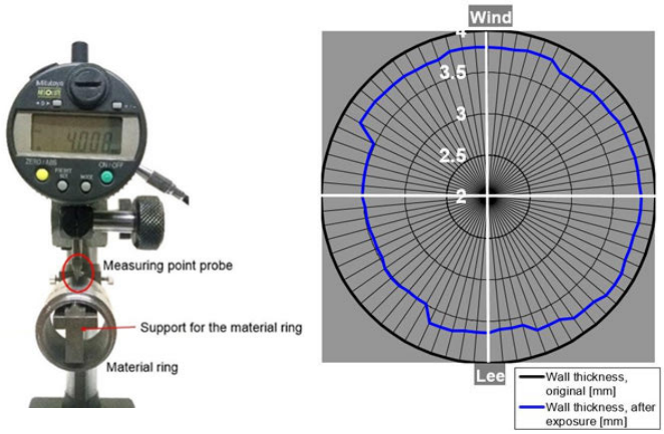

Figure 14. A device used for the wall thickness measurements (on the left) and an image of the measured wall thickness values (on the right) (Paper I).

3.2.3. Fine particle measurements

Fine particle measurements were carried out in the BFB boiler with the help of VTT (**Paper IV**), Figure 15. The method forces gaseous, condensable compounds to form aerosols, which based on aerodynamics are size fractionated and samples on impactor plates [119]. These impactor plates were then further analysed by mass and composition. The sample was sucked into a sampling probe and diluted and quenched with nitrogen (N_2) and sulphur hexafluoride (SF_6). SF_6 was used as a tracer for determining the dilution rate. The diluted sample gas was then again further diluted with N_2 in an ejector before a cyclone and the Dekati Ltd. -type low-pressure mass impactor (DLPI). DLPI is a 13-step cascade impactor which collects and classifies the fine particles with aerodynamic diameters (d_{ae}) between 0.03 and 10 μm. Before the fine particle number impactor (ELPI, electrical low-pressure impactor), the gas was led through a cyclone and once more diluted with N_2 in an ejector. ELPI reveals the number of particles on the different stages online.

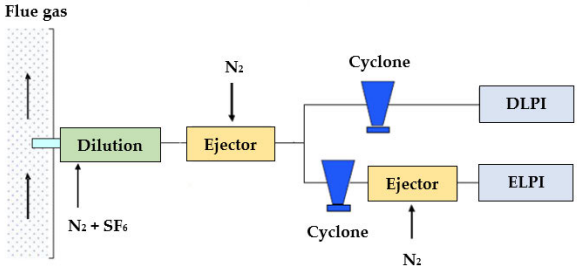

Figure 15. A schematic picture of the fine particle sampling system. Courtesy of VTT.

Particles smaller than 1 μm are known to be in gaseous form and hence the impactor stages containing these particles are of interest [37]. The fine-mode cut size, dp, of DLPI used in this work was 1.6 μm. The mass impactor collects the particles on the plates, from which sample mass and composition are analysed after the sampling. Two parallel samples were collected from each measurement location for the water- and acid leaching. The leaching gives further information on the possible compounds present in the impactor samples. K, Na, Ca, Pb and Zn as well as Cl^-, SO_4^{2-} and bromine (Br) were found in the water-leached fraction, while in the acid-leached fraction a number of 31 elements were found. K, Na, Ca, Zn and Pb concentrations were determined with an inductively coupled plasma mass spectrometer (ICP-MS) while SO_4^{2-} and Cl^- were determined with ion chromatography (IC).

3.3. Thermodynamic modelling

Solidus projections were calculated for the $PbCl_2$-KCl-NaCl (**Paper I**) and $FeCl_2$-KCl-$PbCl_2$ (**Paper II**) systems using FactSage version 7.1 [90]. The thermodynamic data were taken from the FTsalt database, which has been developed for various molten and solid salt mixtures. The thermodynamic data for the $PbCl_2$-KCl-NaCl system have been assessed and optimised on available experimental thermodynamic and phase equilibrium data from the literature by the developers of FactSage. However, the thermodynamic assessment has not been published in the scientific literature. The ternary $FeCl_2$-KCl-$PbCl_2$ system has not been evaluated and compared with experimental data. The binary KCl-$FeCl_2$ system has been evaluated by Robelin et al. [120], and the binary KCl-$PbCl_2$ has been optimised but not published, based on the documentation of FactSage.

The stable gaseous and condensed phases of Pb including compounds during recycled wood combustion were studied with FactSage version 7.2 (**Paper IV**). The thermodynamic databases used in the calculations were the FTsalt databases for the alkali salt phases, and the FactSage pure substance database for the gas components and other solid compounds. In addition, thermodynamic data not available in the commercial FactSage databases were used for the interaction of alkali salts with Ca and Mg compounds in the molten salt phase. Thermodynamic data for $PbCl_2$, $ZnCl_2$ and $FeCl_2$ from the FTsalt databases were also combined with the other data for molten salts. Parts of these data have been published by Lindberg and Chartrand [121] and discussed in the review paper of Lindberg et al. [49]. Fuel data gained

from the BFB boiler full-scale measurements were used as an input for the calculations in Table 7.

Table 7. Chemical composition of the fuel collected from the BFB boiler firing recycled wood (Paper IV).

[wt-% d.s.] *if no other unit*	***BFB boiler*** *(100% recycled wood)*
Moisture	28.9
Ash (815°C)	3.3
C	48.7
H	5.9
N	2.1
O (calculated)	39.6
S	0.08
Cl	0.35
LHV dry [MJ/kg]	18.3
Major ash-forming elements [mg/kg d.s.]	
Al	1400
Si	6200
Ti	1600
Na	1100
K	900
Ca	4500
Minor ash-forming elements [mg/kg d.s.]	
Pb	210
Zn	240

The calculations were carried out with $\lambda = 1.2$, thus considering locations after the secondary air feed in the boiler. Two new gaseous phases, $KPbCl_3$ and $NaPbCl_3$, were added to the database since they, as mentioned in Chapter 2.6, might be formed during recycled wood combustion. Thermodynamic data for $KPbCl_3$ and $NaPbCl_3$ were fitted to reproduce experimentally measured partial pressures of $KPbCl_3$ and $NaPbCl_3$ in equilibrium with molten KCl-$PbCl_2$ and NaCl-$PbCl_2$, respectively [122]. The calculations were based on previously unpublished $KPbCl_3$ and $NaPbCl_3$ thermodynamic data.

3.3.1. DSC/TGA-experiments

Differential scanning calorimetry/thermogravimetric analyses (DSC/TGA) were used to study the melting temperatures of binary or ternary mixtures of KCl, $PbCl_2$ and $FeCl_2$ (**Paper II**). A TA Instruments SDT Q600 simultaneous DSC/TGA apparatus was used in the experiments. The

reagents for the mixtures were anhydrous pro analysis KCl, $PbCl_2$ and/or $FeCl_2$; about 15 mg of the mixtures were added to an alumina cup for the experiments. The experiments were done in nitrogen with a flow rate of 100 ml/min; the heating/cooling rate was 10 °C/min. After the initial heating to the maximum temperature, two cooling/heating cycles were conducted. The maximum temperature was 400 °C for the experiments with KCl, and 500 °C for the $PbCl_2$-$FeCl_2$ mixture. The maximum temperature was kept low to ensure minimal vaporisation of the salts but high enough to achieve a completely molten mixture based on pre-calculations. The results from the first heating ramp were not considered, due to the heterogeneous nature of the unmelted samples. In the subsequent cooling/heating cycles, the sample mixture can be assumed to be homogenised and close to the expected phase equilibria. For simple DSC peaks, the onset temperature was considered to be the relevant transition temperature. For complex peaks, the peak or inflection temperatures were also considered. These temperatures typically coincide with the liquidus of the system.

4. Results and discussion

4.1. Presence and form of lead in the furnace

The presence of Pb in the furnace was studied by performing fine particle measurements in a full-scale BFB boiler firing recycled wood (**Paper IV**). Measurement locations were situated before and after the secondary air inlets and before and after the tertiary air inlets. Parallel samples were collected from each point for water and acid leaching. The concentrations of water-soluble elements in the collected fine particle samples are presented for each of the measurement locations in Figure 16. Particle size distribution is on the x-axis and elemental concentration on the y-axis.

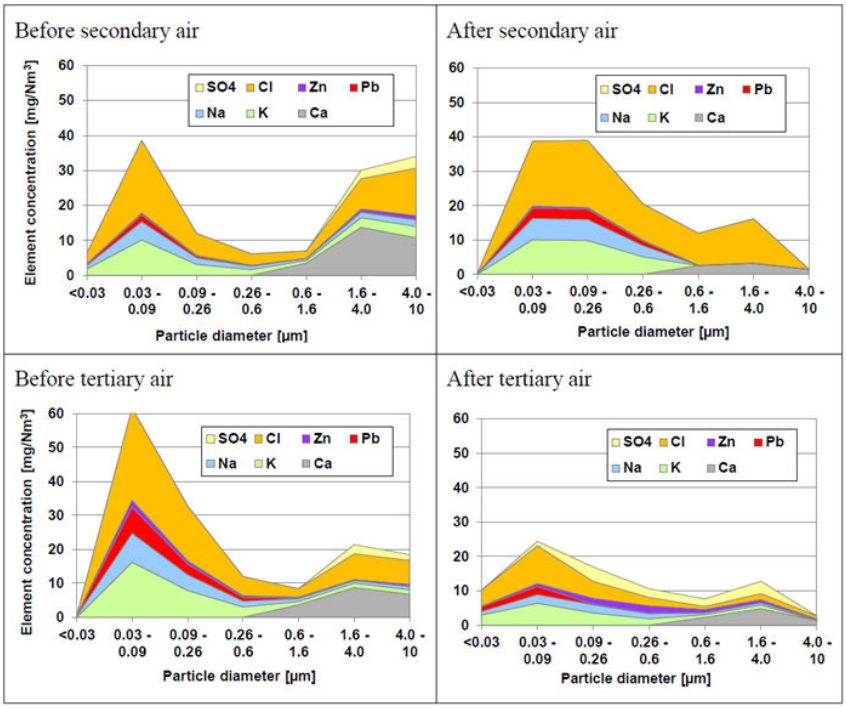

Figure 16. Concentrations of water-soluble elements in fine particle samples collected from the measurement locations. The thickness of each ribbon describes the element concentration (Paper IV).

It can be seen that Na, K and Cl are the main elements when considering fractions < 1.6 µm. In fact, they are the prevailing elements throughout all measurement locations. The concentration of sulphate increases as the Cl concentration decreases after the tertiary air inlet, indicating that some sulphation of chlorides has taken place after the final air inlet. Pb is observed

to be present in all measurement locations, and that the concentration is at its highest between the secondary and tertiary air inlets. This particular location has been reported as one of the problematic areas from the corrosion point of view [123, 124]. As illustrated in Figure 16, the main parts of the Na and K as well as Pb are bound with Cl since sulphates were not present until the tertiary air inlets. Zn was found in quite small amounts; only in the sample after the tertiary air inlet in slightly elevated concentrations.

Pb in forms other than chloride can be calculated by subtracting the water-soluble Pb fraction from the acid-soluble Pb fraction. When considering all the results, the major part of Pb (more than 70 %) is in form of chlorides, Figure 17. The green portions of the columns represent the water-soluble fractions and the blue proportions of the columns represent Pb in forms other than chloride, such as PbO or PbS.

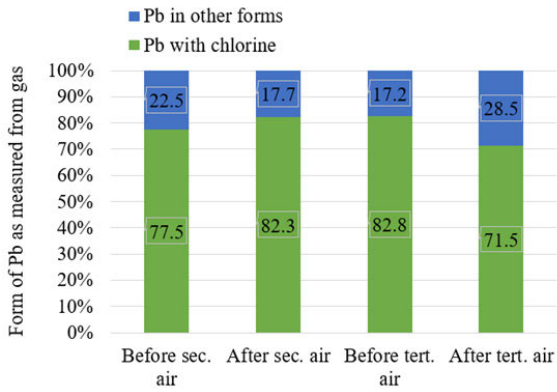

Figure 17. Chemical forms of lead at different measurement locations based on the fine particle measurements (Paper IV).

The results emphasised, that in the areas with observed corrosion, the most dominating compounds are Pb-, K- and Na chlorides. As Pb can be present as gaseous $PbCl_2$, $KPbCl_3$ or $NaPbCl_3$, thermodynamic calculations were performed to study the stable gaseous Pb compounds. The calculations were carried out under oxidising conditions, using the fuel values from the BFB boiler as input data. The new gaseous phases, $KPbCl_3$ and $NaPbCl_3$, were added to the database. The molar distribution of gaseous Pb phases is presented in Figure 18. Temperature is shown on the x-axis and molar distribution fraction of different gaseous compounds on the y-axis.

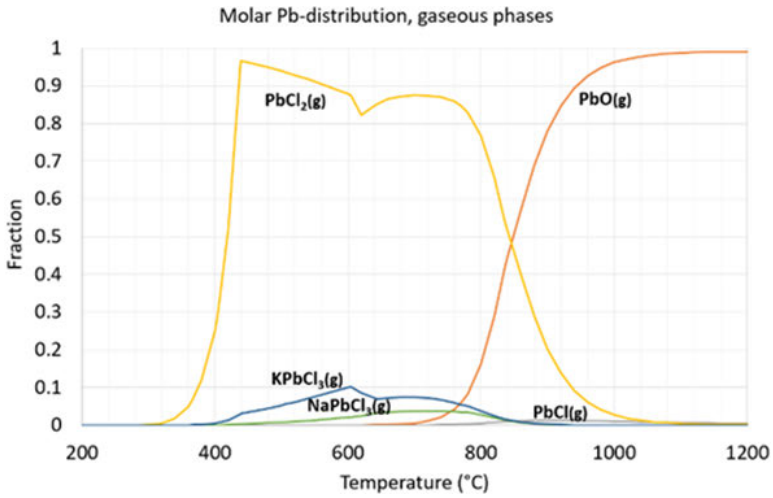

Figure 18. The molar distribution of gaseous Pb phases predicted by FactSage (Paper IV).

The calculations suggest $KPbCl_3$ to be stable between 400 and ~900 °C. The highest share is approximately at 600 °C, which describes the temperature of the superheater pass in a BFB boiler. $NaPbCl_3$ is also suggested to be stable within approximately the same temperature range as $KPbCl_3$, but with a smaller share. The major part of the Pb is suggested to be in the form of $PbCl_2$ between 300 °C and ~850 °C. When considering FB boiler furnace temperatures, PbO is predicted to be the major stable phase. However, this is not supported by the fine particle measurements. Similar differences in the behaviour of Pb between the thermodynamic calculations and full-scale sampling have also been reported by others [52, 53]. According to the calculations carried out in this work, Pb compounds are suggested to be fully oxidised to PbO at ~1200 °C.

4.2. Behaviour of lead in deposits

4.2.1. Short-term deposits

Full-scale deposit probe samples were collected from the CFB (**Paper I**) and BFB boilers (**Paper IV**) firing recycled wood. A detailed characterisation of the samples was carried out with SEM/EDX and with XRD. Cooled deposit samples were collected to study the condensing compounds. An uncooled deposit was collected to reveal the elements coming in contact with the tube surface through mechanisms other than condensation. The results from the wind-side positions were compared with each other, Figure 19. In the BFB boiler furnace, the combustion process at the measurement location in

question is not yet complete; not all the air flows have been introduced, the sulphation process is incomplete and the residence time is shorter compared to the measurement location in the superheater pass and to the CFB boiler measurement locations.

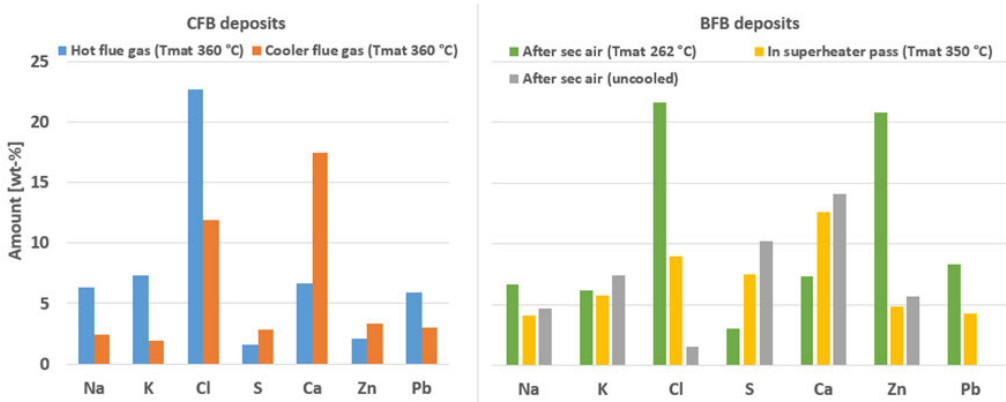

CFB boiler		BFB boiler		
T_{fg} ~800 °C T_{mat} ~360 °C	T_{fg} ~490 °C T_{mat} ~360 °C	T_{fg} ~950 °C T_{mat} ~262 °C	T_{fg} ~950 °C *uncooled*	T_{fg} ~690 °C T_{mat} ~350 °C
NaCl KCl	NaCl KCl	NaCl KCl	NaCl	NaCl KCl
KPb_2Cl_5 $(KPbCl_3)_3{\cdot}H_2O$	KPb_2Cl_5 $(KPbCl_3)_3{\cdot}H_2O$	KPb_2Cl_5 $PbCl_2$, PbO_2		KPb_2Cl_5
$Na_2ZnCl_4{\cdot}3H_2O$	$Na_2ZnCl_4{\cdot}3H_2O$	K_2ZnCl_4, ZnO		

Figure 19. Elements characterised with SEM/EDX and compounds characterised with XRD from the wind side of the short-term deposit probe samples (Paper IV).

In both boilers, NaCl and KCl were identified with XRD from all the cooled deposit samples. NaCl was also identified in the uncooled sample. The share of Cl was significant in each of the analysed deposit samples except for the uncooled one. Cl was present in that sample as well, but at smaller levels. The share of Cl was higher in the samples collected from high flue gas temperature area compared to the samples from lower flue gas temperature.

The XRD results showed that Pb was combined with K and Cl as KPb_2Cl_5 and $(KPbCl_3)_3{\cdot}H_2O$. $KPbCl_3$ does not have a solid form except as a hydrate with crystal water [57, 125]. $(KPbCl_3)_3{\cdot}H_2O$ was not detected in the BFB sample. Instead, small amounts of $PbCl_2$ as well as PbO_2 were detected after the secondary air inlet. As in the case of Cl, the share of Pb decreased when

moving from the hot flue gas temperatures to the cooler temperatures. No Pb was found in the uncooled sample proposing that Pb including compounds come to the surface via condensation.

According to the analyses, Zn was combined with Na or K, as $Na_2ZnCl_4 \cdot H_2O$ in the CFB probe sample and as K_2ZnCl_4 in the BFB sample. The highest share of Zn was observed in the sample with material temperature of 262 °C. Zn was also found in the uncooled sample, indicating that there might be Zn compounds that have come to the surface with a mechanism other than condensation (e.g., impaction of molten or partially molten particles).

Thermodynamic calculations were carried out to predict the condensed phases of Pb-including compounds in the BFB boiler (**Paper IV**). The calculations showed that Pb could be present as KPb_2Cl_5, K_2PbCl_4, $PbCl_2$ or as $PbSO_4$, at temperatures typical to the heat transfer surfaces, Figure 20. Solid KPb_2Cl_5 will be stable at the cooler surface temperatures, below 285 °C. Solid K_2PbCl_4 is predicted to be stable on surfaces with temperatures between 285 °C and 365 °C which represent typical furnace wall temperatures in a boiler with maximum steam pressure of about 100 bar. K_2PbCl_4 was not detected by XRD from the collected deposits; instead, KPb_2Cl_5 was identified from all the cooled deposit samples. The calculations indicate that the highest condensing temperature for solid $PbCl_2$ is ~440 °C. Small concentrations of liquid $PbCl_2$ and $PbSO_4$ are predicted to condense in the multicomponent molten salt phase between 600 °C and 700 °C.

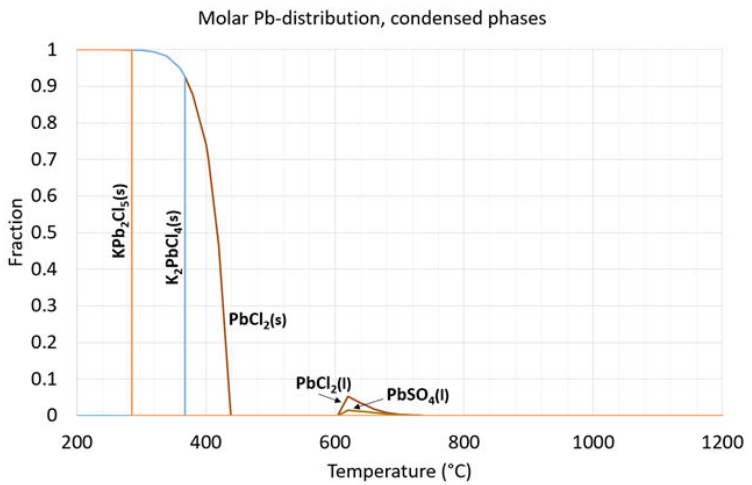

Figure 20. Molar distribution of condensed Pb phases predicted by FactSage (Paper IV).

4.2.2. Long-term deposits

Two five-month corrosion probe measurements were carried out in the CFB boiler to study the effects of flue gas temperature on the deposit composition and on the corrosivity of the deposits (**Paper I**). The set material temperature was in both cases the same, 360 °C, and the flue gas temperatures were 800 °C and 490 °C. During the measurement period, variations in the temperatures were observed. Average temperatures of the sample rings were within two degrees, 358-360 °C. The highest material temperature, 374 °C, of the hot flue gas sample was recorded after two months and the peak lasted for 24 h. The usual variation from the set temperature was no more than +/- 8 °C, if the 24 h temperature peak is not considered. Smaller variations were recorded in the case with the cooler flue gas sample. The maximum material temperature was only four degrees higher than the set temperature, 364 °C. The lowest recorded temperature was 355 °C.

The deposit of the hot flue gas sample was strongly attached to the corrosion probe ring. In contrast, the deposit on the cooler flue gas sample was loose. The thickest deposit layer was located on the wind side of the both rings. High amounts of Pb were found in both probe samples but no Zn was detected. The cross-section of the deposits could be divided into different layers, Figure 21. All the layers were analysed using area analysis with SEM/EDX. Layer 1, closest to the flue gas, consisted mostly of Ca, Cl, K, Na, Fe and oxygen. In the cooler flue gas sample, Pb was also present. When moving closer to the steel surface (layer 2), the amount of Fe was more prevalent and the amount of S decreased. The Cl content increased in the hot flue gas sample, and Pb was also detected. This layer included elements from both the deposit and the ring (corrosion product). Layer 3 consisted of K, Na, Pb and Cl. The composition of layer 3 was almost identical in both the hot and cooler flue gas samples. K was the most predominant alkali metal. Based on the XRD analyses from the short-term deposit samples (Figure 19), the composition was a mixture of NaCl, KCl and K_2PbCl_5. Layer 4 contained Fe oxide and residues of Cl. In the cooler flue gas sample, residues from K and Pb were also detected. Clear signs of $FeCl_2$ (point 5) were observed in the hot flue gas sample. $FeCl_2$ was detected just above the steel surface before the oxide layer, which is a sign that corrosion proceeds via $FeCl_2$ formation. The thickness of the Fe oxide layer underneath the K-Na-Pb-Cl mixture was about 400 μm in the hot flue gas area and roughly 260 μm in the cooler flue gas area.

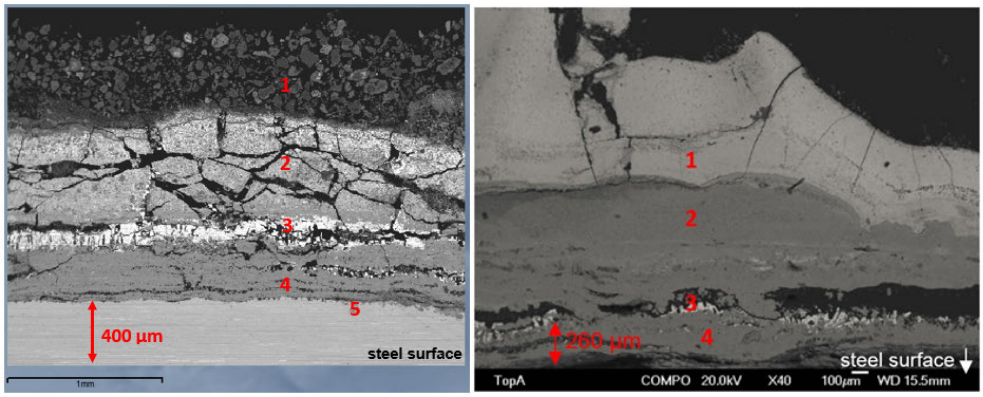

Figure 21. Cross-section and analyses points of the hot and cooler flue gas corrosion probe, wind side (Paper I).

Both rings suffered from severe corrosion. The average measured corrosion rate in the hot flue gas area was ~0.8 mm/year and in the cooler flue gas zone ~0.4 mm/year. The severe corrosion observed in the measurements could be explained by the melt formation as it is known to cause catastrophic corrosion rates. As compounds including Na, K, Pb and Cl were identified from the corrosion probe deposits, a solidus projection for the $PbCl_2$-KCl-NaCl ternary system was calculated with FactSage, Figure 22. Several point analyses were carried out for the K-Na-Pb-Cl areas (point 3 in Figure 21) in the corrosion probe deposits to verify the composition. In order to calculate T_0 values, the elements present in the deposit were determined to form chlorides. Based on the thermodynamics, KCl is the most stable, then leftover Cl reacts with Na and finally with Pb.

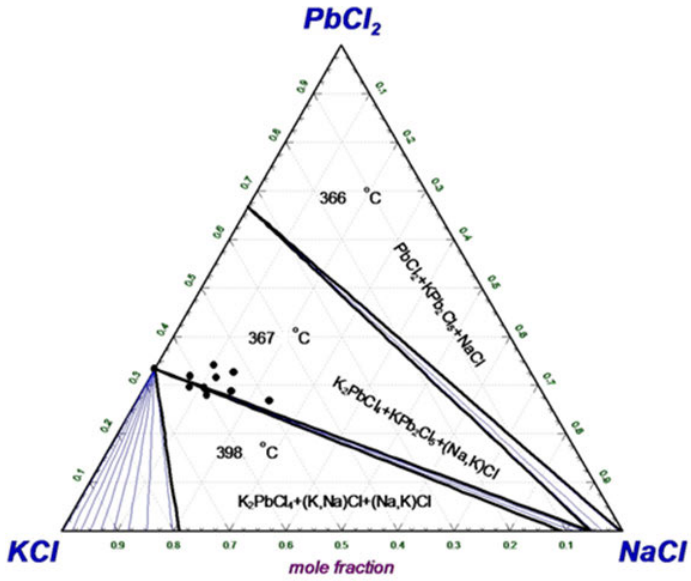

Pb [at-%]	K [at-%]	Na [at-%]	Cl [at-%]	T_0 [°C]	sample
12.44	22.34	4.68	60.53	368	
11.97	24.39	4.4	59.24	392	hot flue gas
11.89	22.79	2.64	62.69	368	sample
14.29	23.32	4.22	58.17	368	
11.81	25.47	5.1	57.62	398	
11.39	24	3.12	61.48	398	
12.97	26.05	0	60.98	483	
11.19	21.53	6.18	61.11	368	cooler flue
13.1	21.21	5.76	59.94	368	gas sample
11.39	21.09	10.08	57.44	368	

Figure 22. Solidus projection of the system $PbCl_2$-KCl-NaCl. Black dots indicate analysed compositions of the hot and cooler deposits presented in the table. The three triangles within the solidus projection show the three solid phases stable at the solidus temperature, and the blue lines show isothermal solidus temperatures (10 °C intervals) in two phase regions (Paper I).

The lowest T_0 of the analysed compositions was 368 °C, which is close to the adjusted probe material temperature (360 °C), indicating that formation of melt could have been possible. Calculated intra-deposit temperature profiles for both the hot and cooler flue gas deposits indicated that formed K-Na-Pb-Cl-including deposits had most probably been molten in the hot flue gas sample but not in the cooler flue gas sample. This could also explain the differences between the corrosivities of the different flue gas temperatures. Theoretical temperature profile calculations were carried out for a cylindrical geometry considering external heat transfer via convection

and radiation in series with conduction through the deposit. Calculations were carried out using deposit surface total emissivity of 0.75 [126] and deposit thermal conductivity of 1.0 W/m-K. A deposit thickness of 2 mm was assumed.

The morphology and structure of a deposit taken from the superheater area of a recycled wood firing CFB boiler were similar to those from the deposits collected with the corrosion probes (**Paper III**), Figure 23. The tube side of the deposit had a dense and layered structure whereas the flue gas side was coarser. Two distinct alternating layers were recognised with SEM/EDX in the lower part of the deposit: Fe oxide (point 4) and K_2PbCl_4 (point 3). Above these alternating layers, a KCl-NaCl mixture was detected (point 2). The uppermost part of the deposit was composed of a mixture of several elements: Na, S, Cl, K, Ca, Fe, Pb, Al and Si (point 1 and area analysis). No Zn was present. Here, as well as in the probe deposits, Na is found as NaCl but K with Cl and Pb. The cracks in the oxide layer were filled with a Pb-including compound, which served as a good pathway towards the steel surface.

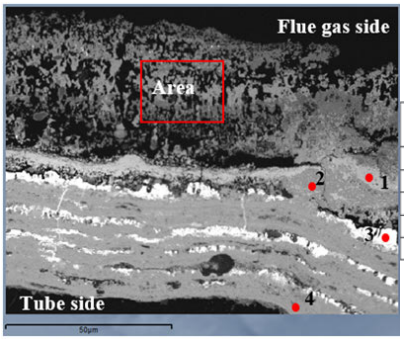

	O	Na	S	Cl	K	Ca	Fe	Pb	Si	Al	Compound
					atomic-%						
Area	43.7	7.4	6.1	20.2	15.6	4.1		0.5	1.3	1.0	Mixed
1	59.2	5.1	11.8	5.6	8.9	54		3.3	0.7		Mixed
2		11.9		50.1	38.0						NaCl, KCl
3				60.3	27.7			12.0			K_2PbCl_4
4	54.5						45.5				Iron oxide

Figure 23. Cross-section with SEM/EDX-results of a collected superheater deposit from a recycled wood fired boiler (Paper III).

4.2.3. Laboratory-scale deposits

As reported, Pb was found together with K and Cl in the full-scale boiler samples and thermodynamic calculations predict the existence of condensed K_2PbCl_4 and KPb_2Cl_5. The formation routes for K_2PbCl_4 (s) and KPb_2Cl_5 (s) compounds can be assumed to occur via $PbCl_2$ (g, l, s) and KCl (g, s) or via $KPbCl_3$ (g) and KCl (g, s); the formation of these compounds within the deposits was studied in the laboratory (**Papers II and III**). Isothermal experiments were carried out with a mixture including pure K_2SO_4 or 50 wt-% $PbCl_2$ mixed with either 50 wt-% K_2SO_4 or 50 wt-% SiO_2 (**Paper II**). SiO_2

was selected as the other mixture component due to its low reactivity and to have equal amounts of $PbCl_2$ as weight-% in both deposits. K_2SO_4 was of interest because it is considered non-corrosive below 500 °C [127]. The steel used in the experiments was low-alloy steel (16Mo3) and the temperature was set to 350 °C. The $PbCl_2$-K_2SO_4 mixture was pre-melted before the experiments.

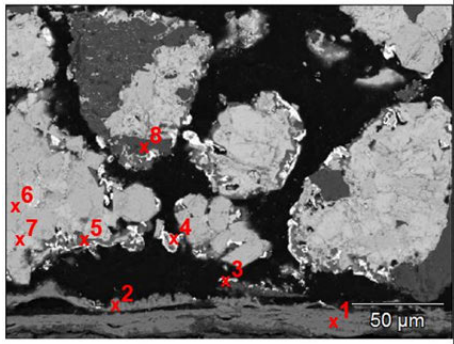

Location	O [at-%]	S	Cl	K	Fe	Pb	Mo
Point 1: **iron oxide**	56.3	res.	res.	-	42.8	res.	-
Point 2: **iron oxide**	56.5	-	1.8	-	40.7	res.	res.
Point 3: **not identified**	40.9	-	18.9	11.1	2.2	23.2	-
Point 4: **not identified**	25.5	-	29.5	8.7	2.0	33.0	1.3
Point 5: **KCl**	14.5	res.	43.6	39.4	res.	1.2	res.
Point 6: **$K_3Pb_2(SO_4)_3Cl$**	53.0	15.1	6.0	15.5	res.	9.4	res.
Point 7: **K_2PbCl_4**	7.4	-	54.4	24.6	res.	12.8	res.
Point 8: **K_2SO_4**	57.2	15.4	res.	26.8	-	res.	-

Figure 24. Cross-section of the sample after exposure with 50 wt-% $PbCl_2$ and 50 wt-% K_2SO_4 mixture on 16Mo3 at 350 °C. Concentrations below 1 at-% are marked as residue, "res." (Paper II).

An Fe oxide layer covered the steel surface (point 1), Figure 24. Above this, another, thinner Fe oxide layer with residues of Cl was detected (point 2) indicating $FeCl_2$ formation as part of the corrosion process. The white areas (points 3 and 4) were composed of Pb, Cl, K and oxygen, and also Mo in point 4. These layers are mixed phases and it is difficult to conclude which compounds are present based on the SEM/EDX analyses. Several greyish areas were observed within the deposit particles. It seems that several different phases were formed due to the interactions between $PbCl_2$ and K_2SO_4 since the compositions of the greyish areas varied significantly. One area consisted mainly of KCl with residues of $PbCl_2$ (point 5) while another area had a composition corresponding to $K_3Pb_2(SO_4)_3Cl$ (point 6). This caracolite-type $K_3Pb_2(SO_4)_3Cl$ compound was detected for the first time in combustion related studies according to the author's knowledge. A similar compound, caracolite $Na_3Pb_2(SO_4)_3Cl$, has been earlier identified and reported by Enestam et al. [128]. Point 7 had an elemental composition corresponding to a K_2PbCl_4 compound, while the dark grey areas were

determined to be K_2SO_4 (point 8). The interaction between the salt particles consisting of $PbCl_2$ and K_2SO_4 was clearly shown with these laboratory tests.

Given the clear interactions based on the above-presented results, vaporisation and condensation of $PbCl_2$ as well as its interaction within deposit with different salts were further studied with a temperature gradient experimental method (**Paper III**). Two different synthetic deposits were applied on two different rings. Ring 1 contained $PbCl_2$ and ring 2 contained either SiO_2, NaCl, Na_2SO_4, KCl, K_2SO_4 or KCl-NaCl (50:50 wt-%). Ring temperature was set either to 200 °C or 400 °C and the exposure times were 4 h and 24 h. The furnace set temperature was 980 °C. The steel used in the experiments was carbon steel (P235GH).

The experiments showed that $PbCl_2$ vaporises from ring 1 and condense to adjacent ring at both test temperatures. $PbCl_2$ was observed to migrate within deposit and react with Na_2SO_4, KCl and K_2SO_4. In contrast, no interactions with NaCl or with SiO_2 were observed. $PbCl_2$ interaction with KCl resulted K_2PbCl_4 formation. In this case no $PbCl_2$ was observed because all the Pb and Cl were associated with K. $PbCl_2$'s interaction with alkali sulphates resulted in the formation of caracolite, $Na_3Pb_2(SO_4)_3Cl$, and the caracolite-type compound $K_3Pb_2(SO_4)_3Cl$, as well as NaCl and KCl, respectively. $K_3Pb_2(SO_4)_3Cl$ interaction further with KCl, resulted K_2PbCl_4 formation. A summary of the observed interactions and compounds at 400 °C are presented in Table 8.

Table 8. Resulted compounds with different deposit material and Pb-compounds within and on top of the oxide layer at 400 °C.

Initial deposit material on Ring 2	**Compounds after interaction with the $PbCl_2$ deposit**	**$FeCl_2$ observed**	**Pb-compounds within the oxide layer**	**Pb-compounds on the oxide layer**
SiO_2	No interaction	yes	$PbCl_2$	$PbCl_2$
NaCl	No interaction	yes	$PbCl_2$	$PbCl_2$
Na_2SO_4	$Na_3Pb_2(SO_4)_3Cl$ + NaCl	yes	$PbCl_2$	$PbCl_2$, $Na_3Pb_2(SO_4)_3Cl$
KCl	K_2PbCl_4	yes	K_2PbCl_4	K_2PbCl_4
K_2SO_4	$K_3Pb_2(SO_4)_3Cl$ + KCl → K_2PbCl_4	no	K_2PbCl_4	K_2PbCl_4
KCl + NaCl	NaCl + K_2PbCl_4	yes	K_2PbCl_4	K_2PbCl_4

The experiments with NaCl showed that $PbCl_2$ migrates from ring 1 to, and within, the deposit via the gas phase, Figure 25. No common solid Na-Pb-Cl was formed; however, indications of melt formation by sintered

particles within the deposit was observed at 400 °C. In the experiments with KCl-NaCl (50:50 wt-%) deposit, the results showed that $PbCl_2$ interacts with KCl, forming K_2PbCl_4, but not with NaCl, Figure 26. A similar behavior was observed in the deposit probe measurements, Figure 19, and with the collected superheater deposit, Figure 23. XRD analyses revealed the common compound with K and Pb but not with Na. Na was found as NaCl and K as KCl and as KPb_2Cl_5.

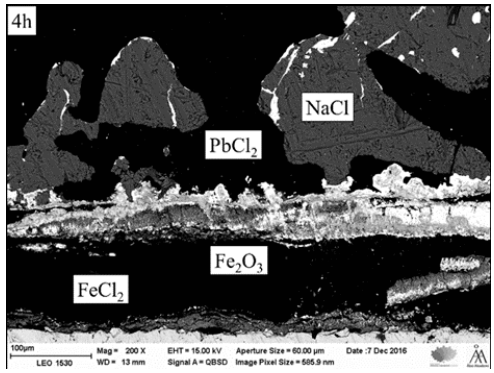

Figure 25. SEM backscatter images of corrosion layers below NaCl deposit at 4h/400 °C (Paper III).

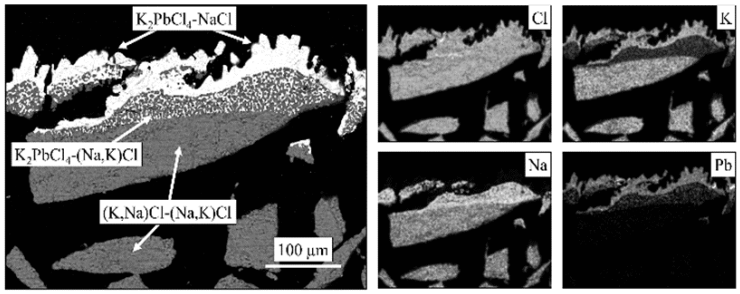

Figure 26. SEM backscatter image and EDX maps of a salt particle in the outer part of the KCl-NaCl deposit in the 24 h/200 °C experiment. The image shows that Pb is enriched on the furnace-facing side of the salt particles and that it has penetrated the original salt particles, resulting in K-depleted areas (Paper III).

Formation of $FeCl_2$ was observed in the steel-oxide interface in each of the cases at 400 ° except with K_2SO_4. In that case, $FeCl_2$ was not clearly observed but its presence could not be completely rule out. An Fe oxide layer with some $PbCl_2$ was observed above the $FeCl_2$ layer in the samples. The presence of $FeCl_2$ supports active oxidation corrosion mechanism theory and is in line with already presented test results.

4.3. Corrosivity of lead-including deposits

Corrosion layer thicknesses of the temperature gradient samples were only measured after the experiments at 400 °C (**Paper III**), since no significant corrosion was observed in the experiments at 200 °C. All the measured corrosion layer thicknesses were high considering the testing time of only 24 hours, Table 9. The highest corrosion rates were measured with compounds in which pure $PbCl_2$ was detected, i.e., with SiO_2 and NaCl. The KCl-NaCl-including mixture resulted in the lowest corrosion. The corrosion seemed to progress with $FeCl_2$ formation and the corrosivity of species was connected to their stability and how easily they release Cl. Based on this, the experiments show that Cl is released more easily from $PbCl_2$, than from $Na_3Pb_2(SO_4)_3Cl$, K_2PbCl_4 or $K_3Pb_2(SO_4)_3Cl$ at 400 °C.

Table 9. Measured corrosion layer thicknesses after the 24 h experiment (Paper III).

Deposit material		**Corrosion layer thickness, Ring 2 [µm]**
Ring 1	*Ring 2*	*24 h test*
$PbCl_2$	SiO_2	630 ± 15
$PbCl_2$	NaCl	260 ± 20
$PbCl_2$	Na_2SO_4	230 ± 57
$PbCl_2$	KCl	110 ± 30
$PbCl_2$	K_2SO_4	70 ± 45
$PbCl_2$	KCl-NaCl	50 ± 13

As the results shown, $PbCl_2$ reacts with alkali sulphates, forming $K_3Pb_2(SO_4)_3Cl$ or $Na_3Pb_2(SO_4)_3Cl$ and inducing corrosion. Thus, a temperature at which the corrosion is significant (threshold temperature) was tested with a small amount of $PbCl_2$ (5 wt-%) mixed with a higher share of K_2SO_4 (95 wt-%) (Paper IV). Experiments were carried out at different temperatures with two low-alloy steels (16Mo3 and 10CrMo9-10) and with a Ni-based alloy (Alloy 625). Ni-based alloys have been shown to be more resistant against Pb attacks compared to the low-alloy steels [56, 67, 129].

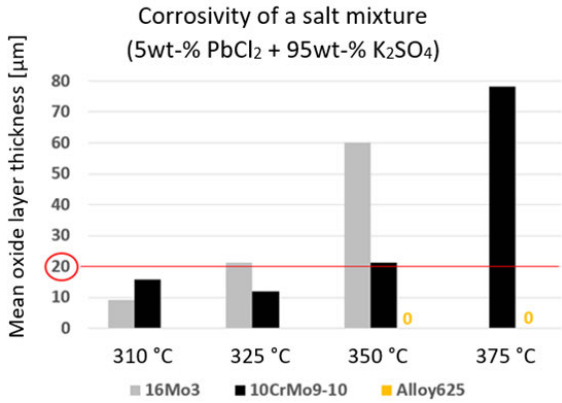

Figure 27. Corrosion test results for low-alloy 16Mo3 and 10CrMo9-10 steels and for nickel-based Alloy 625 (Paper IV).

Based on the previous study, corrosion is assumed to be severe when the oxide layer thickness exceeds 20 µm [18]. According to the test results, the threshold temperature for 16Mo3 can be observed at 325 °C, Figure 27, which is clearly below the first melting temperature of the deposit (the T_0 for a $PbCl_2$-K_2SO_4 system is 403 °C). The threshold temperature for the low-alloy 10CrMo9-10 steel was a bit higher, 350 °C, probably due to the small Cr-alloying. No corrosion was observed with Alloy 625, which was tested only at the two highest temperatures, 350 and 375 °C. 16Mo3 was not tested at 375 °C due to the high corrosion rate already observed at 325 °C.

4.4. Corrosion mechanism of lead-including deposits

Based on the studies presented in the previous chapters, it seems evident that Pb can be present in the deposits together with K, Cl (and S) and that $FeCl_2$ is formed as a corrosion product with Fe-based steels. Corrosion probe measurements and superheater deposits revealed the presence of a K-Pb-Cl compound instead of pure $PbCl_2$. NaCl was shown to have no solid reaction with $PbCl_2$; it can, however, form a common molten mixture. The results presented in this work show that corrosion can start below the first melting temperature of the deposit; this has also been noted in the literature [13, 21, 46]. One accelerating factor for this could be common melt formation together with the deposit and the initial corrosion products [85, 101]. The first melting temperature for the KCl-$FeCl_2$ mixture has been reported to be 355 °C, but no similar data can be found for the $PbCl_2$-KCl-$FeCl_2$ system [130]. Accordingly, a solidus projection was calculated for the $PbCl_2$-KCl-$FeCl_2$ system with FactSage 7.1, Figure 28 (**Paper I**). For additional verification of

the melting temperature of the $FeCl_2$-KCl-$PbCl_2$ system, a synthetic mixture was made and analysed with DSC/TGA.

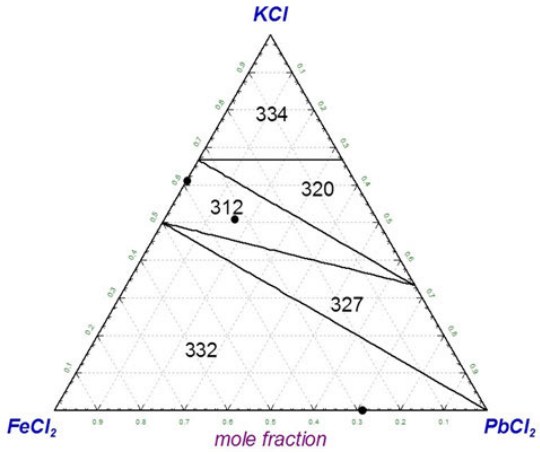

Figure 1. Solidus projections for the $FeCl_2$-KCl-$PbCl_2$ system. Temperatures shown as °C. Black dots indicate experimental mixture compositions (Paper II).

The melting temperatures vary between 312 °C and 334 °C depending on the composition. This might explain why increased oxidation was observed below the deposit's first melting temperature. As earlier mentioned, the presence of $FeCl_2$ just above the steel material was observed in both full-scale and laboratory-scale measurements and above the $FeCl_2$ an Fe oxide layer was reported. The results indicate that corrosion follows the already-known Cl-induced corrosion mechanism by the formation of $FeCl_2$ with Fe-based steels. A corrosion mechanism is suggested, in which a K-Pb-Cl mixture initiates the corrosion reaction by the formation of $FeCl_2$, which in turn further accelerates the corrosion by lowering the melting temperature via formation of a low melting eutectic mixture including Fe, K, Pb and Cl. This could lead to heavy corrosion, in which the steel is dissolved by the formed low-melting ternary eutectic mixture.

The $FeCl_2$ formation and possible melt formation, together with the deposits, were studied in the laboratory (**Papers IV and V**). A carbon steel (P265GH) was exposed isothermally at 300 °C and 340 °C in a tube furnace for 24 h in a gas atmosphere consisting of 100 ppm HCl and 20 vol.-% H_2O in synthetic air, with the deposit mixture including 79 weight-% $PbCl_2$ and 21 weight-% KCl (**Paper V**). The selected experimental temperatures were below and above the lowest first melting temperature of a $FeCl_2$-KCl-$PbCl_2$ system (312 °C). Both pre-oxidised and not pre-oxidised samples were used. The exposed samples were studied by SEM/EDX and XRD.

Both K_2PbCl_4 and KPb_2Cl_5 was observed depending on the surplus of either KCl or $PbCl_2$. If there is a surplus of KCl compared to the $PbCl_2$, K_2PbCl_4 is formed around the KCl particles. If there is more $PbCl_2$, KPb_2Cl_5 will grow around the $PbCl_2$ particles. Some $PbCl_2$ also remained in the salt mixture, more at the 300 °C than at 340 °C. Pre-oxidised samples had less areas with thicker corrosion products compared to the non-preoxidised samples, although oxide layer growth was observed in both samples at both temperatures. The oxide layer growth was smaller at 300 °C.

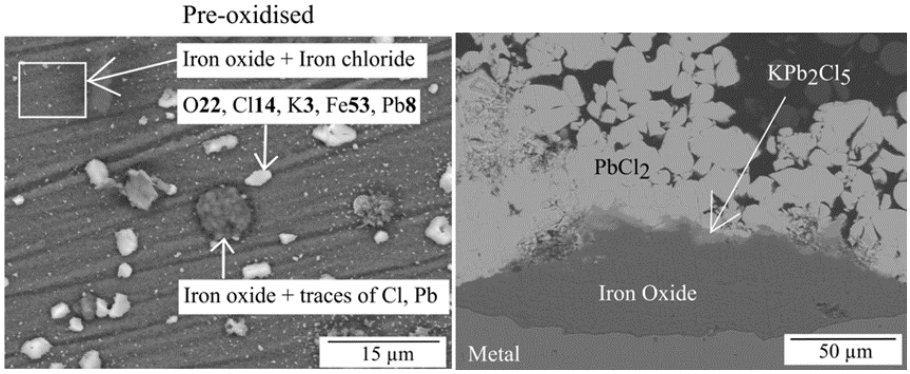

Figure 29. Surface (left, values as atomic-%) and cross-section (right) appearances of the pre-oxidised sample exposed at 340 °C (Paper V).

There were indications of possible melt formation including $FeCl_2$. Areas including O, Cl, K, Fe and Pb were observed, and in the vicinity of these areas were Fe oxide particles with residues of Cl and Pb, Figure 29. A reference exposure was performed without a deposit, with and without HCl to study the role of HCl. A slight increase in corrosion based on the weight gains was observed with HCl. However, no $FeCl_2$ was identified by either SEM/EDX or XRD as a corrosion product for the reference samples, suggesting that the main contribution to increased corrosion is caused by the Pb-K-Cl salt.

The exposures described above provided indications of melt formation (and in particular melt including $FeCl_2$); however, it was not possible to prove its presence in these experiments. To determine whether a melt was present, another set of experiments were conducted in which also $FeCl_2$ was added to the synthetic deposit mixture (**Paper IV**). A test deposit containing of equal weight-% amounts of $FeCl_2$, $PbCl_2$ and KCl was used. $FeCl_2$, an intermediate corrosion product according to the Cl-induced corrosion mechanism, was added to the deposit mixture to study possible reactions with the other deposit components. The tests were carried out again at

300 °C and at 340 °C. The exposure time was 8 hours and the tests were carried out in ambient air.

A narrow $FeCl_2$ ribbon was found just above the steel surface at both temperatures, Figure 30 (point 5). Above the $FeCl_2$ was an Fe-oxide layer, which was much thicker at 340 °C (140 µm) than at 300 °C (30 µm). However, part of the $FeCl_2$ salt may have oxidised during the tests, partially contributing to the increased oxide layer. Pb-including compounds were observed within and above the Fe oxide layer at 300 °C, Figure 30 (point 3). The white areas seem to include all elements from the original deposit mixture (Fe, K, Pb and Cl), indicating that these elements will interact and form a melt or sintered particles. The absence of oxygen in this area shows that oxides are not present. The shape of the particles supports melt formation, as they are round-shaped. If this really is the case, it is already occurring below the calculated T0 for a $FeCl_2$-KCl-$PbCl_2$ system. At 340 °C, no particles including Pb could be found within the Fe oxide layer, Figure 30 (point 4). Instead, Pb-including particles were located above the Fe oxide layer and only small residues of Fe could be detected from those particles (point 2).

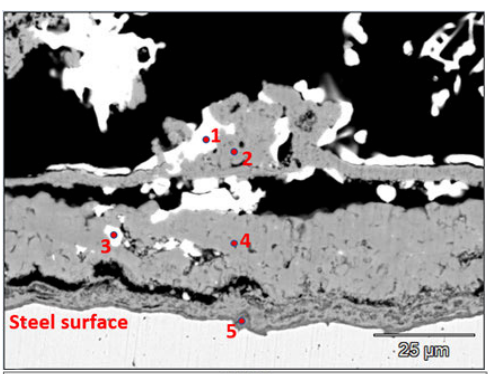

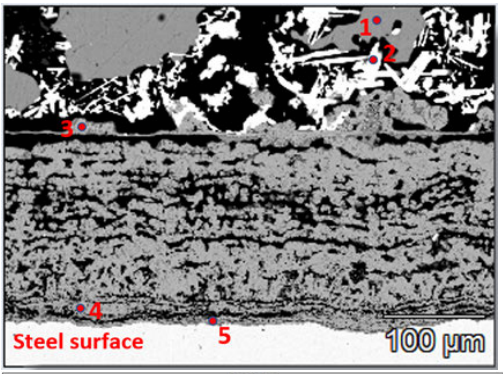

300 °C

Point	O [at-%]	Fe	K	Pb	Cl	Possible compound
1		5.9	29.7	11.1	53.3	K_2PbCl_4 + K-Fe-Cl
2	61.5	37.2	0.3		1.0	Iron oxide
3	34.5	15.5	6.9	12.0	31.1	Not identified
4	59.5	38.3	0.4		1.8	Iron oxide
5	40.4	27.1			32.5	Iron oxide/chloride

340 °C

Point	O [at-%]	Fe	K	Pb	Cl	Possible compound
1			49.5		50.5	KCl
2		0.2	31.6	10.9	57.3	K_2PbCl_4 + KCl
3	61.5	36.1	0.4	0.6	1.4	Iron oxide
4	57.0	41.1	0.6		1.4	Iron oxide
5	57.5	35.1	1.6		5.8	Iron oxide/chloride + KCl

Figure 2. A SEM/EDX image of the cross-section of the exposed steel and its corrosion layer with five-point analyses (300 °C on the left and 340 °C on the right) (Paper IV).

The results argue that corrosion proceeds with $FeCl_2$ formation with Fe-based steels as the $PbCl_2$ including deposits get into contact with the steel.

$PbCl_2$ and K-Pb-Cl-including compounds are all able to initiate the corrosion reaction. In the boiler environment, the most probable compounds are K_2PbCl_4 and KPb_2Cl_5 as $PbCl_2$ interacts with KCl in the deposits. Corrosion probably proceeds following an active oxidation mechanism, in which Cl_2 is formed and which reacts with the steel, producing $FeCl_2$. To initiate the corrosion, no molten phase is needed. Initiation and formation of $FeCl_2$ already occurs at relatively low temperatures (300 °C). In the second stage as the corrosion proceeds, $FeCl_2$ could form a local melt together with Pb-including particles. The melt formation accelerates the growth of the oxide layer and higher material temperatures increase the rate even further.

5. Conclusions

Combustion of recycled wood poses challenges to boiler manufacturers as this kind of fuel typically contains high amounts of Pb, Zn, Cl and alkalis, all contributing to corrosion and limiting the steam parameters. Thus, understanding phenomena occurring from fuel to stack is important in order to find cost-effective solutions related to the boiler design and material selection. The presence, form and behaviour of Pb and Pb-including compounds were widely studied in this thesis with field- and laboratory-scale measurements and with thermodynamic calculations. The results described in this thesis can be used in boiler design when selecting suitable temperatures and materials for furnace walls and superheaters.

Formation and deposition

Fine particle measurements in the furnace area showed the presence of Na, K, Pb and Cl. Over 70 % of Pb was found to be bound with chlorine. The concentration was at its highest between the secondary and tertiary air levels. K_2PbCl_4 and KPb_2Cl_5 were identified in the short- and long-term deposits collected from the recycled wood firing FB boilers. They were observed in the deposits in both high flue gas temperature area (800 °C) and low flue gas temperature area (490 °C). In the presence of alkali sulphates and $PbCl_2$, a caracolite $Na_3Pb_2(SO_4)_3Cl$, or a caracolite-type compound $K_3Pb_2(SO_4)_3Cl$ will form.

The formation of solid binary salts, K_2PbCl_4 and KPb_2Cl_5, in the deposits from $PbCl_2$ and KCl was clearly shown in this work. It was also shown that NaCl does not have a solid-solid reaction with $PbCl_2$ but may form a common melt with K-Pb-Cl including deposit. Thermodynamic calculations suggested solid KPb_2Cl_5 to be stable below 285 °C. Solid K_2PbCl_4 was predicted to be stable on surfaces with temperatures between 285 °C and 365 °C which are typical furnace wall temperatures. The highest condensation temperature of $PbCl_2$ was predicted to be ~440 °C. Gaseous $KPbCl_3$ and $NaPbCl_3$ were predicted to be stable between 400 and 900 °C during recycled wood combustion but the major part of gaseous Pb is suggested to be in the form of $PbCl_2$. PbO was predicted to be the major stable phase at typical FB boiler furnace temperatures which was not supported by the fine particle measurements.

Corrosion mechanism

$FeCl_2$ was observed to form in the full- and laboratory-scale tests as a corrosion product beneath the K-Pb-Cl-including mixtures. The solidus projection for the $PbCl_2$-KCl-FeCl2 mixture proposed melting temperatures between 312 °C and 334 °C depending on the composition. Corrosion tests with the $FeCl_2$-$PbCl_2$-KCl mixture below (300 °C) and above (340 °C) the first melting temperature showed that Fe, K, Pb and Cl will interact and form a melt or sintered particles together and serving the explanation of the corrosion occurring below the deposit's first melting temperature. It is proposed that corrosion proceeds via $FeCl_2$ formation with Fe-based steels when $PbCl_2$-including compounds get into contact with the steel. Formed $FeCl_2$ reacts further with the deposit and might form local melt which could accelerate corrosion.

Corrosivity

Flue gas temperature was observed to have an effect on corrosion rate. The corrosion rate was twice as large at the higher flue gas temperature compared to the lower flue gas temperature, probably due to the presence of a molten deposit in a hot flue gas temperature. No corrosion of carbon steel was observed at 200 °C when exposed to $PbCl_2$-containing deposits. Corrosion was noticed to occur at 300 °C and above. Threshold temperatures for severe corrosion for the low-alloy 16Mo3 and 10CrMo9-10 were 325 °C and 350 °C, respectively. Ni-based alloy 625 was not corroding at the highest test temperature of 375 °C.

Future work

Understanding the corrosion phenomena enables the most cost-effective boiler design and material selection. The results showed that Pb forms corrosive compounds with K and Cl when combusting recycled wood. The formation and corrosivity of these compounds within the deposit were identified. In addition to $PbCl_2$, gaseous $KPbCl_3$ and $NaPbCl_3$ compound might be present during recycled wood firing; these were added to the thermodynamic database. However, additional understanding of the formation and prediction of this $KPbCl_3$ compound is still needed. The tests carried out showed clearly that $PbCl_2$ interacts with alkali sulphates leading to increased corrosion. This was verified within the deposits. Because the gas phase reactions are not known, the effect of S-based additives against heavy metal chloride-induced corrosion needs to be studied further. Fe-based steels were shown to corrode beneath $PbCl_2$-including salts by forming $FeCl_2$, which could promote melt formation together with the deposit, and thus enhance corrosion. High-alloy stainless steels and Ni-based alloys have been shown to be more corrosion-resistant; however, their corrosion mechanism is not yet fully understood.

References

1. Wikipedia. *Renewable energy in the European Union*. Cited: 7th of Feb 2019; https://en.wikipedia.org/wiki/Renewable_energy_in_the_European_Union.

2. Eurostat. *Share of renewable energy in gross final energy consumption*. Cited: 7th of Feb 2019; https://ec.europa.eu/eurostat/tgm/table.do?tab=table&init=1&language=en&pcode=t2020_31&plugin=1.

3. European Comission. *The revised renewable energy directive 2018*. Cited 9th of Apr 2019; https://ec.europa.eu/energy/sites/ener/files/documents/directive_renewable_factsheet.pdf.

4. European Comission. *Renewable energy directive.* Cited 7th of Feb 2019; https://ec.europa.eu/energy/en/topics/renewable-energy/renewable-energy-directive.

5. Tilastokeskus (In Finnish). *Vuosineljännes 2018, Liitekuvio 13. Uusiutuvan energian osuus kokonaisenergiasta 2018. Energian hankinta ja kulutus 2019*. Cited 21st of Apr 2019; http://www.stat.fi/til/ehk/2018/04/ehk_2018_04_2019-03-28_kuv_013_fi.html.

6. Eurostat. Share of renewables in energy consumption in the EU reached 17% in 2016, in Eleven Member States already achieved their 2020 targets. Eurostat Press Office, 2018.

7. Pöyry (In Finnish). *Jätteiden energiahyödyntäminen Suomessa*. 2015, Energiateollisuus RY. p. 39.

8. Pitcher G. *UK 'could become waste wood importer*'. 2018 Cited 7th of Feb 2019]; https://www.mrw.co.uk/latest/uk-could-become-waste-wood-importer/10032497.article.

9. Nilsson L. (In Swedish)*Trädbränsle- och torvpriser. 2017*, Cited 7th of Feb 2019; http://www.google.com/url?sa=t&rct=j&q=&esrc=s&source=web&cd=1&ved=2ahUKEwi90dCxr6ngAhWliKYKHcXfBFMQFjAAegQIARAC&url=http%3A%2F%2Fwww.energimyndigheten.se%2Fcontentassets%2F5b5e7fbcd0f249458f53cbd82675aef1%2Ftidserier_tradbransle_och_torvpriser_master_webben-ver01.xls&usg=AOvVaw1HouD_MjgJAkLRrq2CGWzy.

10. Edo M., Bjorn E., Persson P.E., Jansson S. *Assessment of chemical and material contamination in waste wood fuels--A case study ranging over nine years*. Waste Management, 2016. 49: p. 311-319. doi:10.1016/j.wasman.2015.11.048

11. Krook J., Mårtensson A., Eklund M. *Metal contamination in recovered waste wood used as energy source in Sweden*. Resources, Conservation and Recycling, 2004. 41(1): p. 1-14. doi:10.1016/s0921-3449(03)00100-9

12. Krook J., Mårtensson A. Eklund M., Libiseller C. *Swedish recovered wood waste: linking regulation and contamination*. Waste Management, 2008. 28(3): p. 638-48. doi:10.1016/j.wasman.2007.03.010

13. Skrifvars B.-J., Backman R., Hupa M., Salmenoja K., Vakkilainen E. Corrosion of superheater steel materials under alkali salt deposits Part 1: The effect of salt deposit composition and temperature. Corrosion Science, 2008. 50(5): p. 1274-1282. doi:10.1016/j.corsci.2008.01.010

14. Nielsen H., Frandsen F., Dam-Johansen K., Baxter L. *The implications of chlorine-associated corrosion on the operation of biomass-fired boilers*. Progress in Energy and Combustion Science, 2000. 26(3): p. 283-298. doi:10.1016/S0360-1285(00)00003-4

15. Spiegel M., *Corrosion in molten salts*. Materials Science and Materials Engineering, 2010. 1: p. 316-330. doi: 10.1016/B978-044452787-5.00019-6

16. Albina D. Theory and experience on corrosion of waterwall and superheater tubes of waste-to-energy facilities. Earth and environmental engineering. 2005, Columbia University: New York.

17. Alipour Y. *Furnace Wall Corrosion in a Wood-fired Boiler*. Division of Surface and Corrosion Science. 2015, KTH Royal Institute of Technology: Stockholm.

18. Bankiewicz D. Corrosion behaviour of boiler tube materials during combustion of fuels containing Zn and Pb. Laboratory of Inorganic Chemistry. 2012, Åbo Akademi University: Turku.

19. Enestam S. *Corrosivity of hot flue gases in the fluidized bed combustion of recovered waste wood*. Department of Chemical Engineering. 2011, Åbo Akademi University: Turku.

20. Wu H. Chemistry of potassium halides and their role in corrosion in biomass and waste firing. Laboratory of Inorganic Chemistry. 2016, Åbo Akademi University: Turku.

21. Viklund P. *High temperature corrosion during waste incineration*. Department of Chemistry. 2011, KTH Chemical Science and Engineering: Stockholm.

22. Zevenhoven M., Yrjas P., Hupa M. *Ash-forming matter and ash-related problems*. Handbook of Combustion, 2010.

23. Yin C., Li S. Advancing grate-firing for greater environmental impacts and efficiency for decentralized biomass/wastes combustion. Energy Procedia, 2017. 120: p. 373-379. doi:10.1016/j.egypro.2017.07.220

24. Yin C., Rosendahl L., Kær S. *Grate-firing of biomass for heat and power production*. Progress in Energy and Combustion Science, 2008. 34(6): p. 725-754. doi:10.1016/j.pecs.2008.05.002

25. European Comission. *Waste*, Cited 6th of March 2019, http://ec.europa.eu/environment/waste/landfill_index.htm

26. Alakangas E., Hurskainen M., Laatikainen-Luntama J., Korhonen J. (In Finnish) *Suomessa käytettävien polttoaineiden ominaisuuksia*. Teknologian tutkimuskeskus VTT Oy, 2016.

27. Alakangas E., Koponen K., Sokka L., Keränen, J. *Classification of used wood to biomass fuel or solid recycled fuel and cascading use in Finland*. Book of Proceeding Bioenergy, 2015: p. 79-86.

28. Strömberg B., Svärd S. (In Swedish) *Bränslehandboken*. Värmeforsk, Stockholm, 2012. p. 442.

29. Valmet Technologies Oy. *Fuel database*. 2019.

30. Krutul D., Zielenkiewicz T., Radomski A., Zawadzki J., Antczak A., Drozdzek M., Makowski T. *Metals accumulation in scots pine (Pinus Sylvestris L.) wood and bark affected with environmental pollution*. Wood research, 2017. 62(3): p. 353-364.

31. Krook J., Martensson A., Eklund M. *Sources of heavy metal contamination in Swedish wood waste used for combustion*. Waste Management, 2006. 26(2): p. 158-66. doi:10.1016/j.wasman.2005.07.017

32. Huron M., Oukala S., Lardière J., Giraud N., Dupont C. *An extensive characterization of various treated waste wood for assessment of suitability with combustion process*. Fuel, 2017. 202: p. 118-128. doi:10.1016/j.fuel.2017.04.025

33. Vainikka P., Bankiewicz D., Frantsi A., Silvennoinen J., Hannula J., Yrjas P., Hupa M. High temperature corrosion of boiler waterwalls induced by chlorides and bromides. Part 1: Occurrence of the corrosive ash forming elements in a fluidised bed boiler co-firing solid recovered fuel. Fuel, 2011. 90(5): p. 2055-2063. doi:10.1016/j.fuel.2011.01.020

34. Jones F., Bankiewicz D., Hupa, M. *Occurrence and sources of zinc in fuels*. Fuel, 2014. 117: p. 763-775. doi:10.1016/j.fuel.2013.10.005

35. Clausen C., Kartal S., Arango R., Green F. The role of particle size of particulate nano-zinc oxide wood preservatives on termine mortality and leach resistance. Nanoscale Reasearch Letters, 2011. 6(427).

36. Moradian F. *Ash Behavior in Fluidized-Bed Combustion and Gasification of Biomass and Waste Fuels*. Swedish Centre for Resource Recovery. 2016, University of Borås: Borås.

37. Valmari T. *Potassium behaviour during combustion of wood in circulating fluidised bed power plants*. VTT Chemical Technology. 2000, Helsinki University of Technology: Helsinki.

38. Baxter L., Jenkins B., Miles T., Milne T., Bryers R., Miles Jr. T., Dayton D., Oden L. *The behavior of inorganic material in biomass-fired power boilers: field and laboratory experiences*. Fuel Processing Technology, 1998. 54: p. 47-78. doi:10.1016/S0378-3820(97)00060-X

39. Benson S., Holm P. *Comparison of inorganics in three low-rank coals*. Industrial & Engineering Chemistry Product Research and Development, 1985. 24(1): p. 145-149. doi:10.1021/i300017a027

40. Miles T., Baxter L., Bryers R., Jenkins B., Odens L. *Alkali deposits found in biomass power plants - A preliminary investigation of their extent and nature*. National renewable energy laboratory, 1995.

41. Zevenhoven-Onderwater M. *Ash-forming Matter in Biomass Fuels*. Department of Inorganic Chemistry. 2001, Åbo Akademi University: Turku.

42. Pedersen A., van Lith S., Frandsen F., Steinsen S., Holgersen L. *Release to the gas phase of metals, S and Cl during combustion of dedicated waste fractions*. Fuel Processing Technology, 2010. 91(9): p. 1062-1072. doi:10.1016/j.fuproc.2010.03.013

43. Elled A., Åmand L.-E., Eskilsson D., *Fate of Zinc during Combustion of Demolition Wood in a Fluidized Bed Boiler*. Energy & Fuels, 2008. 22(3): p. 1519-1526. doi: 10.1021/ef700234c

44. van Lith S., Jensen P., Frandsen F., Glarborg, P. *Release to the Gas Phase of Inorganic Elements during Wood Combustion. Part 2: Influence of Fuel Composition*. Energy & Fuels, 2008. 22: p. 1598-1609. doi: 10.1021/ef060613i

45. Silppula O. *Fine particle formation and emissions in biomass combustion*. Department of Environmental Science. 2010, University of Eastern Finland: Kuopio.

46. Talus A., Norling R., Wickström L., Hjörnhede A. *Effect of Lead Content in Used Wood Fuel on Furnace Wall Corrosion of 16Mo3, 304L and Alloy 625*. Oxidation of metals, 2017. 87: p. 813-824. doi: 10.1007/s11085-017-9727-3

47. Jones F. *Characterisation of Waste for Combustion – with Special Reference to the Role of Zinc*. Department of chemical engineering. 2013, Åbo Akademi University: Turku.

48. Lindberg D., Thermochemistry and melting properties of alkali salt mixtures in black liquor conversion processes. Laboratory of Inorganic Chemistry. 2007. Åbo Akademi University: Turku.

49. Lindberg D., Backman R., Chartrand P., Hupa M. Towards a comprehensive thermodynamic database for ash-forming elements in biomass and waste combustion — Current situation and future developments. Fuel Processing Technology, 2013. 105: p. 129-141. doi:10.1016/j.fuproc.2011.08.008

50. Glarborg P., Marshall P. *Mechanism and modeling of the formation of gaseous alkali sulfates*. Combustion and Flame, 2005. 141(1-2): p. 22-39. doi: 10.1016/j.combustflame.2004.08.014

51. Backman R., Hiltunen M., Peltola K.. *Interaction of Pb and Zn with alkalis in fluidized bed combustion or gasification of waste derived fuels*. The 18th international (ASME) conference on fluidized bed combustion. 2005. Toronto.

52. Bankiewicz D., Vainikka P., Lindberg D., Frantsi A., Silvennoinen J., Yrjas P., Hupa M. High temperature corrosion of boiler waterwalls induced by chlorides and bromides – Part 2: Lab-scale corrosion tests and thermodynamic equilibrium modeling of ash and gaseous species. Fuel, 2012. 94: p. 240-250. doi:10.1016/j.fuel.2011.12.023

53. Ménard Y., Asthana A., Patisson F., Sessiecq P., Ablitzer D. *Thermodynamic Study of Heavy Metals Behaviour During Municipal Waste Incineration*. Process Safety and Environmental Protection, 2006. 84(4): p. 290-296. doi:10.1205/psep.05166

54. Spiegel M. *Salt melt induced corrosion of metallic materials in waste incineration plants*. Materials and Corrosion, 1999. 50: p. 373-393. doi: 10.1002/(SICI)1521-4176(199907)50:7<373::AID-MACO373>3.0.CO;2-T

55. Kawahara Y., Kira M. Corrosion Prevention of Waterwall Tube by Field Metal Spraying in Municipal Waste Incineration Plants. Corrosion, 1997. 53(3): p. 241-251. doi:10.5006/1.3280466

56. Viklund P., Hjörnhede A., Henderson P., Stålenheim A., Pettersson R. *Corrosion of superheater materials in a waste-to-energy plant*. Fuel Processing Technology, 2013. 105: p. 106-112. doi:10.1016/j.fuproc.2011.06.017

57. Hagemark K., Hengstenberg D., Blander M. *Association in vapors of ionic salts. The vapor mixtures potassium chloride-lead chloride and rubidium chloride-lead chloride*. Journal of Physical Chemistry, 1967. 71(6): p. 1819–23. doi: 10.1021/j100865a041

58. Jones F., Niklasson F., Lindberg D., Hupa M. Effects of Reduced Bed Temperature in Laboratory- and Full-Scale Fluidized-Bed Boilers: Particle, Deposit, and Ash Chemistry. Energy & Fuels, 2013. 27(8): p. 4999-5007. doi: 10.1021/ef400836e

59. Jones F., Tran H., Lindberg D., Zhao L., Hupa M. *Thermal Stability of Zinc Compounds*. Energy & Fuels, 2013. 27: p. 5663-5669. doi: 10.1021/ef400505u

60. Sorvajärvi T. Advanced Optical Diagnostic Techniques for Detection of Alkali Vapors in High-Temperature Gases. 2013, Tampere University of Technology: Tampere.

61. Viljanen J. *Online Laser Diagnostics for High-Temperature Chemistry in Biomass Combustion*. Faculty of Engineering and Natural Sciences. 2019, Tampere University: Tampere.

62. Toivonen J., Sorvajärvi T., Maunula J., Silvennoinen, K. Laser measurement of KCl vapor in 4 MW CFB boiler during straw combustion and ferric sulfate injection, Automaatioseura.

63. Viljanen J., Toivonen J. Online laser monitoring of metal chloride and oxygen concentration using Collinear Photofragmentation and Atomic Absorption Spectroscopy, Impacts of Fuel Quality on Power Production. 2018. Lake Louise, Canada.

64. Spiegel M., Zahs A., Grabke H. *Fundamental aspects of chlorine induced corrosion in power plants*. Materials at High Temperatures, 2003. 20(2): p. 153-159. doi:10.3184/096034003782749080

65. Daniel P., Barna J., Blue J. *Furnace-wall corrosion in refuse-fired boilers*. National Waste Processing Conference. 1986. Cited 6th of March 2019, http://www.seas.columbia.edu/earth/wtert/newwtert/Research/sofos/nawtec/1986-National-Waste-Processing-Conference/1986-National-Waste-Processing-Conference-22.pdf

66. Bryers R. Fireside slagging, fouling, and high-temperature corrosion of heat-transfer impurities in steam-raising fuels. Prog. Energy Combustion Science, 1996. 22: p. 29-120. doi: 10.1016/0360-1285(95)00012-7

67. Sorell G. *The Role of Chlorine in High Temperature Corrosion in Waste to Energy Plants*. Material at High Temperatures, 1997. 14(3). doi: 10.1080/09603409.1997.11689546

68. Grabke H., Reese E., Spiegel M. *The effects of chlorides, hydrogen chloride, and sulphur dioxide in the oxidation of steels below deposits*. Corrosion Science, 1995. 37(7): p. 1023-1043. doi:10.1016/0010-938X(95)00011-8

69. McNallan M., Liang W., Kim S., Kang C. *Acceleration of the high temperature oxidation of metals by chlorine*. High-temperature corrosion, NACE. 1983. Houston, Texas.

70. Folkeson N., Jonsson T., Halvarsson M., Johansson L.-G., Svensson J.-E. *The influence of small amounts of KCl(s) on the high temperature corrosion of a Fe-2.25Cr-1Mo steel at 400 and 500°C*. Materials and Corrosion, 2011. 62(7). doi: 10.1002/maco.201005942

71. Waldman B., Haider F., Warnecke R. *Corrosion monitoring in waste-to-energy plants*. Eurocorr. 2008. Cited 6th of March 2019, https://www.gks-sw.de/images/pdf2008/117-EuroCorr-08-Korrosionssonde-Waldmann-Manu.pdf

72. Otsuka N. A thermodynamic approach on vapor-condensation of corrosive salts from flue gas on boiler tubes in waste incinerators. Corrosion Science, 2008. 50(6): p. 1627-1636. doi:10.1016/j.corsci.2008.02.004

73. Stålenheim A., Henderson P. (In Swedish) Material for högre ångtemperaturer (upp till 600C) i bio- och avfallseldade annläggningar. Värmeforsk, Stockholm, 2011.

74. Kawahara Y. High temperature corrosion mechanisms and effect of alloying elements for materials used in waste incineration environment. Corrosion Science, 2002. 44: p. 223-245. doi: 10.1016/S0010-938X(01)00058-0

75. Covino Jr B., Cramer S., Bullard S., Ziomek-Moroz M., White M. *Corrosion in a temperature gradient*, A.R. Center. 2003. Albany, USA.

76. Lindberg D., Niemi J., Engblom M., Yrjas P., Laurén T., Hupa M. *Effect of temperature gradient on composition and morphology of synthetic chlorine-containing biomass boiler deposits*. Fuel Processing Technology, 2016. 141: p. 285-298. doi:10.1016/j.fuproc.2015.10.011

77. Purbolaksono J., Khinani A., Rashid A., Ali A., Ahmad J, Nordin N. *A new method for estimating heat flux in superheater and reheater tubes*. Nuclear Engineering and Design, 2009. 239(10): p. 1879-1884. doi:10.1016/j.nucengdes.2009.05.018

78. Kawahara Y. Evaluation of high-temperature corrosion life using temperature gradient corrosion test with thermal cycle component in waste combustion environments. Materials and Corrosion, 2006. 57: p. 60-72. doi:10.1002/maco.200503895|

79. Salmenoja K. Field and laboratory studies in chlorine-induced superheater corrosion in boilers fired with biofuels. 2000, Åbo Akademi University: Turku.

80. Backman R., Khalil R., Todorovic D., Skreiberg Ø., Becidan M., Goile F., Skreiberg A., Sørum L. The effect of peat ash addition to demolition wood on the formation of alkali, lead and zinc compounds at staged combustion conditions. Fuel Processing Technology, 2013. 105: p. 20-27. doi:10.1016/j.fuproc.2011.04.035

81. Norling R., Niklasson F., Wickström L., Hjörnhede A., Talus A. (In Swedish) *Begransad eldstadskorrosion genom reglerad blyhalt* , Energiforsk, Stockholm, 2015.

82. Pettersson J., Asteman H., Svensson J.-E., Johansson L. *KCl induced corrosion of a 304-type austenitic stainless steel at 600 °C; The role of potassium*. Oxidation of metals, 2005. 64(1): p. 23-41. doi:10.1007/s11085-005-5704-3

83. Pettersson C., Pettersson J., Asteman H., Svensson J.-E., Johansson L.-G. *KCl-induced high temperature corrosion of the austenitic Fe–Cr–Ni alloys 304L and Sanicro 28 at 600 °C*. Corrosion Science, 2006. 48: p. 1368–1378. doi:10.1016/j.corsci.2005.05.018

84. Lehmusto J., Yrjas P., Skrifvars B.-J., Hupa M. *Detailed Studies on the High Temperature Corrosion Reactions between Potassium Chloride and Metallic Chromium*. Materials Science Forum, 2011. 696: p. 218-223. doi: 10.4028/www.scientific.net/MSF.696.218

85. Jonsson T., Folkeson N., Svensson J.-E., Johansson L.-G., Halvarsson M. *An ESEM in situ investigation of initial stages of the KCl induced high temperature corrosion of a Fe–2.25Cr–1Mo steel at 400°C*. Corrosion Science, 2011. 53(6): p. 2233-2246. doi:10.1016/j.corsci.2011.03.007

86. Shinata Y., Nichi Y. *NaCl-induced accelerated oxidation of chromium*. Oxidation of metals, 1986. 26(3-4): p. 201-212. doi: 10.1007/BF00659184

87. Mortazavi N., Intiso L., Israelsson N., Johansson L.-G., Halvarsson M. *In Situ ESEM nvestigation of KCl-Induced Corrosion of a FeCrAl and a Model FeNiCrAl Alloy in Lab Air at 450°C*. Journal of Electrochemical Society, 2015. 162(14): p. C744-C753. doi:10.1149/2.0581514jes

88. Nielsen H., Frandsen F., Dam-Johansen K. *Lab-Scale Investigations of High-Temperature Corrosion Phenomena in Straw-Fired Boilers*. Energy & Fuels, 1999. 13(6): p. 1114-1121. doi:10.1021/ef990001g

89. Backman R., Hupa M., Uppstu E. *Fouling and corrosion mechanisms in the recovery boiler superheater area*. Tappi Journal, 1987. 70(6): p. 123-127.

90. Bale C., Bélisle E., Chartrand P., Decterov S., Eriksson G., Gheribi A., Hack K., Jung I.-H., Kang Y.-B., Melancon J., Pelton A., Petersen S., Robelin C., Sangster J., Spencer P. *FactSage thermochemical software and databases, 2010-2016*. Calphad 2016. 54: p. 35-53. doi:10.1016/j.calphad.2016.05.002

91. Nitta K., Nohira T., Hagiwara R., Majima M., Inazawa S. *Physicochemical properties of $ZnCl_2$–NaCl–KCl eutectic melt*. Electrochimica Acta, 2009. 54(21): p. 4898-4902. doi:10.1016/j.electacta.2009.03.079

92. Gabriel A., Pelton A. Phase diagram measurements and thermodynamic analysis of the $PbCl_2$–NaCl, $PbCl_2$–KCl, and $PbCl_2$–KCl–NaCl systems. Canadian Journal of Chemistry, 1985. 63(11): p. 3276-3282. doi: 10.1139/v85-542

93. Chase M. *NIST-JANAF, Thermochemical Tables*, 4th ed. American Institute of Physics, 1998.

94. Seo W., Matsuura H., Tsukihashi F. Calculation of phase diagrams for the $FeCl_2$, $PbCl_2$, and $ZnCl_2$ binary systems by using molecular dynamics simulation. Metallurgical and Materials Transactions B, 2006. 37(2): p. 239-251.

95. Rapp R., Devan J., Douglass D., Nordine P., Pettit F., Whittle D. *High Temperature Corrosion in Energy Systems*. Materials Science and Engineering, 1981. 50: p. 1-17. doi:10.1016/0025-5416(81)90082-3

96. Ruh A., Spiegel M. Thermodynamic and kinetic consideration on the corrosion of Fe, Ni and Cr beneath a molten KCl–$ZnCl_2$ mixture. Corrosion Science, 2006. 48(3): p. 679-695. doi:10.1016/j.corsci.2005.02.015

97. Nordlie B. *Eutectic melting*. Petrology. Encyclopedia of Earth Science, 1989. doi: 10.1007/0-387-30845-8_65

98. Bankiewicz D., Enestam S., Yrjas P., Hupa M. *Experimental studies of Zn and Pb induced high temperature corrosion of two commercial boiler steels*. Fuel Processing Technology, 2013. 105: p. 89-97. doi:10.1016/j.fuproc.2011.12.017

99. Lu W., Pan T., Zhang K., Niu Y. Accelerated corrosion of five commercial steels under a $ZnCl_2$–KCl deposit in a reducing environment typical of waste gasification at 673–773K. Corrosion Science, 2008. 50(7): p. 1900-1906. doi:10.1016/j.corsci.2008.03.004

100. Li Y., Niu Y., Wu W. Accelerated corrosion of pure Fe, Ni, Cr and several Fe-based alloys induced by $ZnCl_2$-KCl at 450 °C in oxidizing environment. Materials Science and Engineering, 2003. 345: p. 64-71.

101. Okoro S., Montgomery M., Frandsen F., Pantleon K. High Temperature Corrosion under Laboratory Conditions Simulating Biomass-Firing: A Comprehensive Characterization of Corrosion Products. Energy & Fuels, 2014. 28(10): p. 6447-6458. doi:10.1021/ef5017335

102. Okoro S., Kiamehr S., Montgomery M., Frandsen F., Pantleon K. Effect of flue gas composition on deposit induced high temperature corrosion under laboratory conditions mimicking biomass firing. Part I: Exposures in oxidizing and chlorinating atmospheres. Materials and Corrosion, 2017. 68(5): p. 499-514. doi:10.1002/maco.201609173

103. Fantozzi D., Kiilakoski J., Koivuluoto H., Vuoristo P., Uusitalo M., Bolelli G., Testa V., Lusvarghi L. *High Temperature Corrosion Properties of Thermally Sprayed Ceramic Oxide Coatings*. in International Thermal Spray Conference and Exposition. 2018. Orlando, Florida.

104. Larsson E., Gruber H., Hellström K., Jonsson T., Liske J., Svensson J.-E. *A comparative study of the initial corrosion of KCl and $PbCl_2$ on a low alloyed steel*. Oxidation of metals, 2017. 87(5-6): p. 779-787.

105. Sørum L., Frandsen F., Hustad J. *On the fate of heavy metals in municipal solid waste combustion. Part II. From furnace to filter*. Fuel 2004. 83: p. 1703–1710. doi: 10.1016/j.fuel.2004.03.002

106. Alipour Y., Henderson P. *Corrosion of furnace wall materials in waste-wood fired power plant*. Corrosion Engineering, Science and Technology, 2015. 50(5): p. 355-363. doi: 10.1179/1743278214y.0000000228

107. Bankiewicz D., Yrjas P., Lindberg D., Hupa M. *Determination of the corrosivity of Pb-containing salt mixtures*. Corrosion Science, 2013. 66: p. 225-232. doi:10.1016/j.corsci.2012.09.024

108. Baker B., Smith G., Shoemaker L. *Performance of Commercial Alloys in Simulated Waste Incineration Environments*. Cited 8th of May, 2019, http://pccforgedproducts.com/web/user_content/files/wyman/Performance%20of%20Commercial%20Alloys%20in%20Simulated%20Waste%20Incineration%20Environments.pdf

109. Larsson E. The corrosive effects of chloride salts on water walls and superheater materials in waste and biomass-fired power plants. Chemical and biological engineering. 2014, Chalmers University of Technology: Gothenburg.

110. Aho M., Silvennoinen J. Preventing chlorine deposition on heat transfer surfaces with aluminium–silicon rich biomass residue and additive. Fuel, 2004. 83(10): p. 1299-1305. doi:10.1016/j.fuel.2004.01.011

111. Öhman M., Nordin A. The role of kaolin in prevention of bed agglomeration during fluidized bed combustion of biomass fuels. Energy & Fuels, 2000. 14: p. 618-624. doi: 10.1021/ef990198c

112. Alipour Y., Talus A., Henderson P., Norling R. The effect of co-firing sewage sludge with used wood on the corrosion of an FeCrAl alloy and a nickel-based alloy in the furnace region. Fuel Processing Technology, 2015. 138: p. 805-813. doi:10.1016/j.fuproc.2015.07.014

113. Viklund P., Pettersson R., Hjörnhede A., Henderson P, Sjövall P. *Effect of sulphur containing additive on initial corrosion of superheater tubes in waste fired boiler*. Corrosion Engineering, Science and Technology 2009. 44(3): p. 234-240. doi: 10.1179/174327809X419203

114. Aho M., Yrjas P., Taipale R., Hupa M., Silvennoinen J. *Reduction of superheater corrosion by co-firing risky biomass with sewage sludge*. Fuel, 2010. 89(9): p. 2376-2386. doi:10.1016/j.fuel.2010.01.023

115. Folkeson N., Pettersson J, Pettersson C., Johansson L.-G., Skog E., Andersson B-Å., Enestam S., Tuiremo J., Jonasson A., Heikne B., Svensson J.-E. *Fireside corrosion of stainless and low alloyed steels in a waste-fired CFB boiler; The effect of adding sulphur to the fuel*. Materials Science Forum, 2008. 595-598: p. 289-297.

116. Slomian A. *Alkali and zinc chlorides in waterwall tube corrosion: Effect of pure salts and mixtures*. Department of Chemical and Biological Engineering. Chalmers University of Tecnology: Gothenburg.

117. DIFFRAC.EVA 4.1.1. Bruker AXS 2010-2015, GmbH. 2015: Karlsruhe, Germany.

118. Powder Diffraction File, PDF-2. Release 2010 RDB: International Centre for Diffraction Data (ICDD): Newtown Square, PA 19073-3273, USA.

119. Vainikka P. Occurrence of bromine in fluidised bed combustion of solid recovered fuel. 2011, Åbo Akademi University: Turku.

120. Robelin C., Chartrand P., Pelton A. *Thermodynamic evaluation and optimization of the ($NaCl + KCl + MgCl_2 + CaCl_2 + MnCl_2 + FeCl_2 + CoCl_2 + NiCl_2$) system*. Journal of Chemical Thermodynamics, 2004. 36(9): p. 809-828. doi: 10.1016/j.jct.2004.05.005

121. Lindberg D., Chartrand P. *Thermodynamic Evaluation and Optimization of the ($Ca + C + O + S$) System*. The Journal of Chemical Thermodynamics, 2009. 41: p. 1111-1124. doi: 10.1016/j.jct.2009.04.018

122. Karpenko N., Sysoev S. *Tensimetric study of the dissociation of mixed chlorides of sodium (or potassium) and lead(II)*. Vestnik Leningradskogo Universiteta, Seriya 4: Fizika, Khimiya, 1974. 1: p. 83-8.

123. Alipour Y., Henderson P., Szakalos P. *Effect of temperature on corrosion of furnace walls in a waste wood fired boiler*. Materials at High Temperatures, 2015. 32(1–2): p. 188-196. doi: 10.1179/0960340914z.000000000100

124. Alipour Y., Viklund P., Henderson P. The analysis of furnace wall deposits in a low-NOx waste wood-fired bubbling fluidised bed boiler. VGB PowerTech, 2012. 12: p. 96-100.

125. Nitsch K., Dusek M., Nikl K., Polak K., Rodova M. *Ternary alkali lead chloride: crystal growth, crystal structure, absorption and emission properties*. Progress in Crystal Growth and Characterization of Materials, 1995. 30(1): p. 1-22. doi: 10.1016/09608974(95)00012-V

126. Wessel R., Denison M., Samretvanich A. The effect of fume on radiative heat transfer in kraft recovery boilers. Tappi Journal, 2000.

127. Bankiewicz D., Yrjas P., Hupa M., *High-temperature corrosion of superheater tube materials exposed to zinc salts*. Energy & Fuels, 2009. 23(7): p. 3469-3474. doi: 10.1021/ef801012z

128. Enestam S., Boman C., Niemi J., Boström D., Backman R., Mäkelä K., Hupa M. Occurrence of zinc and lead in aerosols and deposits in the fluidized-bed combustion of recovered waste wood. Part 1: Samples from boilers. Energy & Fuels, 2011. 25: p. 1396-1404. doi: 10.1021/ef101478n

129. Alipour Y., Henderson P., Szakálos P. *The effect of a nickel alloy coating on the corrosion of furnace wall tubes in a waste wood fired power plant*. Materials and Corrosion, 2014. 65(2): p. 217-225. doi: 10.1002/maco.201307118

130. Häggblom E., Mayrhuber J. *Materials problems in energy utilization from waste*. High Temperature Materials for Power Engineering. 1990. Liége, Belgium.

RECENT REPORTS FROM THE LABORATORY OF INORGANIC CHEMISTRY GROUP OF THE JOHAN GADOLIN PROCESS CHEMISTRY CENTRE:

13-01	Oskar Karlström	Oxidation rates of carbon and nitrogen in char residues from solid fuels
13-02	Frida Jones	Characterisation of Waste for Combustion -with special Reference of the Role of Zinc
13-03	Bingzhi Li	Modeling of Fireside Deposit Formation in Two Industrial Furnaces
13-04	Juho Lehmusto	The Role of Potassium in the Corrosion of Superheater Materials in Boilers Firing Biomass
14-01	Emil Vainio	Fate of Fuel-Bound Nitrogen and Sulfur in Biomass-Fired Industrial Boilers
14-02	Niklas Vähä-Savo	Behavior of Black Liquor Nitrogen in Combustion - Formation of Cyanate
15-01	Petteri Kangas	Modelling the super-equilibria in thermal biomass conversion – Applications and limitations of the constrained free energy method
15-02	David Agar	The Feasibility of Torrefaction for the Co-Firing of Wood in Pulverised-Fuel Boilers
16-01	Tooran Khazraie Shoulaifar	Chemical Changes in Biomass during Torrefaction
16-02	Hao Wu	Chemistry of potassium halides and their role in corrosion in biomass and waste firing
19-01	Jingxin Sui	Initial Stages of Alkali Salt Induced High Temperature Corrosion Mechanisms

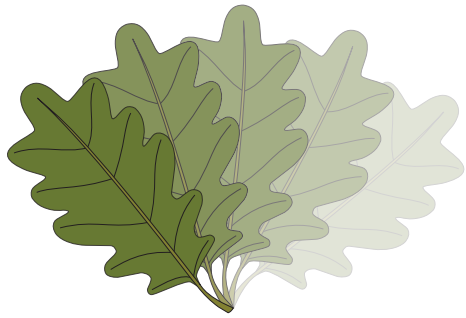

ISBN 978-952-12-3847-5 (printed)
ISBN 978-952-12-3848-2 (digital)
Turku, Finland, 2019

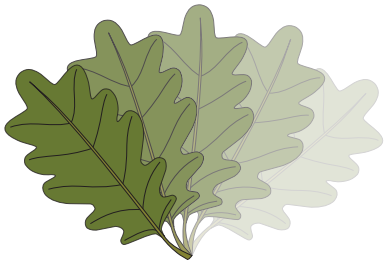

Johan Gadolin
Process Chemistry Centre

ISBN 978-952-12-3847-5